Investigations on the Ski-Snow Contact in Alpine Skiing

A dissertation submitted to the

Faculty of Mathematics, Computer Science, and Physics
of the
University of Innsbruck

for the degree of

Doctor of the Natural Sciences

presented by

Mag. Martin Mössner

Supervisor

A.o. Univ. Prof. Dr. Peter Kaps
Institute for Basic Sciences in Engineering

July 4th 2006

Department of Sport Science, University of Innsbruck
Fürstenweg 185, A-6020 Innsbruck, Austria
email: Martin.Moessner@uibk.ac.at
URL: http://sport1.uibk.ac.at/mm/

This work is available as pdf-document from the author's home page.

Table of Contents

Abstract

Design of skiing equipment for Alpine skiing is in rapid ongoing development. Through the appearance of carver skis, with small ski radii, ski manufacture had been revolutionized. Therefore a detailed knowledge on the contact between ski and snow is necessary. In this work we collect several works contributing to this understanding. The work can be divided in four groups 1) data collection, 2) material research, 3) carving, and 4) ski-snow contact.

For data collection we developed a method for obtaining 3-D data from two or more video recordings. The main benefit of our method is, that cameras may be panned and tilted and lenses zoomed – cameras may even be moved around during the recordings. The method was used in competitive environments, where no markers could be attached to the athlete's bodies. Reconstructed 3-D data proofed to be suitable for biomechanical investigations. In material research we developed experiments to obtain the properties of snow that were needed for simulation. Among these were kinetic friction, resistance against penetration, and shear off strength. For skis we developed methods for obtaining the bending and torsional stiffness of real skis.

For studying the ski-snow contact problem we started with a study of the effects of side-cut on turn radius and strain. Next we studied the quasi-static pressure distribution along the running surface of the ski. Quasi-static means that load is given by gravitation and centrifugal force. The ski-snow contact was implemented by solving the equations of beam deflection with a line load given by the penetration of the ski into the snow. Finally we improved the model to a simulation model, which computes the movement of the ski by solving the Newtonian equations of motion. In the full model reaction forces of snow were computed using a hypoplastic force penetration law with coefficients obtained from material investigations mentioned above.

Introduction

Biomechanical issues had been studied since men began to observe the nature. However, for most of the time investigations were inspired by daily needs, medicine, and wars. Besides that, men tried to realize human dreams, such as flying with one's own muscle strength. For this purpose ancient people tried to build wings for flying. As this example shows, biomechanical issues often are related to the construction and usage of tools. Because of this, biomechanical research needs input from sciences like physics, mathematics, biology, medicine, physiology, etc. A good researcher should master some of these sciences, or at least be able to communicate with scientists of these disciplines.

Biomechanics and Sports have been studied since noble people measured themselves in competitions. But the breakthrough came when practicing sports got popular. Two basic aims are to understand and optimize human movements in sports and to design clothing and tools needed in exercise of sport. In the course of time development of sports equipment got engineered more and more. Skiing, in special, is a good example for this process of mechanization. We just mention the development from wooden skis to modern carver skis and the development from belt bindings to safety release bindings in the last century. Parallel to changes in equipment there is a change in the techniques used by sportsmen.

In this work we give some investigations on the interaction of skis with snow. Because of the author's education, mainly mathematical and physical methods were applied. In particular we dealt with:

- **Data Collection** – especially 3-D reconstruction of 2-D data,
- **Material Research** – in special the properties of snow and skis,
- **Carving Technique**,
- **Ski-Snow Contact**.

Several of the results have been published in journals and conference proceedings, but some of the – quite important detail results – were published as abstracts or posters, only. Each of these subjects will be discussed in the following paragraphs.

Since biomechanics of sports is an applied science almost any investigation needs measured data. A common technique, for obtaining 3-D coordinates of a sportsmen in action, is to record its movements with two or more video cameras. As can be shown by applying geometrical optics, the transformation from real 3-D object coordinates to 2-D image coordinates is described by the direct linear transformation

(DLT). Ten of the 11 DLT-parameters are free and can be related to camera position, resp., image center (2), camera orientation (3), zooming (2), and object center (3). A basic need in recording is, that cameras may be panned and tilted and lenses be zoomed. In some cases it is necessary to move the cameras during the recording. Because of this we developed a method for obtaining 3-D data from 2-D image data [81, 80, 55, 87, 86, 85], that has no restriction for the movement and zooming of the cameras during the recording. For error reduction we used over-determined systems of equations and for stability we used scaling and applied the method of total least squares (van Huffel and Vandewalle [121]). A special version had been developed for planar motion in 3-D. In this case only one camera is needed. Further, distance constraints may be supplied to the landmarks to be reconstructed. In this case one has to solve over-determined, nonlinearly constrained, linear least squares problems (Gill, Murray, and Wright [34], software: `e04unf` from NAG library [105]). Our software for reconstruction was described in [78, 77, 76]. The summit of these investigations was the lecture [79] held on the 10th International Congress of Skiing Trauma and Skiing Safety (STSS) in Zell am See and the publication [85]. In the following the method was supplied at the Department of Sport Science, University of Innsbruck for several biomechanical investigations [101, 61, 75].

The next things to be considered are the materials that are involved. In skiing, we basically are interested in the properties of snow and skis. Therefore we did three groups of investigations: 1) determination of kinetic friction of snow, 2) determination of penetration resistance of snow and shear-off strength, and 3) bending and torsion experiments for Alpine skis.

For determination of the kinetic friction we use runtimes of the skier for a given course [55, 100, 59]. In our case, the motion of the skier is described by the Newtonian equations of motion of a point mass restricted to the snow surface or to the track of the skier. Since the snow surface, resp., the track of the skier is a complicated function, one has to solve a differential-algebraic equation (Hairer and Wanner [41], software: [69, 11, 97]). The coefficient of kinetic friction is a parameter in the differential equation, which had to be computed by parameter identification. For the optimization process we use the damped Newton technique (Deuflhard [23]). For this we needed the derivative of the solution of the differential-algebraic equation with respect to the parameter, i.e. the coefficient of kinetic friction. This was done by solving the variational equations (see [40]). The method was presented by Kaps [53] on the 10th international congress of Skiing Trauma and Skiing Safety (STSS) in Zell am See and published [59]. The method was further applied in [58, 116, 115].

In cooperation with HTM Tyrolia, Schwechat, experiments were designed to determine the snow resistance force due to vertical penetration and to determine the shear strength of snow [84, 74, 73, 61, 88, 93, 92, 95]. Measurements have been done for a long period, results have been published in abstract and poster form, only, but already were used in simulation of skiing [82, 83, 45, 46].

Bending and torsion experiments were designed in order to obtain the ski's bending and torsional stiffness [54, 56]. For the bending stiffness one had to compute the curvature from measurement data of the bending line.

In [94] the influence of the side-cut on turn radius and strain was investigated. In this paper ideas given in Howe's textbook [50], published several years before carver skis were known, were applied. Also very simple, this paper gave, for many readers, a valuable insight to the upcoming carving technique.

Finally the ski-snow contact problem was investigated. Starting from geometrical considerations (Howe [50] or [94]), we investigated the quasi-static deformation of the ski in snow [54, 57, 91, 89, 56]. The word quasi-static means that we computed the load applied from the skier onto the ski by geometrical considerations. The normal force is given by gravitational force and centrifugal force. The edging moment is chosen in such a way, that the resultant force vector directed from the skier's center of mass to the supported running surface of the ski. When the load by the skier onto the ski was given, we calculated the penetration and the deflection of the ski by solving the free boundary value problem for the skis. Note, the snow's reaction force is not supplied by the user, but calculated from the actual penetration depth of the skier. This leads to an optimization problem for the solution of boundary value problems. Since the ski penetrated few millimeters into the snow only, the problem was numerically quite sensitive. Results of these investigations were presented by Kaps [52] at the 2nd International Congress on Skiing and Science (ICSS), St. Christoph am Arlberg and was published [56].

At least a rigid sledge on two skis was implemented in the simulation software LMS Virtual.Lab [67]. This work was done in cooperation with HTM Tyrolia, Schwechat and Lugner et al. [13, 14, 127, 70] from the Department of Mechanics and Mechatronics, Vienna University of Technology. In this software the snow-contact forces were supplied via user defined subroutines. The snow-contact model was improved from pure elastic response to hypoplastic response. Preliminary results were published as abstracts [83, 46] and will be presented at the 6th Engineering of Sport Conference in Munich, DE, papers were submitted and accepted [82, 45].

Biomechanics requires, just as any other science, cooperation in teams. The summit of several scientists working in cooperation is usually more than the sum of the works of each individual. Some things, such as outdoor measurements, can't be done alone, other things, should be done in cooperation. Therefore I, too, have to appreciate the input of my coworkers. At most I have to mention Kaps as well as Nachbauer. Only the cooperation with a mathematician (Kaps) and a biomechanican (Nachbauer), made it possible to write the given thesis. Since outdoor experiments always require a lot of people, I have to thank several people of the department of sport science. Further, I want to dignify the cooperation with Lugner et al. from the Department of Mechanics and Mechatronics of the Vienna University of Technology and Schretter et al. form HTM Tyrolia, Schwechat for the ongoing collaboration. Finally I have to thank all people from the department for the convenient working atmosphere.

1 M. Mössner, P. Kaps, and W. Nachbauer, A Method for Obtaining 3-D Data in Alpine Skiing Using Pan and Tilt Cameras with Zoom Lenses, Ski Trauma and Skiing Safety: 10th Volume, 1996

Reference: M. Mössner[1], P. Kaps[2], and W. Nachbauer[3], *A Method for Obtaining 3-D Data in Alpine Skiing Using Pan and Tilt Cameras with Zoom Lenses*, Ski Trauma and Skiing Safety: 10th Volume, ASTM STP 1266 (Philadelphia, US-PA) (C.D. Mote, R.J. Johnson, W. Hauser, and P.S. Schaff, eds.), American Society for Testing and Materials (ASTM), 1996, pp. 155–164.

Abstract: The direct linear transformation (DLT) was applied for three-dimensional reconstruction in Alpine skiing. Because of the large field of view it is necessary to follow the skier with the cameras to receive frames with a sufficiently large image of the skier. In our implementation, the DLT parameters are computed for each frame of each camera separately. Consequently it is possible to rotate the cameras and to zoom the lenses. The locations of the cameras need not be known. Control points were distributed on the slope. Their coordinates were determined by geodetic surveying. The method requires at least six control points visible in each frame. Using more than six control points reduces the reconstruction error considerably. Under optimal conditions the mean errors are less than 5 cm in each coordinate. This accuracy is sufficient for inverse dynamics if the data are smoothed and the sampling frequency is adequate.

[1]Dept. of Sport Science, Univ. Innsbruck, AT. email: Martin.Moessner@uibk.ac.at
[2]Inst. for Basic Sciences in Engineering, Univ. Innsbruck, AT
[3]Dept. of Sport Science, Univ. Innsbruck, AT

Nomenclature

p	Number of control points
k	Number of cameras
l	Frame number
$\mathbf{b} = (b_1, \ldots, b_{11})$	Calibration vector
$b_1, \ldots, b_{11}$	Calibration coefficients or DLT parameters
$x,\ y$	Image coordinates of a point
$\mathbf{s} = (X,\ Y,\ Z)$	Object vector
$X,\ Y,\ Z$	Object coordinates of a point
$\mathbf{A},\ \mathbf{r}$	Matrix and right hand side of calibration Eq 1.3
$x_i,\ y_i$	Image coordinates of ith control point
$X_i,\ Y_i,\ Z_i$	Object coordinates of ith control point
$\mathbf{B},\ \mathbf{c}$	Matrix and right hand side of image restoration Eq 1.4
$b_1^j, \ldots, b_{11}^j$	Calibration coefficients of the jth camera
$x^j,\ y^j$	Image coordinates corresponding to camera j
ϵ	Absolute error of data
$\sigma_1(\mathbf{A}), \ldots, \sigma_n(\mathbf{A})$	Singular values of a matrix $\mathbf{A}$ (for example Golub and van Loan [5, 36])
$\|\| \cdot \|\|_2$	Euclidean norm, $\|\|\mathbf{x}\|\|_2^2 = \sum_{i=1}^m x_i^2$
$\|\| \cdot \|\|_F$	Frobenius norm, $\|\|\mathbf{A}\|\|_F^2 = \sum_{i=1}^m \sum_{j=1}^n a_{ij}^2$
$s_x,\ s_y,\ s_z$	Standard deviation (mean error) in x-, y-, and z-coordinate

1.1 Introduction

It is a common practice in kinematic analysis of movements in sports to perform three-dimensional (3-D) space reconstruction from 2-D film images using the direct linear transformation (DLT) technique. The DLT technique imposes the restriction that points with known locations (control points) must be distributed in the object space. This is usually provided in form of a calibration frame containing a number of control points (e.g. van Gheluwe [120], Wood and Marshall [126], Hatze [43], Challis and Kerwin [16]). Various shapes of calibration structures with different numbers of control points are used. The calibration frames are usually in a size suitable for analyzing a full stride of a sprinter or a part of a turn in skiing. Extrapolating outside of the calibration frame causes significant inaccuracies (Wood and Marshall [126], Nachbauer et. al. [101]). Larger calibration structures are difficult to construct and to set up. Moreover, the accuracy of the measurements decreases with decreasing size of the subject on the images.

In order to overcome the restriction of the limited object space, 3-D reconstruction techniques were developed that allow rotations of the cameras. Dapena [20] used two cameras that were free to rotate about the vertical axes, and Yeadon [128] reported a method with pan-and-tilt cameras, i.e. rotation about horizontal and vertical axes. In both techniques the camera location must be known and the focal length of the lenses must be constant.

The purpose of this paper is to present a technique for obtaining 3-D data using pan-and-tilt cameras with zoom lenses. The camera locations do not have to be known. We use the method of total least squares (TLS, van Huffel and Vandewalle [121]) for solving the overdetermined linear systems of equations. Proper scaling is essential to yield sufficiently accurate results. An implementation of the method (f3d, version. 3.0) is available.

1.2 DLT method

The direct linear transformation (DLT) was introduced by Abdel-Aziz and Karara [1]. When a space point with object coordinates $(X, Y, Z)^t$ is filmed by a camera, one obtains a 2-D picture. The image coordinates $(x, y)^t$ of this space point are calculated by

$$x = \frac{b_1X + b_2Y + b_3Z + b_4}{b_9X + b_{10}Y + b_{11}Z + 1}\,, \qquad y = \frac{b_5X + b_6Y + b_7Z + b_8}{b_9X + b_{10}Y + b_{11}Z + 1}\,. \tag{1.1}$$

The 11 coefficients $b_1, \dots, b_{11}$ are called DLT or calibration parameters.

There exist several refined models using more than 11 calibration parameters (e.g.: Marzan and Karara [71], Walton [123], Wood and Marshall [126], Ball and

Pierrynowski [7], Challis and Kerwin [16], or Mössner [80]). In such models effects like symmetrical and asymmetrical lens distortion can be considered. We omit such models since the investigation of the model of Marzan and Karara [71] did not show any improvements in our situation.

Hatze [43] proved a nonlinear relationship between the 11 DLT parameters. For his bulky expressions, we have recently found the surprisingly simple equation

$$(1.2)\quad (b_9^2+b_{10}^2+b_{11}^2)(b_1b_5+b_2b_6+b_3b_7)=(b_1b_9+b_2b_{10}+b_3b_{11})(b_5b_9+b_6b_{10}+b_7b_{11}),$$

which will be used in our future work.

We assume that k cameras are available for filming a moving object. The cameras are numbered by j, $j=1,\ldots,k$. An upper index j indicates that the calibration vectors $\mathbf{b}^j$ and the image coordinates x^j, y^j belong to camera j. Synchronized frames are counted by the frame number l. The corresponding recording time is called t_l, $l=1,2,\ldots$ The time history is needed for kinematic analysis. The reconstruction is done for each time t_l separately. Knowledge of t_l is not required for the reconstruction. Therefore, a corresponding index is omitted.

We do not consider the physical meaning of the DLT parameters (see Marzan and Karara [71] or Bopp and Krauss [8]). Therefore, all components of the calibration vector are unknown.

1.2.1 Calibration

In a first step we compute the calibration vector $\mathbf{b}^j$ for the camera j and the frame l. These indices are omitted for simplicity. We assume that the image coordinates x_i, y_i and the object coordinates X_i, Y_i, Z_i, $i=1,\ldots,p$ of p so-called control points are known. Inserting these data into Eq 1.1 leads to a system of linear equations for the 11 DLT parameters $b_1,\ldots,b_{11}$:

$$\mathbf{Ab}=\mathbf{r}$$

$$(1.3)\qquad \mathbf{A}=\begin{pmatrix} X_i & Y_i & Z_i & 1 & 0 & 0 & 0 & 0 & -x_iX_i & -x_iY_i & -x_iZ_i \\ 0 & 0 & 0 & 0 & X_i & Y_i & Z_i & 1 & -y_iX_i & -y_iY_i & -y_iZ_i \end{pmatrix}_{i=1,\ldots,p}$$

$$\mathbf{b}=(b_1,\ldots,b_{11})^t \qquad \mathbf{r}=(x_i,y_i)^t_{i=1,\ldots,p}\,.$$

If the coordinates of at least six control points are available, the system is overdetermined. If the system has full rank there exists a unique $\mathbf{b}$ such that $||\mathbf{Ab}-\mathbf{r}||_2$ is minimal. This solution is called the least squares solution.

Least squares solutions assume an exact $\mathbf{A}$ in Eq 1.3. However, in our case there occur errors in data not only in $\mathbf{r}$, but also in $\mathbf{A}$. Therefore we use the method of total least squares (see Golub and van Loan [37], van Huffel and Vandewalle [121], implementation by Mössner (TLS)).

The above equations may be singular if some of the used control points are coplanar. This happens if there are any four control points in a plane or if there are any three on a straight line or if any two points are coincident.

The computation of the (total) least squares solution smoothes errors in digitized data and object data as well. Residuals give hints for the errors in these data. The residuals are large for control points with erroneous data, which results mainly from mixing up control points.

1.2.2 Reconstruction

In a second step we compute the 3-D object coordinates $(X, Y, Z)^t$ of an unknown space point from its image coordinates $(x^j, y^j)^t$ on the frame of camera j, $j = 1, \ldots, k$. We assume that the frames are synchronized. The calibration coefficients and the image data are camera specific. This is indicated by the upper index j. When the DLT parameters $\mathbf{b}^j = (b_1^j, \ldots, b_{11}^j)$ are known, Eq 1.1 gives two linear equations for the three unknowns X, Y, and Z. Thus, one obtains for k cameras:

$$\mathbf{Bs} = \mathbf{c}$$

$$\mathbf{B} = \begin{pmatrix} b_1^j - x^j b_9^j & b_2^j - x^j b_{10}^j & b_3^j - x^j b_{11}^j \\ b_5^j - y^j b_9^j & b_6^j - y^j b_{10}^j & b_7^j - y^j b_{11}^j \end{pmatrix}_{j=1,\ldots,k} \tag{1.4}$$

$$\mathbf{s} = (X, Y, Z)^t \qquad \mathbf{c} = (x^j - b_4^j,\ y^j - b_8^j)^t_{j=1,\ldots,k}\ .$$

If at least two cameras are used Eq 1.4 is again an overdetermined system of linear equations which is solved by total least squares or least squares. If the angular distance between the optical axes is small, both cameras will have about the same image and the DLT parameters will coincide, which leads to an almost singular $\mathbf{B}$. It is optimal to have an angle of about 90° between the optical axes of the cameras.

1.2.3 Scaling and accuracy

The influence of the error propagation in Eq 1.4 is usually small compared with the one of Eq 1.3. Thus, the error propagation of Eq 1.3 was studied. This was done by comparing the solution $\mathbf{x}$ of

$$\mathbf{Ax} = \mathbf{b}$$

with the solution $\mathbf{y}$ of a disturbed equation

$$\mathbf{A}'\mathbf{y} = \mathbf{b}'.$$

The perturbations are assumed to be errors in the data. ϵ is a measure for the absolute error in the data and is defined by

$$\epsilon = ||\ (\mathbf{A} - \mathbf{A}'|\mathbf{b} - \mathbf{b}')\ ||_F. \tag{1.5}$$

For simplicity we abbreviate $\hat{\sigma}_i = \sigma_i(\mathbf{A})$ and $\sigma_i = \sigma_i(\mathbf{A}|\mathbf{b})$. The error bound for total least squares, given by Golub and van Loan [37], can be refined to

$$\frac{||\mathbf{x} - \mathbf{y}||_2}{||\mathbf{x}||_2} \leq \frac{9\sigma_1}{\sigma_n - \sigma_{n+1}} \left(\frac{1}{1 - \sigma_{n+1}/\hat{\sigma}_n} \right) \frac{1}{||\mathbf{b}||_2 - \sigma_{n+1}} \cdot \epsilon \tag{1.6}$$
$$\text{if} \qquad \epsilon < \frac{1}{6} \left(\hat{\sigma}_n - \sigma_{n+1} \right) .$$

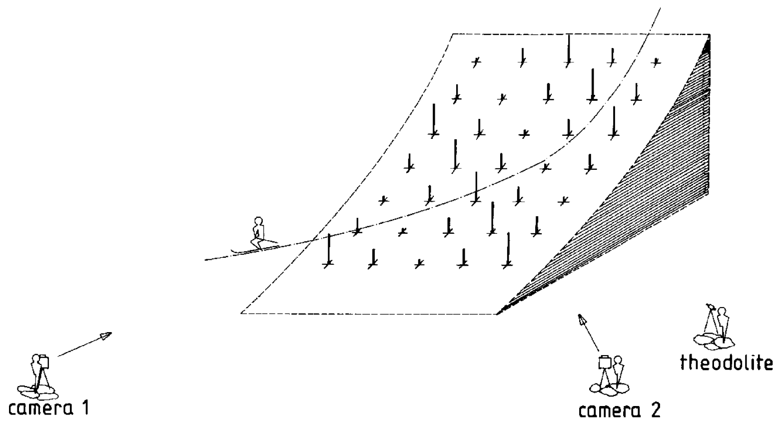

Fig. 1.1: Schematic illustration of the experimental setup on the Rettenbachferner.

Without scaling, the error bound may be fairly high ($> 10^8\,\epsilon$). Therefore, proper scaling is essential. Error bounds less than $10\,\epsilon$ were obtained by the following scaling. In the object space, local coordinate systems were introduced for every frame. The origins of the local coordinate systems were located in the center of the used control points and the image coordinates mapped into the interval $[-1,\,1]$.

Without scaling the linear systems are ill conditioned. Therefore, one has to choose the numerical codes carefully. For least squares we used singular value decomposition (Golub and van Loan [36], LAPACK [5]). The algorithm for total least squares was given by Golub and van Loan [37] and also is based on the singular value decomposition. These methods work even for nearly singular linear systems.

1.3 Data collection

1.3.1 Film measurements

For the film measurements, a testing site was set up on the Rettenbachferner in the Ötztaler Alps in Tyrol (Fig 1.1). Fifty control points were distributed on a field of 7 by 22 m. The distances between the control points were about 2.5 m. Black-painted tennis balls mounted atop wooden posts defined the control points. The height of the posts was alternated between 0.1 and 1.5 m to avoid colinearity. The control points were surveyed with a theodolite to obtain accurate object coordinates. The surveying was repeated after the test runs in order to detect control points moved during the tests.

The skier was filmed using a Locam and a Hycam camera equipped with a 100-200 mm zoom lens (Minolta) and a 12-120 mm zoom lens (Angenieux, Paris), respectively. The film rates were set at 50 and 100 frames/s, respectively. The two film cameras were placed about 30 and 40 m from the marked area. The distance between the film cameras was about 55 m. This resulted in an angle of about

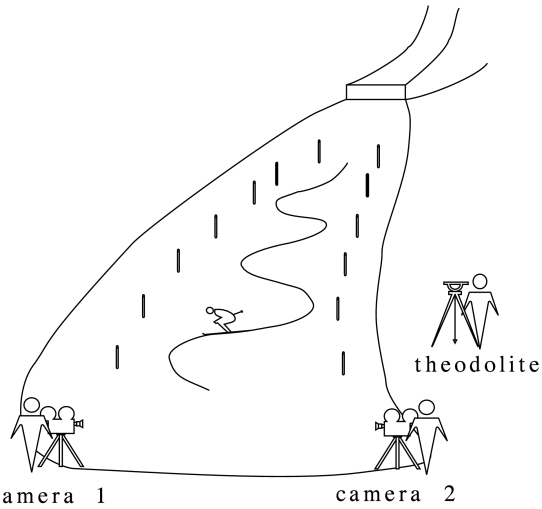

Fig. 1.2: Schematic illustration of the experimental setup in Seefeld.

80° between the optical axes of the cameras. The cameras were not phase-locked. Synchronization was obtained by event synchronization with exploding balloons and an internal timing light which provided a marker on the edge of the film every 100 ms. The slow camera was used as timing baseline.

One run of a skier was analyzed for this study. The frames of the film were projected with a Vanguard projection head onto a Summagraphics digitizer. For each film frame at least 10 control points surrounding the skier and the toepieces of the bindings were digitized.

1.3.2 Video measurements

For the video measurements, a testing site was built on the runout of the 70 m Olympic jumping hill in Seefeld near Innsbruck (Fig 1.2). Thirty-two control points were located laterally on both sides of the runout. The horizontal distances between the control points varied from 10 to 17 m and the distances along the runout were about 5 m. The control points were surveyed with a theodolite to obtain accurate object coordinates.

Several runs of one skier were recorded using two electronically shuttered video cameras (Panasonic F15) equipped with 10.5-126 mm zoom lenses (Panasonic). The cameras were genlocked to ensure shutter synchronization and identical frame rates. This required a cable connection between the cameras. Both cameras were located at the end of the runout in a distance of about 150 m to the marked area. The distance between the cameras was about 45 m. This resulted in an average angle of about 15° between the optical axes of the cameras. The sampling frequency of the cameras was 50 frames/s and the exposure time 1/2000 s.

One run of one skier was analyzed. For each image the toepieces of the bin-

control points	s_x [cm]	s_y [cm]	s_z [cm]
9	1.91	1.38	1.70
8	1.99	1.56	1.68
7	2.17	2.36	1.95
6	4.55	4.48	2.92

Tab. 1.1: Mean errors of a fixed point – film analysis.

control points	s_x [cm]	s_y [cm]	s_z [cm]
7	9.73	1.35	2.85
6	9.82	1.33	3.25

Tab. 1.2: Mean errors of a fixed point – video analysis.

dings and eight control points were digitized using the Peak Videosystem (Peak Technologies Inc., US).

1.4 Results

The results are presented in a Cartesian coordinate system. The z-axis is in the vertical direction and the x-axis is chosen in a way that the fall line of the slope is in the x-z plane approximately.

Tab 1.1 gives the mean errors of the coordinates of a fixed point obtained by geodetic surveying and DLT reconstruction for the film analysis. The number of control points used for calculating the DLT parameters was increased from six to nine. Except in the case of six control points, the mean errors were between 1.4 and 2.4 cm. The errors decreased with increasing number of control points.

Fig 1.3 shows the absolute errors for the case of nine control points used in the DLT. The maximum absolute errors were 6.1, 5.6, and 3.4 cm in the x-, y-, and z-directions, respectively, for the 1.2 s analyzed.

Tab 1.2 gives the mean errors of a fixed point for the video analysis. Results for six and seven control points used in the DLT were calculated. The accuracy of the y- and z-coordinates was about the same as for the film analysis. In the x-direction, a relatively large error occurred. This is due to the small angle between the optical axes of the cameras which affected the accuracy mainly in the x-direction.

Fig 1.4 shows the projection of the displacement of the toepiece of the binding in the x-y plane for the film analysis. The DLT results are compared with a cubic smoothing spline approximation (see de Boor [22]) in order to estimate the random error part of the coordinates. The mean errors were 2.3, 1.3, and 1.7 cm in the x-, y-, and z-directions, respectively.

Fig 1.5 shows the projection of the displacement of the toepiece of the binding

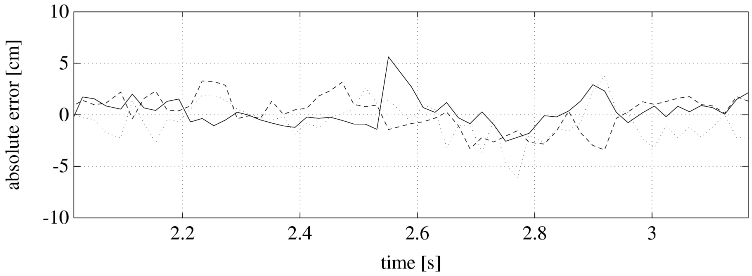

Fig. 1.3: Absolute errors of a fixed point – film analysis. Nine control points were used in the DLT. Dotted line x-, solid line y-, and slashed line z-coordinate.

in the x-y plane for the video analysis. The mean errors were 22.2, 4.0, and 5.0 cm in the x-, y-, and z-directions, respectively. The relatively large error in the x-direction is due to the insufficient angle between the optical axes of the cameras.

1.5 Discussion

The accuracy of the 3-D reconstruction was assessed in two different ways:

(a) *Comparison of the coordinates of a fixed point obtained by geodetic surveying and DLT reconstruction.* For the comparison we chose one control point which was not used for the calibration and which was visible in both camera images. In this way synchronization errors, blurred images, and problems with the identification of body landmarks do not occur. The mean errors between the results obtained by DLT and theodolite were smaller than 2 cm for the film analysis if at least eight control points were used. In video analysis the mean errors are comparable. The error in the x-direction was 10 cm. As reasons, one has to consider the larger test field, the larger distances of the cameras to the test field, and the small angle between the optical axes of the cameras.

(b) *Comparison of the DLT reconstruction of a moving point and its cubic smoothing spline approximation.* The displacement curve of the toe binding of the skier was approximated by smoothing cubic splines. The smoothing spline depends on an unknown parameter p, the so-called smoothing parameter. By varying p one can change the smoothing between interpolation and least squares line fitting. By this comparison the random error in the DLT results can be estimated; however, systematic errors cannot be detected. In the case of oversmoothing an additional systematic error is introduced. If the smoothing is too small the differences between the DLT results and the smoothing spline approximation decrease, which yields a too small error estimation. Both types of errors can be detected optically: systematic differences in the smoothed and unsmoothed displacement/time data indicate oversmoothing and strongly oscillating accelerations undersmoothing.

The number of control points used in the DLT affects the accuracy. The applied DLT technique needs at least six control points, which can be different ones for

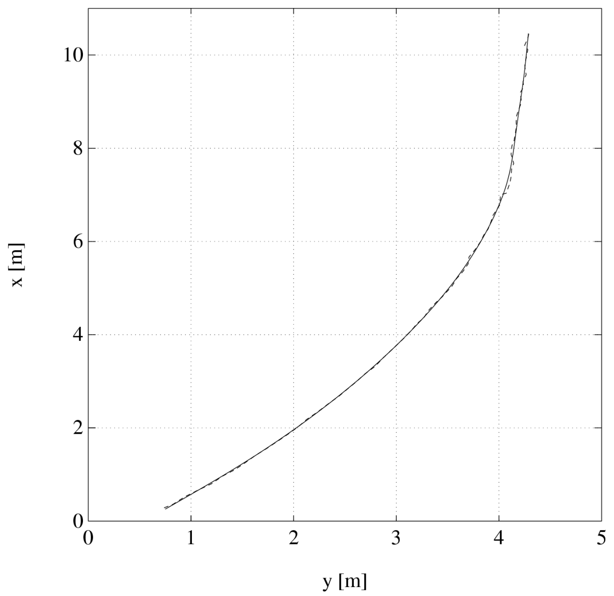

Fig. 1.4: Displacement of a moving point in the x-y plane – film analysis. Dashed line: piecewise linearly interpolated DLT results, solid line: smoothed by cubic smoothing spline.

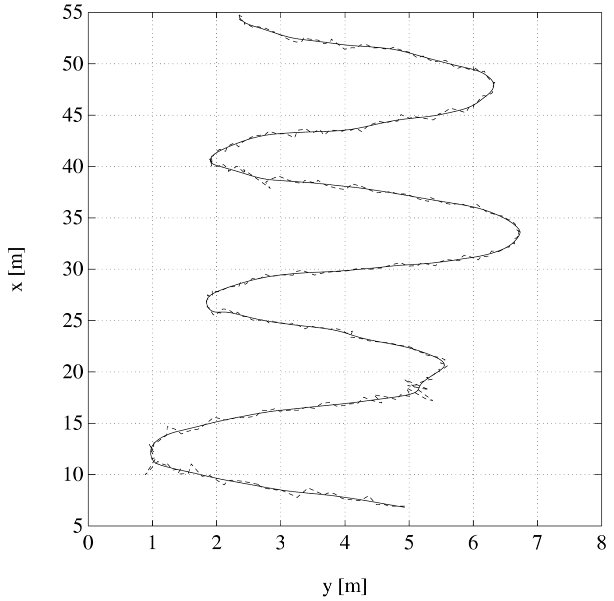

Fig. 1.5: Displacement of a moving point in the x-y plane – video analysis. dashed line: piecewise linearly interpolated DLT results solid line: smoothed by cubic smoothing spline.

each frame of each camera. The use of more control points improves the results considerably. This is shown by the decrease in the mean error from about 4.5 to 1.9 cm using six and nine control points, respectively (Tab 1.1).

High mean errors for the x-coordinate of 9.8 cm (fixed point) and 22 cm (moving point) were calculated for the experimental setup in Seefeld. This error occurred in the direction close to the optical axes of the two video cameras and was due to the small angle of about 15° between the optical axes. Because of the terrain, it was not possible to align the optical axes in the optimal angle of 90°. Small angles cause decreased accuracy mainly in the direction of the optical axes.

The estimation of the random error part of a moving point showed a mean coordinate error of up to 2.3 cm in the film analysis but up to 5.0 cm in the video analysis. The error in the x-coordinate due to the insufficient angle between the optical axes caused an increase up to 20 cm. Two control point configurations were studied. The gridlike control point system of the film analysis allowed a relatively large size of the skier on the images, whereas the control point system of the video analysis required a much larger field of view in order to have the necessary control points on the images. This may be the main reason for the differences in the observed accuracies. Control points located on the left and the right side of the course show the advantage to be suitable not only for experimental setups but also in competitions.

In order to maximize the size of the skier on the images and thus increase the accuracy, the skier was recorded using pan and tilt cameras with zoom lenses. Nevertheless the accuracy assessment of the method gave a considerably high error for the investigated setups. The main reason for this is the need to record, in addition to the skier, at least six control points which should surround the skier. This causes an increase of the field of view particularly in a control point system suitable in competitions. After smoothing, the obtained 3-D data appeared to be appropriate to analyze displacement/time curves.

Similar to Kaps, Nachbauer, and Mössner [59] the reaction forces between skier and snow can be computed. In a recent paper (Nachbauer et al. [101]), the flight and the landing phase of a jump were investigated at the 1994 Olympic downhill race. The reconstructed data were sufficiently accurate to compute resultant knee joint forces and moments by inverse dynamics.

1.6 Conclusion

It is concluded that the developed DLT technique is relevant for sports events like Alpine skiing, where the movement takes place over a large distance. One can obtain mean errors less than 5 cm in each coordinate. This accuracy is sufficient for inverse dynamics if the data are smoothed and the sampling frequency is adequate. A disadvantage of the method is the high number of control points which have to be distributed on the slope.

Acknowledgment

This study was supported in part by a grant of the Austrian Research Foundation and the Austrian Ski Federation. We are grateful to F. Brunner for his help in data collecting.

2 P. Kaps, W. Nachbauer, and M. Mössner, Determination of Kinetic Friction and Drag Area in Alpine Skiing, Ski Trauma and Skiing Safety: 10th Volume, 1996

Reference: P. Kaps[1], W. Nachbauer[2], and M. Mössner[3], *Determination of Kinetic Friction and Drag Area in Alpine Skiing*, Ski Trauma and Skiing Safety: 10th Volume, ASTM STP 1266 (Philadelphia, US-PA) (C.D. Mote, R.J. Johnson, W. Hauser, and P.S. Schaff, eds.), American Society for Testing and Materials (ASTM), 1996, pp. 165–177.

Abstract: The coefficient of friction of skis on snow appears to be influenced by several factors, for example, speed, contact area, snow type and ski properties. The purpose of this study was to determine simultaneously the coefficient of kinetic friction and the drag area in straight running on a slope with varying inclination and in traversing on an inclined plane. Experimental measurements were taken using photo cells for straight running and by film analysis for traversing. The skier was modeled as a particle that moves on the surface of a slope. The equation of motion with the algebraic constraints of the track of the skier represents a differential-algebraic equation which was solved numerically. The coefficient of friction and the drag area were calculated by minimizing the sum of the square errors between computed and measured time data.

For straight running, the computed coefficient of friction and the drag area were in the same range as obtained by other methods. For traversing, the coefficient of friction could be determined but not the drag area. The skier traversed in an upright position at a speed from 0 to 17 m/s. In this range of velocity the drag area is not constant. It corresponds to critical Reynolds numbers where a sudden drop in the drag coefficient occurs if the body segments are approximated by cylinders.

The results indicate that in both cases the applied method is adequate for determining simultaneously the coefficient of kinetic friction and the drag area if these parameters are independent of the velocity.

[1]Inst. for Basic Sciences in Engineering, Univ. Innsbruck, AT. email: Peter.Kaps@uibk.ac.at
[2]Dept. of Sport Science, Univ. Innsbruck, AT
[3]Dept. of Sport Science, Univ. Innsbruck, AT

Nomenclature

A	projected area
A_c	contact area
α	slope inclination
β	traverse angle between fall line and direction of travel
C_d	drag coefficient
d	thickness of water film
D	diameter of a cylinder
η	coefficient of viscosity
F_c	friction force due to snow compaction, ploughing, etc.
F_d, F_f	drag and friction force
$\mathbf{F}_g$	gravitational force
$\mathbf{F}_a, \mathbf{F}_r$	vector of applied and reaction forces
k_1, k_n	air friction constant, see Eq 2.6, 2.7
l	height of a skater
L	characteristic length in Re
m	mass
μ	coefficient of friction
μ_1	velocity dependent part of coefficient of friction
N	normal force
ν	kinematic viscosity
Re	Reynolds number
ρ	density
s	arc length of path of skier
s_i	arc length at time t_i
t_i	measured time at ith photocell or for ith picture
θ_0	knee angle
θ_1	angle between trunk and horizontal line
v	velocity
V	characteristic velocity in Re
x_i, y_i	measured coordinates of skier at ith photocell

2.1 Introduction

When a ski glides over snow, the snow exerts forces on the ski. The ratio of the tangential force and the normal force is called the *coefficient of kinetic friction*. It is influenced by several factors, e.g. speed, contact area, loading, temperature, snow type (snow temperature, hardness, liquid-water content, texture) and ski properties (stiffness, thermal conductivity, base material, base roughness). The air resistance comprises all interactions between skier and air. The component parallel to the direction of motion is called *drag*, the normal component *lift*. The drag coefficient seems to be nearly constant for high velocities whereas it decreases for low velocities (Gorlin et al. [38]). In laboratory investigations, the coefficient of friction was commonly determined by means of friction meters consisting of rotational devices with built-in force transducers (e.g. Kuroiwa [62]). In skiing investigations, measurements were obtained in straight running using the towing method (e.g. Habel [39]) or the runout method (e.g. Habel [39], Leino and Spring [63]). The drag area is determined usually in wind channels (Gorlin et al. [38]). Erkkilä et al. [27] used roller-skis. The purpose of this study was to present a method to determine the coefficient of kinetic friction and the drag area simultaneously in straight running on a slope with varying inclination and in traversing on an inclined plane. The paper starts with a review on results for the kinetic friction and the drag area. The experimental work was performed in the surroundings of Seefeld, Austria. Then the equations of motion are formulated as differential-algebraic equations and results are presented for schussing in the fall line and for traversing.

2.2 Data collection

The straight running experiments were conducted on a 342 m long run with an altitude difference of 73 m (Fig 2.1). Nine photocells were installed about 25 cm above the snow surface and distributed along the run. The location of the photocells was determined by geodetic surveying using a theodolite. Time data of a skier gliding straight down the fall line in a tucked position were collected from all photocells (see Nachbauer et al. [102]).

In traversing, the path of the downhill ski boot was determined by film analysis. The length of the run was about 25 m, located on an 18° inclined plane (Fig 2.2). The traversing angle was about 40° to the horizontal. The sides of the traverse were marked by ropes equipped with black-painted tennis balls that defined a 1 m reference marker system. The skier was filmed with a 16 mm high-speed camera located laterally to the plane of motion of the skier. The width of the film field ranged from 4 to 6 m. The film speed was set at 100 frames per second. Ball-shaped markers were placed on the toepiece of the binding. The skier had to traverse in a straight line in an upright position. Side slipping was to be avoided. The coordinates of the marker were determined using the DLT method (Kaps et al. [55], Mössner et al. [85]). Barometric pressure and air temperature were measured in

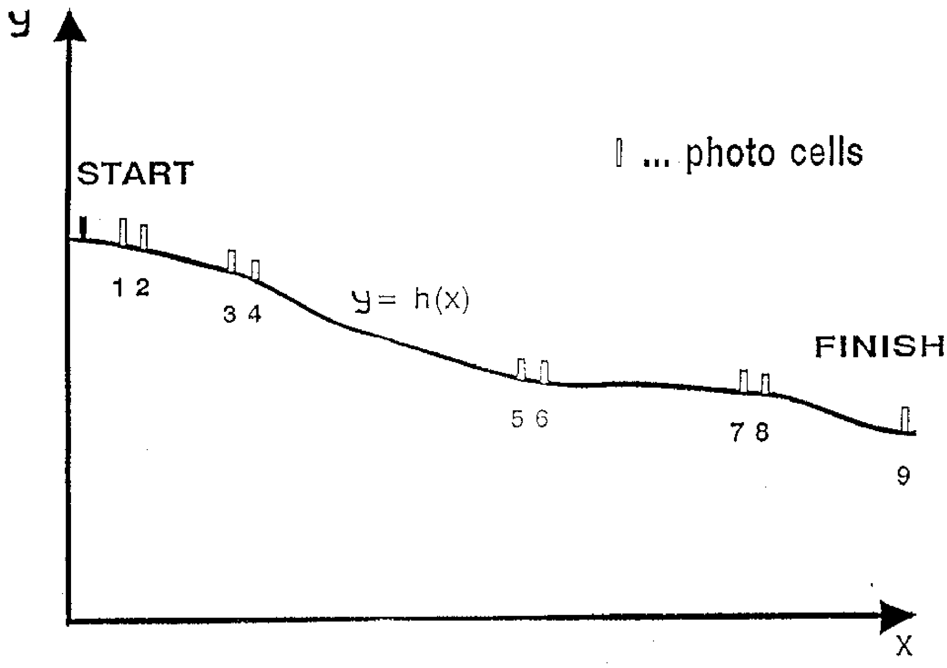

Fig. 2.1: Straight running experiments.

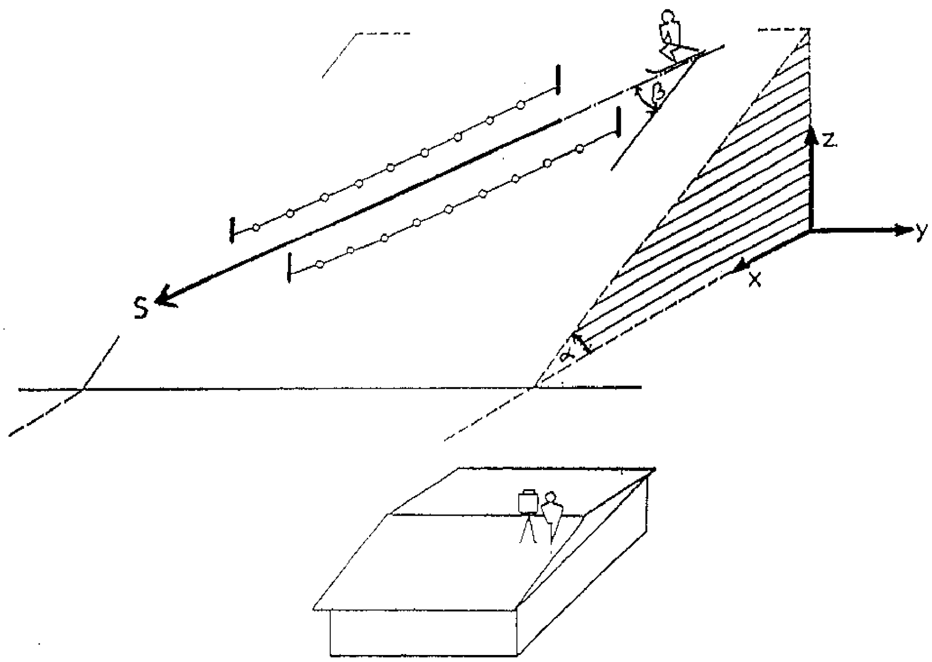

Fig. 2.2: Traversing experiments.

order to calculate the air density. The mass of the skier including his equipment was measured as well (see Haug [44]).

2.3 Kinetic friction

The friction between ski and snow is relatively small because the snow melts at the contact surface of the ski due to the heat produced by friction (Bowden and Hughes [10], Bowden [9]), but it is a complicated phenomenon which is understood only partly.. A thin water film covers at least part of the contact surface. Before we discuss kinetic friction more carefully, two facts from basic mechanics are stated.

1. Coulomb friction: If a rigid body is sliding on a rigid surface, there is a friction force F_f which is proportional to the normal force N by which the body is pressed onto the surface

$$F_f = \mu N, \tag{2.1}$$

where μ is the coefficient of kinetic friction. It is almost independent of the velocity.

2. Viscous friction: If two rigid bodies are moving on a liquid film of thickness d in between with a relative velocity v, the friction force is given by

$$F_f = \frac{\eta A_c v}{d}, \tag{2.2}$$

where A_c denotes the contact area and η the coefficient of viscosity.

For a review of the current research on the kinetic friction between ski and snow see Colbeck [17], Colbeck and Warren [19], Glenne [35], and Perla and Glenne [106]. The snow friction force can be separated into two components. One component is due to the ploughing, shearing, and compression action of a ski; this component is called F_c. The second component is the frictional interaction at the ski-snow interface, where three mechanisms dominate at different film thicknesses: dry, lubricated, and capillary friction. Dry friction occurs at low temperatures or low velocities when the water film is insufficient to prevent solid-to-solid interactions between ski and snow. For thick water films, there is a bridging between the slider and ice grains which are not carrying any load. This leads to an increase in friction (Colbeck [18]). Evans et al. [28], and Akkok et al. [3] presented careful investigations of *thermally controlled* kinetic friction of *ice*. However, they obtained results which suggest that the coefficient of kinetic friction μ is proportional to $1/v$, which is doubtful for our conditions in which higher velocities occur. For hard snow, F_c is usually disregarded. However, it seems that the influence of the ski stiffness on the ground pressure distribution is an important factor (Aichner [2]). The dry sliding friction can be described by a formula of type Eq 2.1. For the wet sliding friction, a formula of type Eq 2.2 should hold. Note that the thickness of the water film and the area of contact are not known. Ambach and Mayr [4] measured the thickness of the water film. We have the impression that the theoretical and empirical results are not consistent. Without doubt, μ depends on the velocity and the loading. As a guess, we modified Eq 2.1 by introducing a velocity dependent part

$$F_f = (\mu + \mu_1 v)N. \tag{2.3}$$

A partial result of the experimental results given later encourages such investigations. Note that a term proportional to v^2 cannot be separated from the air drag, at least for small changes of the load. Moreover, the dependence assumed in Eq 2.3 for the load is doubtful.

2.4 Drag area

The drag force F_d is given by

$$F_d = \frac{1}{2} C_d A \rho v^2, \tag{2.4}$$

where C_d denotes the drag coefficient, A the frontal projected area, ρ the density, and v the relative velocity between air and body. The drag coefficient C_d is usually assumed to be independent of the velocity. Habel [39], the Austrian pioneer in ski friction measurements, strongly stated that the drag coefficient for a skier does not depend on velocity as long as no aerodynamic means such as spoilers are used. Also, in Leino et al. [64] and Leino and Spring [63] a constant drag coefficient was used, but the traversing results given later could not be explained by this hypothesis. For the interpretation of these results we must recall some facts of aerodynamics (see Schlichting [117], Hoerner [49], and Schenau's excellent investigation of speed skating [122]). Especially for low velocities (up to 15 m/s) the drag coefficient depends on the velocity. Already 1972 Gorlin et al. [38] presented plots of the drag coefficients of skiers in different positions for the velocity range from 10 up to 45 m/s. The drag coefficient is roughly halved from its initial value at a velocity of 10 m/s to a “nearlyconstant value for velocities between 15 and 45 m/s.

In fluid dynamics the Reynolds number Re plays an essential role. We ask, under what conditions do geometrically similar bodies produce a similar picture of streamlines. The answer is that at similar points the ratio of the forces must be the same, independent of time. We consider a stationary flow which streams with a velocity u mainly in direction x. If one assumes inertial forces $\rho u \frac{\partial u}{\partial x}$ and friction forces $\eta \frac{\partial^2 u}{\partial y^2}$ only, the ratio of these forces is a dimensionless number which is called the Reynolds number:

$$\frac{\rho u \partial u/\partial x}{\eta \partial^2 u/\partial y^2} = \frac{\rho V^2/L}{\eta V/L^2} = \frac{\rho V L}{\eta} = \frac{V L}{\nu} =: Re \tag{2.5}$$

where V is a characteristic velocity and L a characteristic length. $\nu = \eta/\rho$ is called kinematic viscosity. Thus, the flow around two similar bodies is similar in all situations, for which Reynolds numbers are equal (see e.g. Schlichting [117]). In air, the flows around cylinders with diameters 1 and 2 are similar when the unperturbed velocities are 10 and 5, respectively.

The drag force has two components, the *friction* drag and the *pressure* drag. Friction drag is determined by friction forces in the boundary layer. When friction drag dominates, C_d is inversely proportional to the velocity v (Stokes' law) and F_d is proportional to v. This situation occurs for $Re \leq 1$. When Re increases from $Re = 1$ to $Re = 10^3$, the air behind a body becomes turbulent. The velocity in front of the body is almost zero and increases behind the place where the boundary layer is separated from the surface. This high velocity v leads to a low pressure behind the body. In front of the body the pressure is about $\frac{1}{2}\rho v^2$ higher than behind the body. The pressure drag force is nearly proportional to $\frac{1}{2}A\rho v^2$. The drag coefficient contains the other influences such as shape or nature of the surface (clothing). For regular bodies such as spheres or cylinders (including elliptical cross sections) the dependence of C_d as a function of Re is known. Wind tunnel experiments show that C_d is nearly constant for Reynolds numbers in the range $10^3 < Re < 10^5$. This is due to the fact that the boundary layer separates from the surface at the same location. In the range $10^5 < Re < 10^6$, C_d rapidly decreases to a lower level. Due to turbulence in the boundary layer itself, the place of separation of the boundary layer from the surface shifts to a more downstream position resulting in a smaller wake behind the body. The kinematic viscosity ν of air is given by $\nu = 1.4 \times 10^{-5}\ m^2/s$. If one puts the diameter of the trunk $D = 0.4\ m$ or the thighs $D = 0.2\ m$ as characteristic length, one obtains from a critical Reynolds number 2.8×10^5 critical velocities of $V = 9.8\ m/s$ and $V = 19.6\ m/s$, respectively. Already Gorlin et al. [38] point out that the value of C_d for different positions may be individually strongly different. An optimal position must be choosen for each skier separately. Changes in the position which are in the first view not essential might affect the value of C_d by 10 to 20%. Even during the test, elite skiers were not able to remain completely in an optimal position.

Schenau [122] investigated skaters with a knee angle θ_0 and an angle θ_1 between the trunk and a horizontal line. The air friction constant k_1 at a velocity $v = 12\ m/s$

$$k_1 = \frac{1}{2} C_d A \rho \tag{2.6}$$

depends obviously on θ_0 and θ_1. The value of k_1 at a reference position of $\theta_1 = 15°$ and $\theta_0 = 110°$ is denoted by k_n. Schenau [122] found the relation

$$k_1 = k_n(0.798 + 0.013\theta_1) \times (0.167 + 0.00757\theta_0) \tag{2.7}$$

for values near to the reference position. Although C_d depends strongly on the individual skater, Schenau [122] found the following relationship between k_n, the height l, and the mass m of a skater:

$$k_n = 0.0205\ l^3\ m. \tag{2.8}$$

In Nachbauer and Kaps [99], the drag area of skiers in a tucked position was considered as a function of the mass only. With the help of Eq 2.8, Schenau [122] could predict the drag force of six skaters within a standard deviation of 2%. For the dependence of k_1 on the velocity, Schenau [122] found

$$\frac{k_1(v)}{k_n} = \begin{cases} 4.028 - 0.809 \ln v - 0.189v + 0.00866v^2 & \text{for } 7 < v < 14 \text{ m/s}, \\ 1.561 - 0.0705v + 0.00188v^2 & \text{for } 14 < v < 19 \text{ m/s}. \end{cases} \tag{2.9}$$

The correlations of the first and second expression within the brace are given by $r = 0.99$ and $r = 0.81$, respectively.

Erkkilä et al. [27] measured the drag of a skier with roller-skis. The drag area was found to decrease linearly with velocity increase in the velocity range 5.5 to 10 m/s. The slope was 0.043 for a skier in a semi-squatting position. Spring et al. [119] measured the drag area of cross country skiers gliding on roller-skis. In the velocity range from 5.5 to 10.5 m/s the drag area was nearly constant. For a skier in a racing suit the drag area was 0.65 ± 0.05 m^2 in an upright posture, and 0.27 ± 0.03 m^2 in a semi-squatting posture.

Roberts [113] used a model in which he approximated the trunk, the lower legs and the upper arms as cylinders. Depending on the Reynolds number he used the following values for the drag coefficient:

$$C_d = \begin{cases} 1.2 & \text{for } 6 \times 10^3 < Re < 2 \times 10^5, \\ 1.0 & \text{for } 2 \times 10^5 < Re < 4 \times 10^5, \\ 0.3 & \text{for } Re > 4 \times 10^5. \end{cases} \tag{2.10}$$

2.5 Equations of motion

The equations of motion are formulated as a system of differential-algebraic equations (DAEs):

$$\begin{aligned} \mathbf{M}\ddot{\mathbf{x}} &= \mathbf{F}_a + \mathbf{F}_r \\ \mathbf{g}(\mathbf{x}) &= \mathbf{0}. \end{aligned} \tag{2.11}$$

The first expression is a system of n_x second order differential equations for the n_x unknown components of $\mathbf{x}$. $\mathbf{M}$ denotes the mass matrix, $\mathbf{F}_a$ the applied forces, and $\mathbf{F}_r$ the constraint or reaction forces. $\mathbf{g}(\mathbf{x}) = \mathbf{0}$ is a system of n_g algebraic equations which are called *position* constraint equations. From d'Alembert's principle it follows for the reaction forces

$$\mathbf{F}_r = -\mathbf{G}^T \boldsymbol{\lambda}. \tag{2.12}$$

$\mathbf{G}^T$ denotes the transpose of the Jacobian matrix

$$\mathbf{G} = \frac{\partial \mathbf{g}(\mathbf{x})}{\partial \mathbf{x}} = \mathbf{g}_{\mathbf{x}}. \tag{2.13}$$

The vector $\boldsymbol{\lambda}$ is called the Lagrange multiplier. Its components are additional unknowns. Equation 2.11 represents a system of DAEs with *index* 3 since it is necessary to differentiate Eq 2.11 three times to obtain a system of ordinary differential equations in the variables $(\mathbf{x}, \boldsymbol{\lambda})$. If the position constraints in Eq 2.11 are differentiated with respect to time, one obtains the *velocity* constraints

$$\mathbf{g_x}\dot{\mathbf{x}} = \mathbf{0}. \tag{2.14}$$

Replacement of the position constraints in Eq 2.11 by the velocity constraints yields a system of DAEs of index 2. This can be solved by recently developed codes, for example, MEXX21 (Lubich [68], Lubich et al. [69]). The reaction forces $\mathbf{F}_r$ are computed automatically and need not be provided by the user of such a code.

The skier is modeled as a mass point with coordinates $\mathbf{x} = (x, y)$ or $\mathbf{x} = (x, y, z)$ in the two-dimensional or three-dimensional case, respectively. The dimension n_x of $\mathbf{x}$ is given by 2 or 3, correspondingly. With help of the constraints $\mathbf{g}(\mathbf{x}) = \mathbf{0}$ an arbitrary path can be defined, for example in two dimensions by

$$y = h(x) \tag{2.15}$$

or in three dimensions by

$$z = h(x, y), \quad y = y(x). \tag{2.16}$$

Thus n_g the dimension of $\mathbf{g}$ is given by 1 or 2. If the applied forces $\mathbf{F}_a$ are known, the motion $\mathbf{x}(t)$ of a skier can be computed as a function of time t. We have used an earlier version of the code MEXX21. More detailed information on DAEs is given in Hairer and Wanner [41], and representation of the equations of motion as DAEs in Haug [44]. The applied forces consist of the gravitational force $\mathbf{F}_g$, the drag force $\mathbf{F}_d$ and the friction force $\mathbf{F}_f$

$$\mathbf{F}_a = \mathbf{F}_g + \mathbf{F}_d + \mathbf{F}_f. \tag{2.17}$$

2.5.1 Straight running

The path of the skier is given by Eq 2.15, the slope by

$$\tan\alpha = h'(x) \tag{2.18}$$

(see Fig 2.3). Note in the situation of Fig 2.3, it holds that $\alpha < 0$.

For the unit vectors $\mathbf{t}$ and $\mathbf{n}$ in the tangential and normal directions, respectively, and the reaction force $\mathbf{F}_r$ in Eq 2.11 it holds that

$$\mathbf{t} = \begin{pmatrix}\cos\alpha\\ \sin\alpha\end{pmatrix}, \quad \mathbf{n} = \begin{pmatrix}-\sin\alpha\\ \cos\alpha\end{pmatrix}, \quad \mathbf{F}_r = -\begin{pmatrix}-\tan\alpha\\ 1\end{pmatrix}\lambda = N\,\mathbf{n} \text{ with } N = -\frac{\lambda}{\cos\alpha}. \tag{2.19}$$

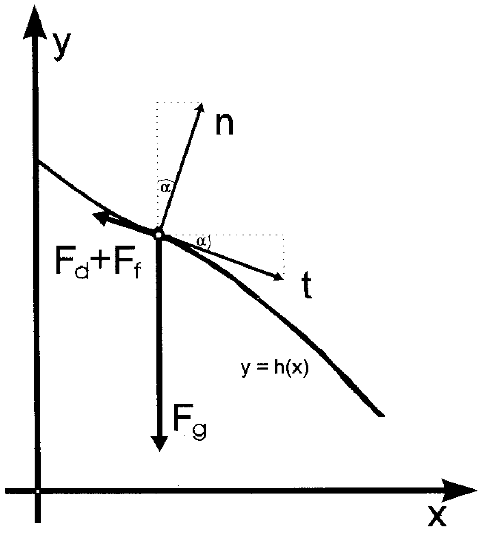

Fig. 2.3: Model of skier.

The normal force N depends on the Lagrange multiplier λ. If one considers the kinetic friction Eq 2.1 and the drag Eq 2.4, one obtains

$$\mathbf{F}_f + \mathbf{F}_d = -(\frac{1}{2}\rho(\dot{x}^2 + \dot{y}^2)C_d A + \mu N)\mathbf{t}. \tag{2.20}$$

The equation of motion is given by:

$$m\begin{pmatrix}\ddot{x}\\ \ddot{y}\end{pmatrix} = \begin{pmatrix}0\\ -mg\end{pmatrix} + \mathbf{F}_f + \mathbf{F}_d + \mathbf{F}_r, \quad y - h(x) = 0. \tag{2.21}$$

The applied force depends on the Lagrange multiplier λ. If λ becomes positive, the skier will be in the air and the constraint equation is no longer valid.

2.5.2 Traversing

For traversing on an inclined plane (Fig 2.2) α and β are constant. By introducing the arc length s as the dependent variable, one obtains for the equation of motion the well known ordinary differential equation (see Kaps et al. [55]):

$$\begin{aligned}\ddot{s} &= a + b\dot{s}^2\\ a &= -g\sin\alpha\cos\beta - \mu g\cos\alpha\\ b &= -\frac{1}{2m}\rho A C_d.\end{aligned} \tag{2.22}$$

The initial conditions are given by

$$s(0) = s_0, \qquad \dot{s}(0) = v_0. \tag{2.23}$$

Usually we choose $s_0 = 0$. We tried to vary the initial velocity v_0 to obtain different mean velocities in the test runs (slow, moderate, fast). To this aim, the skier started from different heights. Therefore, the initial velocity is treated as an unknown parameter. Writing Eq 2.22 as a first order system, the new variables s and $w = \dot{s} - v_0$ are introduced. This yields to

$$\begin{aligned} \dot{s} &= w + v_0 \\ \dot{w} &= -\frac{\rho}{2m} C_d A (w + v_0)^2 - \mu g \cos\alpha - g \sin\alpha \cos\beta \\ s(0) &= 0, \qquad w(0) = 0. \end{aligned} \tag{2.24}$$

The drag area and the coefficient of friction must remain nonnegative. Thus, these expressions are written as squares of the corresponding parameters

$$p_1^2 = C_d A, \qquad p_2^2 = \mu, \qquad \text{and} \qquad p_3 = v_0. \tag{2.25}$$

To obtain a least-squares solution, one needs the derivatives of the components of Eq 2.24 with respect to the parameters. A numerical differentiation is not satisfactory since the numerical code would usually stop before reaching the minimum. With the following abbreviations

$$\begin{aligned} y_1 &= s, & y_3 &= \frac{\partial s}{\partial p_1}, & y_5 &= \frac{\partial s}{\partial p_2}, & y_7 &= \frac{\partial s}{\partial p_3}, \\ y_2 &= w, & y_4 &= \frac{\partial w}{\partial p_1}, & y_6 &= \frac{\partial w}{\partial p_2}, & y_8 &= \frac{\partial w}{\partial p_3} \end{aligned} \tag{2.26}$$

one obtains the so-called *variational equations* (see, e.g., Hairer et al. [40]):

$$\begin{aligned} \dot{y}_1 &= y_2 + p_3 \\ \dot{y}_2 &= -\frac{\rho}{2m}(y_2 + p_3)^2 p_1^2 - g\cos\alpha\, p_2^2 - g\sin\alpha\cos\beta \\ \dot{y}_3 &= y_4 \\ \dot{y}_4 &= -\frac{\rho}{m}(y_2 + p_3) y_4 p_1^2 - \frac{\rho}{m}(y_2 + p_3)^2 p_1 \\ \dot{y}_5 &= y_6 \\ \dot{y}_6 &= -\frac{\rho}{m}(y_2 + p_3) y_6 p_1^2 - 2g\cos\alpha\, p_2 \\ \dot{y}_7 &= y_8 + 1 \\ \dot{y}_8 &= -\frac{\rho}{m}(y_2 + p_3)(y_8 + 1) p_1^2 \end{aligned} \tag{2.27}$$

with the initial values

$$y_i(0) = 0, \qquad i = 1, \ldots, 8. \tag{2.28}$$

This system of ordinary differential equations is integrated numerically.

2.6 Experimental results

2.6.1 Straight running

According to the experimental setup given earlier we have measured the time t_i and the coordinates x_i, y_i when the skier passed the ith photo cell. The solution of the equation of motion (Eq 2.21) depends on the parameter $\mathbf{p} = (\sqrt{C_d A}, \sqrt{\mu}, v_0)$. We have computed the times $t(x_i, \mathbf{p})$ at which the x-component of the solution was equal to x_i. Note that a root finding algorithm is necessary. The parameters were computed by minimizing the sum of error squares

$$\Sigma(\mathbf{p}) = \sum_{i=1}^{9} (t(x_i, \mathbf{p}) - t_i)^2. \tag{2.29}$$

We used the program E04FCF of the NAG library [105]. This program is based on the Gauss-Newton method near to the solution. It computes the derivatives with respect to the parameters numerically. We include an additional computation where the kinetic friction in Eq 2.19 was replaced by Eq 2.3. In Tab 2.1, results of a fast run are presented. In addition to the deviations Σ, the gradient g of Σ is given. At a minimum it holds $g = 0$. $g^T g$ is the square of the Euclidean length of g.

v_0	$C_d A$	μ	μ_1	Σ	$g^T g$
3.4	0.22	$8.5 \cdot 10^{-3}$	0	0.11	0.11
3.1	0.22	$8.1 \cdot 10^{-3}$	$8.3 \cdot 10^{-5}$	0.18	0.47

Tab. 2.1: Results for straight running.

The results show that it has been difficult to obtain the real minimum, since the value of $g^T g$ is relatively high. The computed coefficient of friction was 0.0085, which is below the range obtained by the towing and runout method. By these methods values between 0.01 and 0.25 were obtained. The drag area was 0.22 m^2. This is in agreement with unpublished wind tunnel experiments of the Austrian Ski Federation, in which the drag area of male world class racers was between 0.13 and 0.19 m^2. The results for a velocity dependent kinetic friction gave errors which are only slightly higher.

2.6.2 Traversing

According to the experimental setup of Fig 2.2, we have measured the position of a point at the ski binding s_i at time t_i corresponding to the ith picture. For the computation of the minimum, we used the algorithm E04GDF of the NAG library [105], which needs the derivatives of s and $\dot{s}$ with respect to the parameters. Therefore, we solved the equation of motion (Eq 2.27) in variational form. The

μ	$\Delta\mu$	$v_0(m/s)$	$v_f(m/s)$
0.064	0.060 – 0.067	0.6	10.6
0.128	0.108 – 0.150	11.0	13.4
0.153	0.136 – 0.171	14.7	16.6

Tab. 2.2: Results for traversing: Coefficients of friction (μ) with 90% confidence intervals ($\Delta\mu$), initial (v_0) and final velocities (v_f).

parameters $\mathbf{p}$ were computed by minimizing the sum of error squares

$$\Sigma(\mathbf{p}) = \sum_{i=1}^{m}(s(t_i, \mathbf{p}) - s_i)^2. \tag{2.30}$$

In Tab 2.2 the traversing results for different velocities are summarized. The computed coefficients of friction were between 0.06 and 0.15. Note that the normal force N in the equation of motion was given by $N = mg\cos\alpha$. We ignored the fact that the skier is actually gliding on a small band which is cut out of the inclined plane. The values of the friction coefficients are relatively high compared with those of straight running. A reason might be that compression, ploughing, and shearing forces contribute to a larger μ. The increase of μ with increasing velocity is not necessarily a velocity effect, as the snow conditions varied considerably throughout the measurements due to increasing solar radiation. The increase in the length of the confidence interval $\Delta\mu$ for increasing velocities is not caused by a decreasing number of data points for low, medium, and high velocity, as one might expect. We used in all cases approximately 100 data points. For low velocities, only every third picture was used. For the drag area the value 0 was obtained. The confidence interval was infinitely large.

In the earlier „drag area“section, arguments (Gorlin et al. [38], Schenau [122], Roberts [113]) were given that the drag area depends on the velocity in the investigated range of velocities. This leads us to the assumption that the model (Eq 2.4) is not correct for traversing. Note that during straight running the skier used a tucked position, whereas during traversing he used an upright position. We have also performed an experiment in which the skier was loaded in order to investigate the dependence of the kinetic friction on the load. The mass of the skier was 88 kg, the load 69 kg. One obtained $\mu = 0.049$ and $C_dA = 0.89$. The 90% confidence intervals were $\Delta\mu = [0.049, 0.053]$ and $\Delta(C_dA) = [0.61, 1.12]$, and the velocities were $v_0 = 0.37\ m/s$ and $v_f = 10.5\ m/s$. Thus the drag area could be computed within a still acceptable interval of confidence. An explanation could be that in the case of a skier loaded with a lead vest and a knapsack, the critical Reynolds number was reached at a lower velocity.

2.7 Conclusion

In this study a new method to determine the coefficient of kinetic friction μ and the drag area C_dA was presented. For straight running μ and C_dA were computed simultaneously for a track with variable inclination. The results correspond well with literature values. To our knowledge, we have performed the first measurements for traversing. We could determine the kinetic friction. Values of 0.06 to 0.15 appear to be high compared with those for straight running. However, due to increasing solar radiation the snow became wet and soft - a situation in which the friction is usually high. The drag area could not be determined. This failure is probably due to inappropriate model assumptions. The skier traversed in an upright position at speeds from 0 to 17 m/s. In this velocity range the drag area is probably not constant as it was assumed in the calculations.

The method requires the collection of position/time data of the skier. Two measurement techniques were tested: timing and cinematography. In the first case, accurate time (± 0.1 ms) and position data (± 1 cm) of nine photocells were obtained at a long test run of about 340 m. In the second case the time data are assumed to be exact and the position data have an error of ± 10 cm. This relatively large error is mainly caused mainly by two facts: first, the test course was not ideally planar; and second, the track of the skier was approximated by a straight line. This task could not be performed by the skier exactly. The results indicate that both methods are adequate for collecting the required data. However, the analysis of the cinematographical data is much more complicated and time consuming.

For more detailed investigations regarding the dependence of the drag area on velocity and the dependence of kinetic friction on velocity or loading, one has to improve the measurement setup. This was accomplished on the runout at the Olympic ski jumping site in Seefeld, where 20 photocells were built up and geodetically surveyed. Time data of straight runs of a skier were collected but have not yet been analyzed. At the same time, video measurements were taken which will allow to compare the two data collection methods.

Acknowledgment

This study was supported in part by a grant of the Austrian Research Foundation and the Austrian Ski Federation.

3 W. Nachbauer, P. Kaps, B.M. Nigg, F. Brunner, A. Lutz, G. Obkircher, and M. Mössner, A Video Technique for Obtaining 3-D Coordinates in Alpine Skiing, Journal of Applied Biomechanics, 1996

Reference: W. Nachbauer[1], P. Kaps[2], B.M. Nigg[3], F. Brunner[4], A. Lutz[5], G. Obkircher[6], and M. Mössner[7], *A Video Technique for Obtaining 3-D Coordinates in Alpine Skiing*, Journal of Applied Biomechanics **12** (1996), 104–115.

Abstract: A video technique to obtain 3-D data in Alpine skiing competition was investigated. The flight and landing phases of a jump were recorded during the 1994 Olympic combined downhill race. A direct linear transformation (DLT) implementation was applied, which computes the DLT parameters for each video image of each camera separately. As a consequence, one is able to pan and tilt the cameras and zoom the lenses. The problem of distributing control points in the large object space could be solved satisfactorily. The method proved to be suitable for obtaining 3-D data with reasonable accuracy, which is even sufficient for inverse dynamics. The computed resultant knee joint forces and moments compare well with results reported by other authors.

[1]Dept. of Sport Science, Univ. Innsbruck, AT. email: Werner.Nachbauer@uibk.ac.at
[2]Inst. for Basic Sciences in Engineering, Univ. Innsbruck, AT
[3]Human Performance Laboratory, Univ. Calgary, CA
[4]Dept. of Sport Science, Univ. Innsbruck, AT
[5]Dept. of Sport Science, Univ. Innsbruck, AT
[6]Dept. of Sport Science, Univ. Innsbruck, AT
[7]Dept. of Sport Science, Univ. Innsbruck, AT

3.1 Introduction

Film analysis of Alpine ski racing has been used for different purposes, such as performance enhancement (Fetz [30], Nachbauer [98], Förg-Rob and Nachbauer [32], Müller, Brunner, Kornexl, and Raschner [96]), safety improvement (Herzog and Read [47], Read and Herzog [111]), and studying the friction between ski and snow (Erkkilä, Hämäläinen, Pihkala, Savolainen, and Spring [27], Kaps, Nachbauer, and Mössner [59], Leino and Spring [63]). In recent years, there has been considerable progress in video technology, which is now used as an alternative to cinematography. Comparisons of film and video techniques have indicated that within a small field of view (4 m), video and film analyses provide the same accuracy (Kennedy, Wright, and Smith [60]). Angulo and Dapena [6] reported that with a large field of view (8 m), the accuracy of video analysis is inferior to that of film analysis. However, video analysis is precise enough for most practical purposes. A video technique has been proposed for conducting field research in Alpine skiing (Schaff and Hauser [114]). Fixed cameras are used, a technique that restrains the analysis to a few meters or parts of a turn.

Restricted object space due to the use of fixed cameras concerns various kinds of sport. Three-dimensional (3-D) reconstruction techniques allowing rotations of the cameras in order to follow the athlete's motion have been developed. Dapena [20] used two cameras that were free to rotate about the vertical axes. Drenk [26] and Yeadon [128] reported methods with pan and tilt cameras. Mössner, Kaps, and Nachbauer [85] introduced a direct linear transformation (DLT) method that allows the operator to pan and tilt the cameras and zoom the lenses.

The purpose of this study was to apply a video technique with pan and tilt cameras and zoom lenses in an Alpine skiing competitive environment and to test the technique's suitability for obtaining accurate 3-D data. The video technique proved to be suitable. Thus, numerous questions raised by coaches and athletes can be investigated in controlled settings as well as in competitions. The comparison of kinematic variables of skiers at different performance levels may lead to performance improvement. Kinematic analysis combined with inverse dynamics may provide insight into injury mechanisms and may bring about methods to prevent injuries. In high-speed downhill racing, anterior cruciate ligament (ACL) injuries occur frequently, predominatly during the landing phase following a jump (Figueras, Escalas, Vidal, Morgenstern, Bulo, Merino, and Espadaler-Gamisans [31]). In the present paper the method to obtain kinematic data of the jumping movement is investigated. Additionally, resultant knee joint forces and moments of one skier are presented.

3.2 Methods

3.2.1 Collection of Video Data

Video data were collected on the Russi jump during the men's special and combined downhill event of the 1994 Olympic Winter Games in Lillehammer, February 13 and 14. The flight and landing phases of all competitors, as well as the recovery phase back into the aerodynamic downhill position, were recorded. The jump, named after the former Swiss downhill racer Bernhard Russi, was located in the upper part of the downhill course at an altitude of about 800 m. The jump was caused by a natural terrain edge. Approaching the edge, the racers skied on the flat slope maintaining the tucked downhill position at a speed of more than 100 km/h. Shortly before takeoff the racers raised the low body position somewhat in order to rotate their bodies forward, thus maintaining the body orientation during flight and landing phases. The slope inclination of the landing area was about 27°. Pre-jumping was rarely used. The racers jumped between 30 to 50 m at speeds around 100 km/h.

The recording system consisted of two monochrome CCD-cameras (510 x 240 lines) and two high-speed modified Panasonic AG-1970 videocassette recorders (320 x 240 lines). The system operated on a VHS-NTSC technique basis (Motion Analysis Corporation, Santa Rosa, US-CA). The cameras were equipped with 12- to 120-mm (Angenieux, Paris, FR) and 12.5- to 75-mm (Schneider, Kreuznach, DE) zoom lenses. The lenses were zoomed in the range of 25 to 40 mm. Camera shutters were set to 1/2000 s and the f-stops between 5.6 and 11. The recordings were made on Sony S-VHS tapes. A control unit provided camera synchronization and consecutive numbering of the recorded video images. The noninterlaced video system operated at the maximum sampling frequency of 180 Hz. A power source of 110 V AC, 50-60 Hz was required.

The skiers required a distance of about 40 m for landing and recovery. In order to calibrate the large object space, 108 control points were distributed on both sides of the course (Fig 3.1) ensuring that in each video image 6 to 10 control points were visible. After considering safety guidelines, the jury of the competition gave us permission to establish the control point system. Two different kinds of control points were used. Black painted tennis balls (diameter = 65 mm) were attached to 250 x 200 mm white plastic plates and were screwed on poles of different lengths. The poles were placed slightly shifted along the course boundary at about 2-m intervals. In order to identify the control points in the video images, every 5th control point was a yellow tennis ball on a black plate. Additionally, on both sides close to the line of the skiers, black 100 x 200 mm carpet stripes were drilled into the snow facing the cameras. Sketches of the control points are shown in Fig 3.1.

Before and after the competitions, the positions of the centers of the tennis balls and the carpet stripes were determined using an SET4CII theodolite (Sokkia, JP) with a CP01 miniprism (Sokkia, JP). The tripod of the theodolite was mounted on three wooden poles that were fixed in the frozen ground. Metal fittings on the

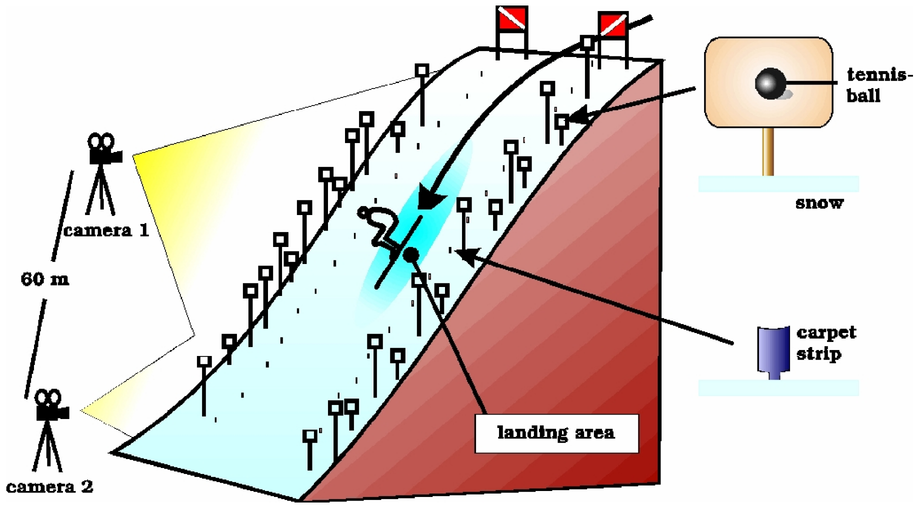

Fig. 3.1: Schematic illustration of the measurement site including the control points: tennis ball and carpet stripe.

wooden poles ensured the stability of the tripod. Surveying the control points took about 1.5 h. The measurements were stored on a memory card and then transferred to a notebook computer for further calculations.

In Fig 3.1 the camera positions are shown schematically. The cameras were panned and tilted and the lenses zoomed in order to follow the skier's motion. Camera 1 covered a field of view of approximately 8 by 6 m with an image depth of 15 m and camera 2 covered a field of view of approximately 7 by 11 m with an image depth of 30 m. The cameras were positioned to ensure angles between their optical axes between 30 and 150°. The camera operators practiced recording the competitors during the training runs.

3.2.2 Processing of Video Data

The videotapes were digitized using a NTSC Panasonic AG-7350 videocassette recorder and an IBM 486-compatible personal computer equipped with a 16 grey level NTSC frame grabber and a 15-in SVGA monitor. The computer was operated with the manual digitizing software of Motion Analysis Corporation (Santa Rosa, US-CA). In each video image, 8 to 10 control points, 2 points on each ski, and 19 anatomical landmarks representing the endpoints of 13 segments were digitized manually. Fig 3.2 shows a typical picture with the digitized points.

Our own DLT implementation was used to calculate 3-D coordinates from the digitized points (Mössner, Kaps, and Nachbauer [85]). First, the DLT parameters were computed for each video image of each camera separately and, subsequently, the 3-D coordinates of the landmarks were computed for each pair of synchronized video images. This enables the user to rotate the cameras and zoom the lenses. The method requires at least 6 control points visible in each video image. With

Fig. 3.2: Photograph of a video image used for digitizing.

a minimum of 6 control points, any 3 of them must not be colinear and any 4 not coplanar. For each camera, a different set of control points can be used. The main error in reconstruction arises from inaccuracies in the digitized data. The digitized data occur both in the matrix and in the right-hand side of the linear equations for calibration and reconstruction. The method of total least squares was applied (van Huffel and Vandewalle [121]). It considers errors in the matrix and the right-hand side of a system of linear equations, whereas the method of least squares would assume only errors in the right-hand side of the equations. Proper scaling of the data was essential to yield sufficiently accurate results. An orthogonal coordinate system with its origin in the average location of the control points was defined for each video image. The image coordinates were scaled in the interval of -1 to 1. The error propagation caused by solving the systems of linear equations was considerably reduced by this scaling. If the linear equations become close to singular, the scaling is absolutely necessary.

The object coordinates were presented in an orthogonal reference system with the z-axis vertical and the x- and y-axes horizontal. The traveling direction of the skier was in the x-z plane. The displacement time data were smoothed with the routine `csaps` of the MATLAB Spline Toolbox (The MathWorks Inc., Natwick, US-MA). The smoothing parameter was set to $p = 0.999$. $p = 0$ corresponds to a straight line fit and $p = 1$ to a natural cubic spline interpolant. After smoothing, the first and last 20 data points were excluded to avoid poor approximation near the interval ends. MATLAB does not provide smoothing quintic splines.

3.2.3 Evaluation of Measurement Errors

Errors in geodetic surveying, in reconstruction of a fixed landmark, and due to digitizing were investigated. The error was defined as absolute value of the difference between the measured value and the „true“ value. The „true“ value was the most accurate value available, for example, the arithmetic mean of two measurements in geodetic surveying or the geodetically obtained coordinate in the reconstruction of a fixed landmark. Objectivity and reliability of digitizing were examined. To determine objectivity two persons digitized the same data set. To determine reliability, the same person digitized the same data set twice. 3-D coordinates were calculated and compared with the arithmetic mean of the two digitizations, which was taken as true value. The effect of repeated digitizing was studied. The same data set was digitized three times, 3-D coordinates were calculated, averaged, and smoothed. Velocities and accelerations were computed from the smoothed average. Coordinates, velocities, and accelerations from the smoothed average were taken as true values and compared with the smoothed coordinates, velocities, and accelerations of a further digitization of the same data set. Mean errors denote the arithmetic mean of the errors taken over the values indicated in the context.

3.2.4 Calculation of Resultant Knee Joint Forces and Moments

Resultant knee joint forces and moments were calculated with a two-dimensional inverse dynamics approach in the sagittal plane. The skier with equipment was modeled as a linked system composed of 13 rigid segments: head, upper trunk, lower trunk and pairs of pole/hand/forearm, upper arm, thigh, shank/upper boot, and foot/lower boot/binding/ski (Fig 3.3). The inertial parameters of the human body segments were determined based on the geometric model of Hanavan [42] and the code of Preiss [108]. The dimensions of the geometric segments were approximated by taking 32 anthropometric measurements from the skier presented in the study. The inertial parameters of the equipment were calculated based on mass and shape measurements. Air resistance and snow friction were neglected. The influence of air resistance on knee joint resultants during the landing movement was found to be small (Read and Herzog [111]).

A one-legged landing was studied to avoid complications due to the closed loop formed by both legs in contact with the ground. The corresponding segment pairs were combined for this purpose. We used Cartesian generalized coordinates $y = (\ldots, x_i, z_i, \varphi_i, \ldots)$, where x_i, z_i denote the center of mass of segment i and φ_i denotes the orientation of this segment with respect to the vertical axis. The segments were connected by hinge joints. For a joint between the proximal end of a segment i and the distal end of a segment j, there are two kinematic constraints of the type

$$x_i + c_i \sin\varphi_i = x_j - d_j \sin\varphi_j,$$
$$z_i + c_i \cos\varphi_i = z_j - d_j \cos\varphi_j,$$

where c_i, d_j denote the distances between the joints and the centers of mass. As driving constraints the angular orientations of the segments and the coordinates of the right foot were used. The constraints can be written as an algebraic system $g(y,t) = 0$ of the same dimension as y. Thus, the equations of motion are a system

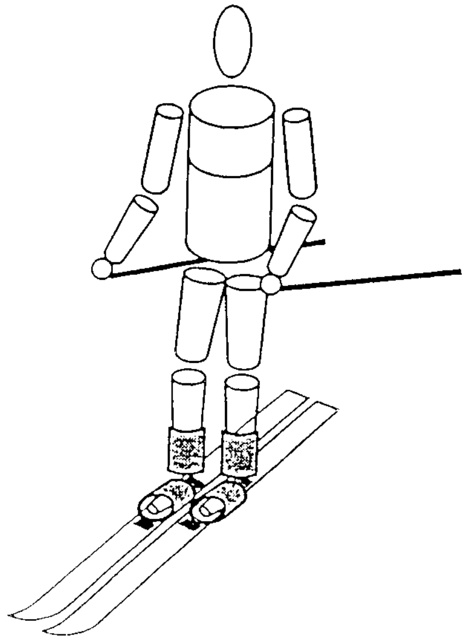

Fig. 3.3: Skier model with equipment.

of differential-algebraic equations:

$$M\ddot{y} = f_a + f_c, \qquad g(y,t) = 0.$$

The mass matrix $M = Diag(\ldots, m_i, m_i, I_i, \ldots)$ is diagonal, $f_a = (\ldots, 0, -m_i g, 0, \ldots)$ denotes the generalized applied forces, and f_c the generalized constraint forces. The resulting knee loads were calculated by inserting the accelerations $\ddot{y}$ obtained from the analytically differentiated smoothing splines. The computations were performed using MATLAB.

The knee joint resultants acting on the proximal end of the shank segment, that is, loads exerted by the thigh on the shank, were calculated. The resultants were expressed in a shank embedded reference frame. The y'-axis was defined by the longitudinal axis of the shank (line connecting the digitized endpoints of the shank); positive was directed proximally. The x'-axis was perpendicular to the y'-axis with positive in the anterior direction.

3.3 Results

3.3.1 Accuracy of the Measurements

The mean errors of the geodetic surveying of the 78 control points used were 0.4, 0.8, and 0.4 cm in x-, y-, and z-directions. The large errors in y-direction were mainly found at the carpet stripes. The technical accuracy of the theodolite was

Number of control points	mean error [m] x	y	z
6	0.135	0.158	0.116
7	0.075	0.108	0.070
8	0.061	0.083	0.054
9	0.059	0.079	0.050
10	0.063	0.058	0.038

Tab. 3.1: Mean errors in the 3-D reconstruction of a fixed landmark in 10 subsequent video frames.

5 mm + 3 mm x distance in km for distances and 1.5 mgon for angles. Thus, for an object in a distance of 0.1 km one obtains an error of $5 + 3 \cdot 0.1 = 5.3$ mm in the distance and a perpendicular deviation of $100 \cdot 0.0015 \cdot \pi/200 = 2.36$ mm.

In the reconstruction of a fixed landmark the mean errors over 10 frames were 6.3, 5.8, and 3.8 cm in the x-, y-, and z-coordinates when 10 control points were used for calibration. These errors are relatively high. The investigated landmark was located close to the edge of the jump, and in this area the angle between the optical axes of the cameras was small. Moreover, since the theodolite was positioned at the bottom of the jump, the distance to these control points was the largest resulting in the largest surveying error.

The reconstruction error was strongly affected by the number of control points used for the calibration (Tab 3.1). With the minimal number of 6 control points, the reconstruction error was up by a factor of 2.5. In 95 % of the images, 10 control points were used to calculate the DLT parameters. The main error in the calibration was due to the digitization of the control points. The effect of this error was averaged by using more control points than necessary. Another reason for the observed increase of accuracy with a higher number of control points may be that some of the control points were nearly colinear or coplanar. The carpet stripes were placed on the surface of the slope. Therefore, the stripes visible in a video image were approximately in the tangential plane to the surface and consequently nearly coplanar. The carpet stripes were placed in two lines on each side of the course as near as possible to the line of the skiers. Thus, three or more control points were often nearly colinear. For safety reasons, the poles with the tennis balls had to be located near the closing off the course. Although the poles differed in the height, the distance to the closing fence did not vary much. Thus, the tennis balls were also nearly coplanar. Using 6 control points with inappropriate locations for calibration could yield reconstruction errors considerably greater than 1 m. Reconstruction error is further affected by the position of the investigated landmark with respect to the calibration volume. Reconstructing landmarks about 5 m outside of the calibration volume enlarged the reconstruction error by a factor of approximately 10. No attempt was made to improve the DLT parameters by smoothing.

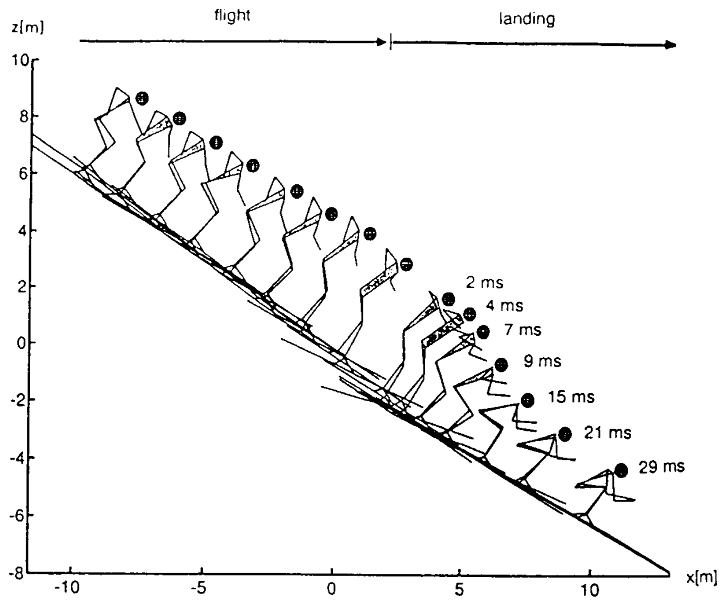

Fig. 3.4: Stick figure diagrams of the movement analyzed.

For objectivity, the mean errors averaged over 70 frames and 23 landmarks were 2.4, 2.3, and 1.6 cm in the x-, y-, and z-coordinates. The reliability was about 20 % better with mean errors of 1.9, 1.9, and 1.3 cm in the x-, y-, and z-coordinates. The largest errors occurred at the ski tails, which showed little contrast to the surrounding snow, and in the body landmarks of the left body side, which were frequently covered by the right body side.

Comparing the smoothed single digitization with the smoothed average of the three digitizations yielded mean errors averaged over 70 frames and 23 landmarks of 3.3, 2.4, and 2.0 cm in the x-, y-, and z-coordinates. The mean errors in the velocities were 0.20, 0.19, and 0.15 m/s and in the accelerations 3.18, 3.37, and 2.10 m/s^2 in x-, y-, and z-directions.

3.3.2 Resultant Knee Joint Forces and Moments

The resultant knee joint loading of one skier performing a good landing is presented next. Fig 3.4 shows stick figures of the analyzed skier during the last part of the flight and landing. In the landing phase a time scale is provided that corresponds to the time axis of Fig 3.5, in which the knee joint resultants are presented. The skier touched the ground with the left ski tail first (t = 2 ms), at t = 4 ms both skis had snow contact from the tail to the middle part, and at t = 7 ms the whole skis were on the snow (Fig 3.4). In this time range, the loading results might be erroneous since the coordinates of the right foot were used as a driving condition, which is not valid when the skier is in the air.

Fig 3.5 shows the components of the resultant knee joint force and the resultant

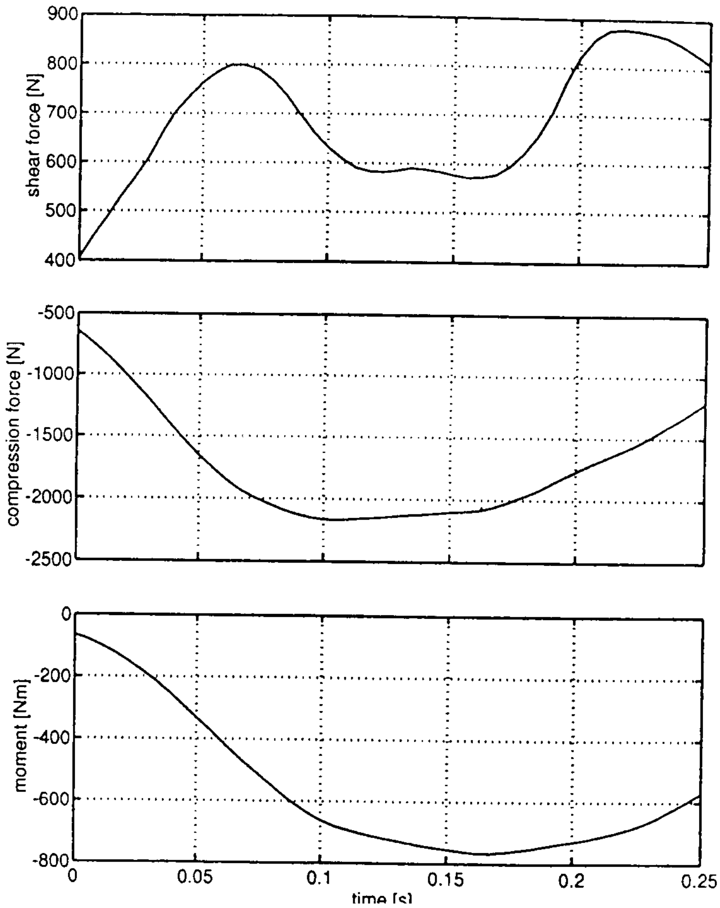

Fig. 3.5: a) Shear component of the resultant knee joint force acting perpendicular to the longitudinal axis of the shank. Positive forces are directed anteriorly. b) Compression component of the resultant knee joint force acting along the longitudinal axis of the shank. Negative forces are directed downward. c) Resultant knee joint moment. Extensor moments are negative and flexor moments positive.

knee joint moment as a function of time for the one-legged landing. The component acting perpendicular to the longitudinal axis of the shank was always positive varying between 400 and 880 N. This force tends to translate the shank posteriorly with respect to the thigh. The component acting along the longitudinal axis of the shank was always compressive with an extreme of -2200 N. The resulting knee joint moment was always an extensor moment with an extreme of -790 Nm.

These values compare well with results presented by other authors. Read and Herzog [111] obtained loading at the knee joint of two skiers during a World Cup Downhill race by means of inverse dynamics. Assuming a one-legged landing for the skier who executed the landing with difficulties, force extremes of 800 N in anterior and -2300 N in downward direction were calculated. Additionally, Read and Herzog consistently observed an anterior shear force and an extensor moment for the skier

Study	Shear force [N] Anterior	Posterior	Compression force [N]	Extensor moment [Nm]
Force measurements:				
Maxwell and Hull (1989)[1]	660		-625	-200
Quinn and Mote (1993)	1298	-242	-1778	-303
Inverse dynamics:				
Read and Herzog (1992)	800	-280	-2300	-630
Present study	880		-2200	-790

[1] Only averaged forces during turn were reported.

Tab. 3.2: Extremes of the resultant knee joint forces and moments during skiing.

who executed the landing well, which is also in agreement with our calculations. In two studies, loading at the knee joint was predicted during normal skiing (snowplow, parallel turn, Stem Cristiana turn). Maxwell and Hull [72] calculated forces and moments at the knee joints from force and moment measurements at the base of the boot neglecting inertial forces and ankle joint flexion movement. Quinn and Mote [110] improved the prediction by considering dorsiflexion at the ankle joint. The maximum of the anterior shear force was 1298 N, of the compression force -1778 N, and of the extensor moment -303 Nm (Tab 3.2).

3.4 Discussion

A DLT method to obtain 3-D data was applied in the environment of Alpine ski racing. Two main problems had to be solved before the data could be collected:

- In order to capture the skier's body as large as possible on the video image, we had to follow the skier's motion with the cameras. A DLT implementation was developed that allows the operator to pan and tilt the cameras and zoom the lenses.
- In order to calibrate the large object space where the movement took part, points with known location had to be distributed on the slope. The 108 control points used had to satisfy the geodetic requirements. A more demanding requirement was that they not disturb the athletes or cause any injury risk. Carpet stripes and poles with tennis balls were chosen as control points (Fig 3.1).

Errors in 3-D reconstruction are caused by errors in calibration and in the image coordinates of the landmarks. Errors in calibration are determined by the accuracy of object and image coordinates of the control points. The main reason for errors in the object coordinates of the control points used here was difficulty with identification of the centers of the control points. The centers were not marked and had to be estimated during positioning of the prism. Limitations in the technical accuracy of the theodolite and small displacements of the control points (e.g. caused by accidentally side slipping over carpet stripes during course inspection and preparation) were other error sources. Apparently moved control points were detected by resurveying. Errors in the image coordinates of the control points are discussed below. Their effect on the calibration was reduced by using 8 to 10 control points. By this and the geodetic surveying of the control points, the calibration errors could be kept so small that their influence on 3-D reconstruction was less important than the influence of errors in the image coordinates of the landmarks.

Errors in image coordinates of control points and landmarks are caused by technical limitations of the video system and by manual digitizing. Resolution of the video system was restricted by the high-speed cassette recorder, which operates in the VHS mode (320 x 240 lines). The video images covered a field of view of approximately 8 by 6 m. In the best case, each line of the video image covered a real-life distance of 800 cm / 320 = 2.5 cm in horizontal and 600 cm / 240 = 1.9 cm in vertical direction. Furthermore, the control points were often located at the margin of the images, where inaccuracies caused by lens distortion and jittering of the image were large. Control points as well as body landmarks had to be digitized manually. Digitizing body landmarks was difficult: Segment endpoints were not defined exactly, and the use of contrast markers was not possible in the competition. The landmarks on the left body side were often covered by other body parts. This was partly due to terrain restrictions regarding the camera setup. For an improvement the use of more than two cameras would be necessary. The digitizing error of body landmarks was estimated by objectivity and reliability. The mean error was smaller than 2.5 cm in each coordinate, which is surprisingly accurate.

It is interesting that the relative error in the 3-D reconstruction was in the range of laboratory measurements. Dividing a typical reconstruction error (0.03 m) by a typical length of the calibration volume (15 m) yields a relative error of 0.2 %. In laboratory measurements 0.05 to 0.5 % can be achieved. Their best accuracy can only be obtained by fixed cameras and fixed focal lengths and by averaging control point data and digitized image data.

As discussed previously, the raw data are erroneous. For various investigations the computation of accelerations and forces is of interest. By interpolation we obtained irregularly oscillating accelerations in the order of magnitude of 10^4 m/s^2. Therefore, smoothing was a necessity. As well known, there are a variety of different smoothing techniques, all of which provide better results with a higher number of data points. The sampling rate of 180 Hz provided enough data points for smoothing. The mean absolute difference between raw and smoothed data was less than 3 cm (in x- and z-directions) for the chosen smoothing parameter. Since this difference is small, there was no oversmoothing. One could suspect undersmoothing, but this would lead to strong oscillations in accelerations, which was not the case.

Our objective in measuring phases of the Russi jump was to improve understanding of ACL injury mechanisms occurring during landing in downhill skiing.

Further analyses will include determining of knee joint resultants of several racers performing the landing movement differently and estimating of the forces in the ACL. Being aware of the limitations of the inverse dynamics approach, we developed a simulation model (Gerritsen, Nachbauer, and Bogert [33]). The video data were used as initial values for the simulations and for validation of the model. The validated simulation model will be used to study the influence of isolated variables by varying them systematically.

Acknowledgments

The study was supported by the IOC Medical Commission, the International Ski Federation, and the Austrian Ski Federation. We are grateful to Thomas Weinold for instructions in geodetic surveying and Thomas Fetz for performing the MATLAB computations.

4 M. Mössner, W. Nachbauer, and K. Schindelwig, Einfluss der Skitaillierung auf Schwungradius und Belastung (Influence of the Ski's Sidecut on the Turning Radius and Strain), Sportverletzung Sportschaden, 1997

Reference: M. Mössner[1], W. Nachbauer[2], and K. Schindelwig[3] *Einfluss der Skitaillierung auf Schwungradius und Belastung (Influence of the Ski's Sidecut on the Turning Radius and Strain)*, Sportverletzung Sportschaden **11** (1997), 140–145.

Zusammenfassung: Um den Einfluss der Skitaillierung auf den Schwungradius zu untersuchen, wird im ersten Teil dieser Arbeit der Radius der Spur eines selbstfahrenden Schlittens ermittelt und mit der Vorhersage nach Howe verglichen. Es zeigt sich, dass die Schwungradien zu Beginn des Schwunges zwischen 65 und 85 % des theoretisch erwarteten Wertes betragen. Im zweiten Teil wird der Verlauf des Schwungradius eines Carverfahrers bestimmt und daraus, mittels Geschwindigkeitsmessung, die angreifenden Kräfte berechnet. Es ergibt sich eine starke Reduktion des Schwungradius, welche zu einer deutlichen Erhöhung der Belastung führt. Modellrechnungen zeigen den großen Einfluss von Skitaillierung und Geschwindigkeit auf die Belastung. Schon kleine Geschwindigkeitsänderungen führten bei Carverski zu großen Belastungsänderungen.

Abstract: The first part of this paper deals with the influence of the side cut on the turn radius, which was examined by measuring the turn radius of a self-running sledge-like construction and by comparing it to Howe's prediction. The turn radius at the beginning of the turn has proved to be between 65 and 85 % of the theoretically expected result. In the second part a carver's turn radius was determined and the reaction force acting on the skier was calculated. The result shows a strong reduction of the turn radius along the path which increases the load on the skier. The effect of side cut and velocity on the load was examined. Using carver skis even small changes in velocity resulted in considerable load changes.

[1]Dept. of Sport Science, Univ. Innsbruck, AT. email: Martin.Moessner@uibk.ac.at
[2]Dept. of Sport Science, Univ. Innsbruck, AT
[3]Dept. of Sport Science, Univ. Innsbruck, AT

4.1 Problemstellung

Die Taillierungsradien herkömmlicher Ski lagen viele Jahre zwischen ca. 40 und 80 m. Carverski weisen mit ca. 15 bis 25 m deutlich geringere Radien auf. Die veränderte Seitengeometrie erlaubt geschnittene Schwünge mit kleinen Schwungradien wie sie früher nicht gefahren werden konnten.

Howe [50] formulierte einen Zusammenhang zwischen Skitaillierung, Kantwinkel und Schwungradius. Einflussgrößen wie Skisteifigkeit und Schneebeschaffenheit werden dabei vernachlässigt. In der ersten Zielsetzung der Arbeit wurde deshalb die Anwendbarkeit der Formel von Howe zur Vorhersage des Schwungradius aus der Skitaillierung geprüft. Um Aktivitäten des Skifahrers auszuschließen, wurde ein selbstfahrender Schlitten gebaut und die Fahrspur des Schlittens geodätisch vermessen.

Die Verkleinerung des Schwungradius bedingt eine Erhöhung der auf den Skifahrer wirkenden Kräfte. Die zweite Zielsetzung beinhaltete die Bestimmung der Belastung beim Carven anhand eines Fallbeispiels. Dazu wurden aus Spur- und Geschwindigkeitsmessung die auf den Skifahrer wirkenden Kräfte bestimmt und anhand von Modellrechnungen der Einfluss der Skitaillierung und der Fahrgeschwindigkeit auf die Kräfte abgeschätzt.

4.2 Theoretische Grundlagen

4.2.1 Kräfte beim Schwung

In den durchgeführten Berechnungen wirken auf den Skifahrer nur Schwer- und Zentripetalkraft. Reibungskräfte, Luft- und Schneewiderstand, sowie vom Skifahrer erzeugte Kräfte werden vernachlässigt. Ferner sind die Ski zu einem Monoski zusammengefasst. In diesem Fall übt der Skifahrer auf den Schnee die laterale Kraft

$$L = \frac{mv^2}{r} - mg \sin\alpha \cos\beta \tag{4.1}$$

und die Normalkraft

$$N = mg \cos\alpha \tag{4.2}$$

aus. Zusammen ergibt sich die Reaktionskraft des Ski auf den Schnee

$$R = \sqrt{L^2 + N^2}. \tag{4.3}$$

m ist die Masse des Skifahrers mit Ausrüstung, v die Geschwindigkeit, ϑ der Kantwinkel und r der Schwungradius des Skifahrers. g steht für die Erdbeschleunigung, α für die Hangneigung und β für den Winkel zwischen Hangwaagrechten und Tangente an die Fahrspur. Bei einem Schwung aus der Hangwaagrechten in diese zurück steigt β von 0 auf 180° an.

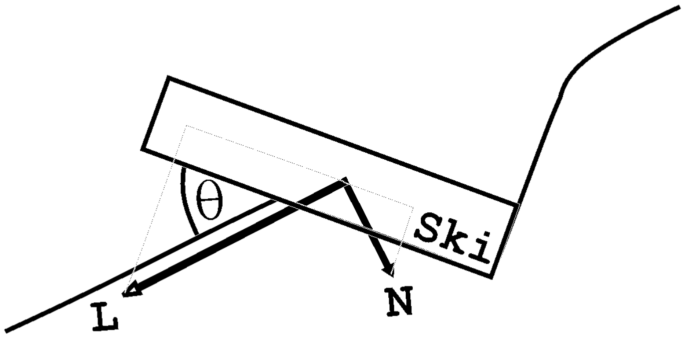

Fig. 4.1: Kräfte des Ski auf den Schnee

Aufgrund der Normalkraft gräbt sich der Ski in den Schnee und bildet einen Schneekeil (Fig 4.1). Solange der Ski nicht seitlich aus der Spur geschoben wird und die Schneefestigkeit die laterale Kraft kompensieren kann, bewegt sich der Skifahrer entlang dieses Schneekeils.

Seitliches Rutschen tritt auf, wenn $L \cos\vartheta > N \sin\vartheta$ ist. Einsetzen von L und N ergibt:

$$\frac{v^2}{gr\cos\alpha} - \tan\alpha\cos\beta > \tan\vartheta. \tag{4.4}$$

Abscheren von Schnee wurde von Lieu und Mote [65] untersucht. Sie bestimmten eine empirische Formel für die Festigkeit von Eis. Bei einer Eindringtiefe von d [m] und einem Kantwinkel von ϑ [°] kann Eis Belastungen bis zu

$$F = \left(\frac{16120}{\sin^{3.7}\vartheta} - 15510\right)(39.37d)^{0.7-0.37\vartheta} \tag{4.5}$$

[N/m] aufnehmen. Die Autoren geben für Schnee einen Korrekturfaktor von 0.02 an.

4.2.2 Schwungradius geschnittener Schwünge

In diesem Abschnitt folgen wir den Überlegungen von Howe [50]. Der aufgekantete Ski wird unter Belastung durchgebogen bis der Schneewiderstand den angreifenden Kräften entspricht. Die Projektion der verformten Skikante auf den Hang ergibt in erster Näherung ein Kreissegment. Man spricht von einem geschnittenen Schwung, wenn sich der Ski entlang dieses Kreises weiterbewegt. Bei solchen Schwüngen verliert der Skifahrer keine Energie durch seitliches Rutschen und/oder Abscheren.

Die Projektion der Durchbiegung zwischen Schaufel und Skimitte auf den Hang b ergibt sich aus der Taillierung T und der Eindringtiefe d (Fig 4.2 a). Als Taillierung T wird die maximale Einbuchtung des Ski entlang der Seite bezeichnet. Aus den drei Breitenmessungen an Schaufel S, Skimitte M und Skiende H berechnet sich

$$T = \frac{S + H - 2M}{4}. \tag{4.6}$$

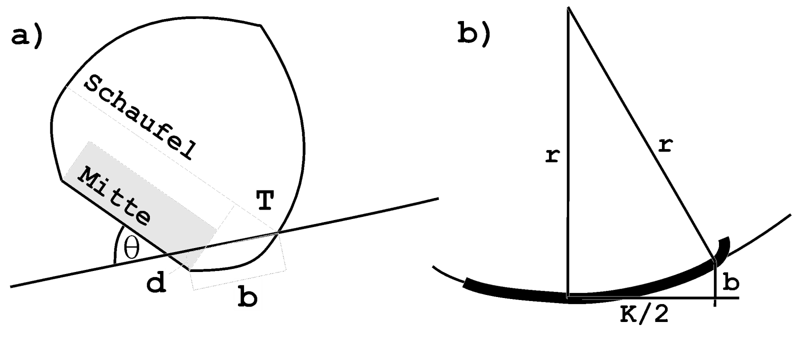

Fig. 4.2: a) Ski von vorne. b) Skispur des schneidenden Ski von oben.

Aus Fig 4.2 a entnimmt man die Beziehung

$$b = \frac{T}{\cos\vartheta} + d\tan\vartheta. \tag{4.7}$$

Wenn unterschiedliche Eindringtiefen von Schaufel d_S, Skimitte d_M und Skiende d_H berücksichtigt werden, ist

$$d = \frac{2d_M - d_S - d_H}{2} \tag{4.8}$$

zu setzen.

In Fig 4.2 b ist eine Aufsicht des Hanges dargestellt. r bezeichnet den Radius des geschnittenen Schwunges. Die Skispitze weist von der Tangente an die Skimitte einen Normalabstand von b auf. Ist K die Länge der Kontaktfläche zwischen Ski und Schnee, so gilt $r = \frac{K^2+4b^2}{8b}$. Unter Vernachlässigung von b^2 ergibt sich mit Eq 4.7

$$r = \frac{K^2\cos\vartheta}{8(T + d\sin\vartheta)}. \tag{4.9}$$

Im Grenzfall verschwindend kleiner Eindringtiefe vereinfacht sich die Beziehung weiter zu

$$r_H = r_S\cos\vartheta \qquad \text{mit} \qquad r_S = \frac{K^2}{8T}. \tag{4.10}$$

Der Skiradius r_S ist eine Approximation an den Krümmungsradius der Taillierungskurve. r_H steht für den Schwungradius nach Howe.

4.2.3 Veränderung des Schwungradius geschnittener Schwünge

Beim geschnittenen Schwung sind Kantwinkel ϑ und Schwungradius r durch $r = r_S\cos\vartheta$ verknüpft. Die Innenlage des Skifahrers φ ergibt sich aus $\tan\varphi = \frac{N}{L}$. Innenlage und Kantwinkel sind nicht unabhängig voneinander: $\varphi = \frac{\pi}{2} - \vartheta + \gamma$, wobei

γ die Differenz zwischen Innenlage des Skifahrers und Innenlage des Unterschenkels ist. Dieser Winkel kann nur in einem schmalen Bereich variiert werden. Ist $\gamma < 0$, so beginnt der Skifahrer wegen Eq 4.4 seitlich zu rutschen. Bei beliebiger Vorgabe von γ erhalten wir eine nichtlineare Gleichung zwischen Schwungradius r, Geschwindigkeit v und gefahrenem Kreissegment β:

$$\frac{v^2}{gr} - \sin\alpha\cos\beta = \tan\left(\operatorname{acos}\left(\frac{r}{r_S}\right) - \gamma\right)\cos\alpha. \tag{4.11}$$

Im einfachsten Fall γ gleich 0 reduziert sich (4.11) zu:

$$r^2(\cos^2\alpha + \sin^2\alpha\cos^2\beta) - 2r\frac{v^2}{g}\sin\alpha\cos\beta + \frac{v^4}{g^2} - r_S^2\cos^2\alpha = 0. \tag{4.12}$$

Der Schwungradius verkleinert sich entlang der Spur (β ansteigend). Die Reduzierung des Radius ist umso größer, je größer die Geschwindigkeit und je kleiner der Skiradius ist. Durch die Abnahme des Schwungradius steigt die laterale Kraft. Im Laufe des Schwunges kann es passieren, dass Eq 4.4 erfüllt wird und der Ski seitlich zu rutschen beginnt. Ebenso kann durch das Ansteigen der lateralen Kraft die Festigkeit des Schnees überschritten werden. In diesen Fällen ist ein geschnittener Schwung nicht mehr möglich.

4.3 Methode

4.3.1 Messung mit Skischlitten

Zur Bestimmung des Schwungradius wurde ein selbstfahrender Schlitten (Fig 4.3) gebaut. Dieser besteht aus einem Gestell von Stahlschienen und Rohren, welche gelenkig miteinander verbunden sind. An der Unterseite des Schlittens wurden die Ski so montiert, dass mit Kantwinkeln und Gewichtsverlagerungen experimentiert werden kann.

In dieser Arbeit werden ausgewählte Messungen von Sölden im Ötztal, Hochfügen im Zillertal und St. Christoph am Arlberg präsentiert. Die Hänge waren nahezu eben mit Neigungen von 8°, 11° und 13°. Als Kantwinkel wurde bei allen Fahrten 18° gewählt. Der Schlitten wurde durch Gewichtsscheiben soweit belastet, dass das Gesamtgewicht dem einer erwachsenen Person entsprach. Nach jeder Fahrt wurden 6 bis 40 Punkte der Spur des Außenski geodätisch vermessen. Begleitende Daten wie Skimodell, Kantwinkel, Schneehärte etc. wurden registriert. Die Messungen wurden unter Mitwirkung von Jenner im Rahmen ihrer Diplomarbeit durchgeführt [51].

4.3.2 Messung eines Skifahrers mit Carverski

Neben den Schlittenmessungen wurde auch eine Fahrt mit einem Carving-erfahrenen Skilehrer durchgeführt und geodätisch vermessen. Die Messung fand in Sölden im

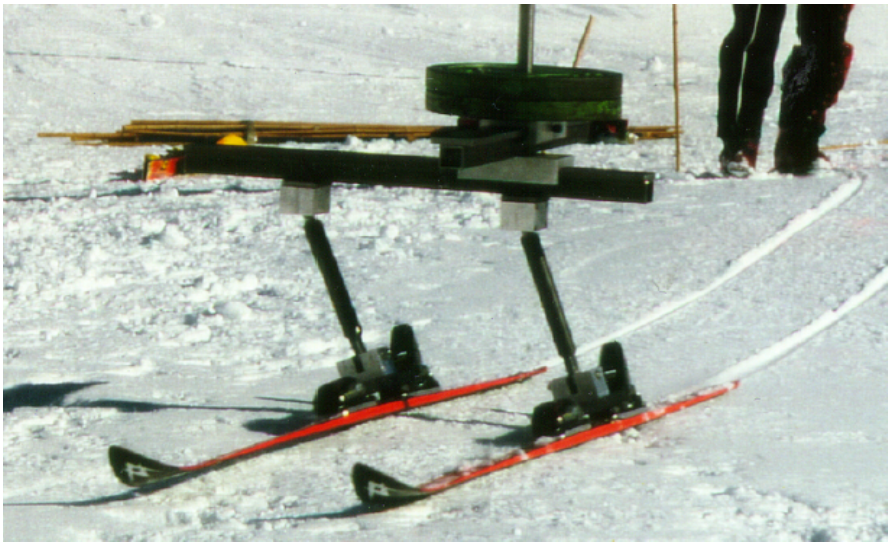

Fig. 4.3: Skischlitten

Ötztal auf einem ebenen Hang mit einer Neigung von 16° statt. Die Masse des Skifahrers samt Ausrüstung betrug 92 kg. Zur Bestimmung der Geschwindigkeit in der Endphase des Schwunges wurden zwei Lichtschranken in einem Abstand von 7.5 m aufgebaut.

4.3.3 Verwendete Skier

Die geometrischen Merkmale der verwendeten Ski sind in Tab 4.1 zusammengefasst.

Ski	S [mm]	M [mm]	H [mm]	K [m]	L [m]	T [mm]	r_S [m]
V	89	63	78	1.80	1.95	10	39.5
B	109	61	96	1.77	1.93	21	18.9
A	91	61	78	1.84	2.03	12	36.0
H	109	61	97	1.60	1.80	21	15.2

Tab. 4.1: Geometrische Merkmale der verwendeten Ski. Völkl RS P20 (V), Blizzard Carver (B), Atomic RS Arc (A) und Head Cyber Space (H). Breite von Schaufel S, Skimitte M und Skiende H, Kontaktlänge K, Skilänge L, Taillierung T, Skiradius r_S.

4.3.4 Auswertung

Zum Ausgleich von Unebenheiten des Hanges wurden die geodätischen Messdaten auf die Ausgleichsebene projiziert. Dies führte zu ebenen Datenpunkten (x_i, y_i), $i = 1, 2, \ldots$

Als mittleren Radius verwendeten wir den Radius des Ausgleichskreises [109]. Der Kreis ist durch Angabe des Mittelpunktes (u, v) und des Radius r eindeutig bestimmt. Als Maß für die Abweichung der Messdaten vom Kreis berechneten wir die Residuen

$$\epsilon_i = (x_i - u)^2 + (y_i - v)^2 - r^2. \tag{4.13}$$

u, v und r wurden so bestimmt, dass die quadratische Summe der Residuen minimal wird:

$$f(u, v, r) = \sum \epsilon_i^2 \longmapsto \min\,. \tag{4.14}$$

Das Verfahren ist ab drei Messpunkten anwendbar. Zum Ausgleich von Messfehlern wurden jedoch bis zu 40 Datenpunkte verwendet.

Zur Bestimmung der Veränderung des Schwungradius entlang der Spur wurden glättende Splines $x(s)$ und $y(s)$ durch die Datenpunkte gelegt. Die Krümmung im Kurvenpunkt $(x(s), y(s))$ ist gegeben durch [25]:

$$\kappa(s) = \frac{\dot{x}(s)\ddot{y}(s) - \ddot{x}(s)\dot{y}(s)}{(\dot{x}(s)^2 + \dot{y}(s)^2)^{\frac{3}{2}}}. \tag{4.15}$$

Der Schwungradius ist der Kehrwert des Betrages der Krümmung

$$r(s) = \frac{1}{|\kappa(s)|}. \tag{4.16}$$

4.4 Ergebnisse

4.4.1 Skischlitten

In Tab 4.2 sind die theoretisch erwarteten Schwungradien (Radius nach Howe r_H) und die mittleren Schwungradien aus den Schlittenmessungen (Radius des Ausgleichskreises r_A) gegenübergestellt. Es sind jeweils Mittelwerte aus ein paar Fahrten angegeben. Nach Gleichung Eq 4.9 sollten die gemessenen Werte etwas kleiner als die berechneten sein. Dies trifft für die Messungen V und B zu, nicht jedoch für A und H. Aufgrund des konstanten Kantwinkels bei den Schlittenversuchen müsste nach der Theorie auch der Schwungradius einen konstanten Wert aufweisen. Die Residuen der Ausgleichskreise zeigen systematische Fehler, was auf die Veränderung des Schwungradius hindeutet. Die Ergebnisse der Krümmungsberechnung entlang der Spur zeigen 1) dass die Schwungradien entweder konstant sind oder zunehmen und 2) dass die Schwungradien zu Beginn des Schwunges zwischen 64 und 86 % des theoretisch erwarteten Wertes betragen.

Versuch	r_H [m]	r_A [m]	n	σ [m]
V	37.6	35.0	10	2.3
B	17.9	15.7	1	
A	34.2	41.8	4	3.6
H	14.5	19.5	6	1.0

Tab. 4.2: Gegenüberstellung der theoretischen r_H zu den mittleren gemessenen Schwungradien r_A der Ski Völkl (V), Blizzard (B), Atomic (A) und Head (H). Anzahl der Datenpunkte n, Streuung der Messwerte σ.

4.4.2 Skifahrer mit Carverski

In Fig 4.4 ist der gemessene und berechnete Schwungradius entlang der Spur für den Skifahrer mit dem Carverski dargestellt. Der gemessene Krümmungsradius verkürzt sich von 14 auf 6 m. Der berechnete Verlauf nach Eq 4.12 stimmt qualitativ mit der Messung überein.

Zur Berechnung der Reaktionskraft R (Eq 4.3) wird neben dem Schwungradius auch die Fahrgeschwindigkeit benötigt. Aus der Lichtschrankenmessung und der Bogenlänge der Spur zwischen den Lichtschranken ergibt sich eine Geschwindigkeit von 11.2 m/s für den letzten Teil des Schwunges. Basierend auf Luft- und Gleitreibungsangaben [59] schätzen wir eine Geschwindigkeitszunahme im Laufe des Schwunges von 9 auf 11 m/s. Die Reaktionskraft für den gemessenen Schwungradius steigt von 1000 auf 2500 N an (Fig 4.5). Aufgrund des kleineren berechneten Schwungradius liegen die theoretischen Kraftwerte etwas über den Werten für den gemessenen Schwungradius.

Am Ende des Schwunges ($\beta = 180°$) beträgt $v = 11$ m/s und $r = 6$ m. Daraus ergibt sich eine Innenlage φ von 23° und ein Kantwinkel ϑ von 67° für den Monoskifahrer. Ein geschnittener Schwung ist bei diesen Bedingungen nicht mehr möglich, laut Eq 4.4 beginnt der Ski seitlich zu rutschen und laut Eq 4.5 wird Schnee abgeschert.

4.5 Diskussion

4.5.1 Vergleich gemessener und berechneter Schwungradien

Der Vergleich gemessener und berechneter Schwungradien wurde anhand der Schlittenversuche und eines Carverschwunges durchgeführt. Bei den Schlittenversuchen wurde der Kantwinkel mit 18° konstant vorgegeben. Nach der Formel von Howe sollte der Schlitten eine kreisförmige Spur beschreiben, was nur teilweise der Fall war. Bei mehreren Fahrten wurde ein deutliches Anwachsen des Schwungradius beobachtet. Dieses Anwachsen führen wir auf seitliches Rutschen aufgrund des kleinen Kantwinkels von 18° zurück. Deshalb wurden zur Überprüfung der Formel von Ho-

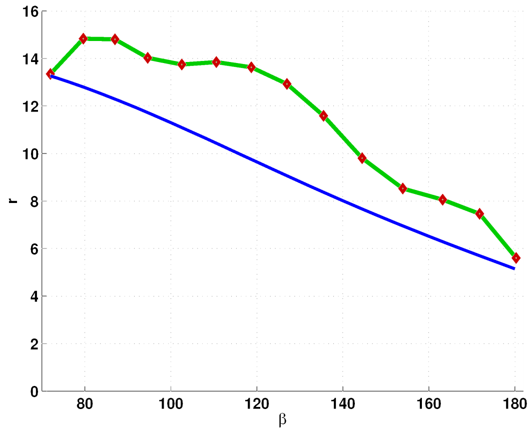

Fig. 4.4: Schwungradius des Skifahrers entlang der Spur von Messung (–*–) und Berechnung (—-).

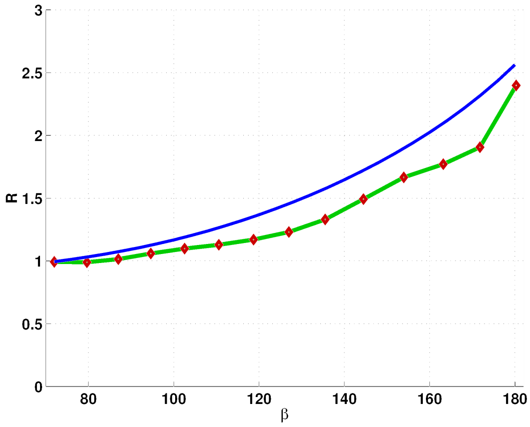

Fig. 4.5: Reaktionskraft des Skifahrers auf den Schnee für Messung (–*–) und Berechnung (—-).

we nur die Anfangswerte der Schwungradien verwendet. Diese betragen zwischen 65 und 85 % der theoretischen Werte. Für die Fahrten mit konstantem Schwungradius treffen dieselben Prozentangaben zu.

Die kleineren gemessenen Radien lassen sich durch das Eindringen des Ski in den Schnee, welches in der Formel von Howe nicht berücksichtigt ist, erklären. Bei einer Eindringtiefe von 10 mm reduziert sich für einen Carver mit 10 mm Taillierung der Schwungradius um 23 % und liegt damit im Bereich der gemessenen Werte. Das Eindringen des Ski hängt neben der Skigeometrie von Schneebeschaffenheit sowie Biege- und Torsionssteifigkeit des Ski ab [112]. In der Formel von Howe wird das Eindringen des Ski in den Schnee überhaupt nicht berücksichtigt. Dennoch ergibt sich eine qualitativ richtige Vorhersage des Schwungradius. Dies spiegelt den großen Einfluss von Skiradius und Kantwinkel auf den Schwungradius wider.

Im Gegensatz zu den Schlittenfahrten ergibt sich beim Carverschwung eine deutliche Reduktion des Schwungradius entlang der Spur. Die Verkleinerung wird durch die Zunahme der lateralen Kraft verursacht. Um diese Kraft auszugleichen, muss sich der Skifahrer immer stärker nach innen legen. Als Folge wird der Ski stärker aufgekantet und der Schwungradius verkleinert. Dieser Vorgang wird durch Gleichung Eq 4.12 beschrieben. Die Lösung dieser Gleichung ergibt eine qualitativ gute Übereinstimmung der gemessenen und berechneten Schwungradien für den Carver-

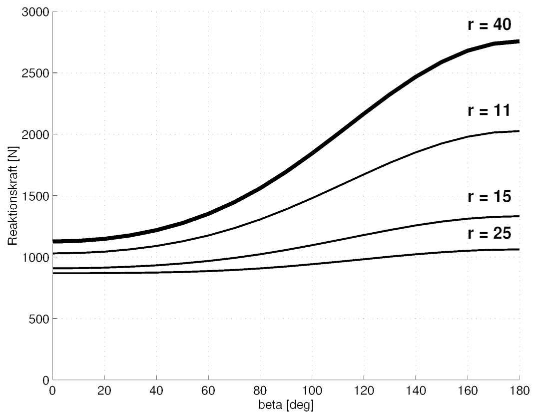

Fig. 4.6: Reaktionskraft auf den Skifahrer. Es werden Carverschwünge mit 9 m/s und Skiradien von 11, 15 und 25 m und ein Super-G Schwung mit 18 m/s und 40 m Skiradius verglichen.

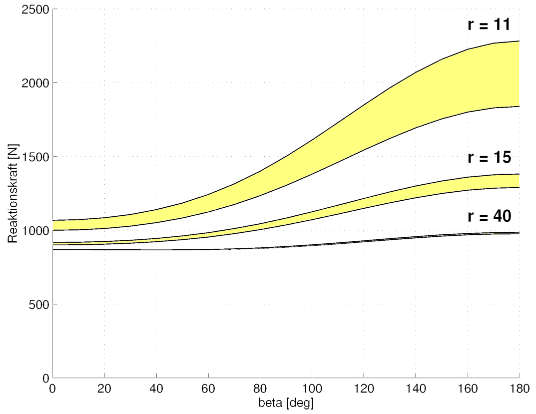

Fig. 4.7: Reaktionskraft auf den Skifahrer mit Skiradien von 11, 15 und 40 m für Geschwindigkeiten im Bereich von 9 ± 0.2 m/s.

schwung.

4.5.2 Belastung des Skifahrers

Anhand eines Fallbeispieles wurde gezeigt, dass beim Carverschwung große Belastungen auftreten können. Verursacht werden diese Belastungen durch 1) den kleinen Schwungradius aufgrund der großen Taillierung und 2) die starke Reduktion des Schwungradius im Laufe des Schwunges.

Die qualitativ gute Übereinstimmung von gemessenen und berechneten Radien beim Carverschwung erlaubt die Verwendung von Eq 4.12 zur Vorhersage des Schwungradius. Aus dem Schwungradius- und Geschwindigkeitsverlauf ergibt sich die Reaktionskraft.

Fig 4.6 zeigt die Reaktionskraft für Skiradien von 11, 15 und 25 m und einer Geschwindigkeit von 9 m/s. Zum Vergleich wird auch die Reaktionskraft für einen Super-G Schwung mit einem Skiradius von 40 m und einer Geschwindigkeit von 18 m/s dargestellt. Die Reaktionskraft steigt mit abnehmender Taillierung nichtlinear an. Wechselt man von einem Ski mit 25 m Radius zu einem Ski mit 15 m Radius, so steigt die Reaktionskraft am Ende des Schwunges lediglich um 330 N an. Eine weitere Skiradiusverkürzung von 15 auf 11 m erhöht die Reaktionskraft um 630 N. Bei der geringen Geschwindigkeit von 9 m/s bleibt die Reaktionskraft deutlich unter der eines Super-G Schwunges. Bei der geringfügig größeren Geschwindigkeit von 9.5 m/s wird diese jedoch bereits überschritten, was die große Bedeutung der Geschwindigkeit auf die Reaktionskraft zeigt.

In Fig 4.7 ist der Einfluss einer geringfügigen Geschwindigkeitsänderung auf die Reaktionskraft dargestellt. Gezeigt wird die Reaktionskraft für Skiradien von 11, 15 und 40 m bei Geschwindigkeiten von 9±0.2 m/s. Sowohl die absolute Größe als auch die Variation der Reaktionskraft ist bei den Skiradien von 15 und 40 m unbedenklich. Dies trifft jedoch nicht auf für den Ski mit 11 m Radius zu. Der absolute Wert steigt auf etwa 2000 N und hat eine Schwankungsbreite von 440 N. Schon eine sehr kleine Änderung der Geschwindigkeit führt zu einer deutlichen Änderung der Reaktionskraft.

Zusammenfassend kann gesagt werden, dass bei Carverski eine starke Reduktion des Radius entlang der Spur auftritt und damit, in Abhängigkeit von der Fahrgeschwindigkeit, hohe Belastungen entstehen können. Bei stark taillierten Ski wirken sich geringe Änderungen der Geschwindigkeit stärker auf den Schwungradius und damit auf die Belastung aus als bei herkömmlichen Ski.

Dank

Wir danken F. Brunner für die Mithilfe bei der Ausführung der Messungen. Die Messung mit dem Skifahrer wurde von der Skibindungsfirma Tyrolia finanziert.

5 P. Kaps, M. Mössner, W. Nachbauer, and R. Stenberg, Pressure Distribution Under a Ski During Carved Turns, Science and Skiing, 2001

Reference: P. Kaps[1], M. Mössner[2], and W. Nachbauer[3], R. Stenberg[4] *Pressure Distribution Under a Ski During Carved Turns*, Science and Skiing (Hamburg, DE) (E. Müller, H. Schwameder, C. Raschner, S. Lindiger, and E. Kornexl, eds.), Verlag Dr. Kovac, 2001, pp. 180–202.

[1]Inst. for Basic Sciences in Engineering, Univ. Innsbruck, AT. email: Peter.Kaps@uibk.ac.at
[2]Dept. of Sport Science, Univ. Innsbruck, AT
[3]Dept. of Sport Science, Univ. Innsbruck, AT
[4]Dept. of Mathematics, Univ. Tampere, FI

5.1 Introduction

For a dynamic analysis of skiing turns (see for example [15, 48, 103, 112] the interaction between ski and snow plays an essential role. In the present paper we study this interaction in a static case, which is fundamental for carved turns. For a detailed discussion of carved turns see Howe [50] or Lind and Sanders [66]. Assume that a skier performs a carved turn with a certain instantaneous turn radius and a given velocity. These two quantities determine the centrifugal force, which acts on the skier. We neglect body-generated forces like weighting or unweighting, leg and trunk actions, poling or skating. Then, the resultant force acting on the skier is given by the vector sum of the centrifugal force and the gravitational force. To maintain equilibrium the skier tilts toward the center of the turn. He has to take such a position that the resultant force acting on his center of gravity is directed to the region between the skis, usually to the loaded edge of the outer ski. Thus, the resulting force is approximately normal to the running surface of the ski. Further, torques about the longitudinal axis of the ski (edging torque), the transversal axis (forward or backward leaning) and the vertical axis act on the skier. Forces and torques can be transmitted from the skier to the ski in the boot-binding region only. The snow has to sustain the forces that the ski exerts onto the snow. We assume compacted snow and a linear relation between compaction pressure and penetration. However, when the compaction pressure exceeds a certain limiting value, the yield pressure, the snow starts yielding. The aim of this study is the computation of the pressure distribution under the loaded ski during purely carved turns. In an ongoing study, the yield pressure is measured for different snow conditions. With this information one can determine whether in a certain situation the pressure under the ski exceeds the yield pressure. Then, skidding will occur and a purely carved turn is not possible for the given loading of the ski.

In our study the ski is modeled as an elastic beam on a snow foundation. In the boot region it is loaded by a force normal to the running surface and by an edging (or longitudinal) and a transversal torque. The investigation is static. The loading is applied from a carved turn. To compute the centrifugal force one has to know the turn radius. The turn radius depends both on the loading and the edging angle of the ski. In our model, the skier can only edge the ski without angulation, because the ski can be loaded by a force normal to the running surface of the ski only. Then, the edging angle depends on the ratio of the normal to the lateral force. The centrifugal force gives the main contribution to the lateral force. Consequently, one has to compute the loading iteratively. From the differential equation of beam deflection and torsion the contact area between ski and snow and the penetration depth is computed. The pressure distribution under the ski is computed with help of the constitutional law of snow. We recall Howe's theory for carved turns since it provides an analytic solution for the turn radius, which can be used as initial value for the computation of the loading. Further, the penetration of the ski into snow can be calculated in a rather good approximation when the contact length and the penetration depth are known. We start with our notation for the ski geometry.

Ski geometry. In the top view (Fig 5.1) a ski has the width $2w(x)$. The waist is the region of the ski with the smallest width. Shovel and tail are the regions at tip and end with the largest width. We denote these widths with W, S, and T, respectively. The side cut is characterized by the parameter D

$$D = \frac{T + S - 2W}{4}. \tag{5.1}$$

The contact length L of the ski is the distance between shovel and tail. In the side view (Fig 5.2), the ski has a variable thickness $d(x)$ and a camber $c(x)$.

Ski radius. In the top view (Fig 5.3) the edge of a ski is the arc of a circle. The radius of this circle, the so-called ski radius or side cut radius R, can be computed by elementary geometry. Assume that the ski is pressed onto a plane surface. In a coordinate system with origin at that point of the edge, where the waist is situated, the equation of this circle is given by $x^2 + (y - R)^2 = R^2$. We assume for simplicity that there is no taper, i.e. $S = T$, and that the waist is exactly in the middle between tail and shovel. Inserting the point $(\pm L/2, D)$ in the front or rear part of the edge into this equation yields to $L^2/4 + D^2 - 2DR + R^2 = R^2$. Neglecting the very small term D^2 one obtains for the ski radius

$$R = \frac{L^2}{8D}. \tag{5.2}$$

The forces between ski and snow [12, 65] as well as the turn radius [50] depend both on the edging angle and the penetration depth. Thus, a skier can vary the turn radius and the forces between ski and snow by edging. Angulation and other body movements like weighting and unweighting, bending or extending the knees, or actions of the upper body influence the resultant force the skier exerts on a ski. Variations of the resultant force change its component normal to the snow surface and consequently the penetration depth of the ski. Thus, forces generated by angulation or extending the knees might further increase the penetration depth of the ski into snow and prevent skidding in limiting situations.

Howe's theory for carved turns. During skiing turns the ski follows a certain trajectory. The arcs of the turns are not circular in general. In carved turns, the ski should be bent in such a way, that the edge of the ski is circular and that the radius of this circle coincides with the radius of curvature of the trajectory. This radius is called instantaneous turn radius. We repeat some fundamental results of Howe [50] on the turn radius. An edged ski is put on a rigid and plane surface. In Fig 5.4, the situation is given schematically in the front view. First, the edge has contact with the surface at two points of tail and shovel due to the side cut. Afterwards, the ski is loaded until it is bent such that the waist has contact with the surface. Surprisingly, then the whole edge between shovel and tail has contact with the surface, too. The line of contact is the arc of an ellipse and can be represented by a circle with turn radius r in a very good approximation. To compute this radius,

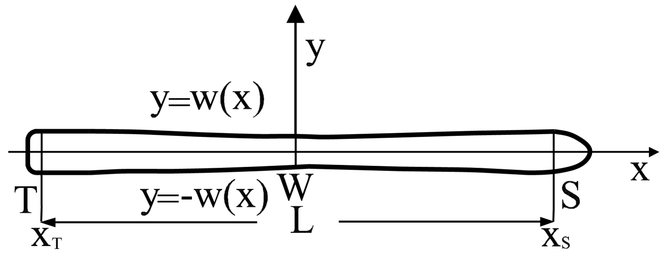

Fig. 5.1: Top view of a ski.

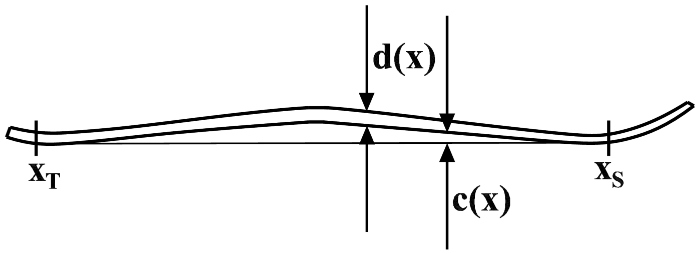

Fig. 5.2: Side view of a ski.

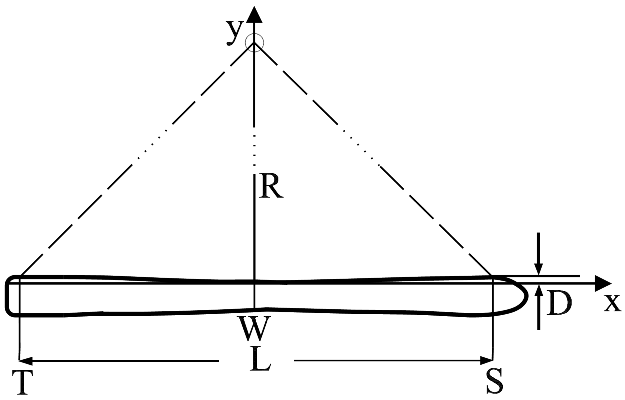

Fig. 5.3: Ski radius.

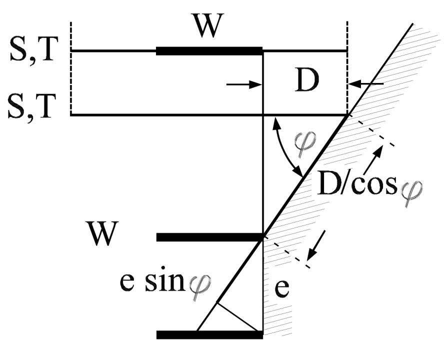

Fig. 5.4: Turn radius.

one has to replace the side cut D in Eq 5.2 by $D/\cos\varphi$, where φ denotes the edging angle (Fig 5.4). One obtains for the turn radius on hard snow (more exactly on a rigid plane surface)

$$r = \frac{L^2}{8(D/\cos\varphi)} = R\cos\varphi. \tag{5.3}$$

If the surface is not rigid, like in the case of snow, the ski penetrates a distance $e(x, y)$ into the snow. This distance is measured normal to the running surface of the ski and not normal to the snow surface. It depends on the position (x, y) at the ski. The ski edge penetrates at the waist further into the snow than at the shovel and tail. We call the difference of these penetration depths the penetration depth e of the ski (Fig 5.4). It depends on the characteristics of the snow, the ski, and the loading. Thus, one has to add the projection $e\sin\varphi$ to the term $D/\cos\varphi$. This yields the turn radius on soft snow (more exactly on a nonrigid plane surface)

$$r = \frac{L^2}{8(D/\cos\varphi + e\sin\varphi)} = \frac{R\cos\varphi}{1 + (e/D)\sin\varphi\cos\varphi}. \tag{5.4}$$

The penetration depth e has to be known in this formula.

Computation of the turn radius. For a dynamic analysis of skiing turns one has to compute the penetration depth. We perform a static computation with the loads from a dynamic case. We determine the contact area between ski and snow and the penetration depth for all points on the contact area. Then, we project the position of the penetrated edge onto the snow surface as above. The resulting curve is a circle in a good approximation. The radius of this circle is called turn radius. It depends both on ski and snow properties. Among the ski properties we mention geometric properties like length L and side cut D as well as elastic properties like flexural stiffness EI and torsional stiffness GJ. The snow properties are determined by the constitutional law of snow Eq 5.6. If the pressure under the ski exceeds the limiting pressure for yielding, skidding might occur. The yield pressure has to be determined experimentally.

5.2 Method

The penetration depth of the ski into the snow is computed from the deflection and torsion of a ski on a snow foundation under a loading in the boot region. To this aim, the equations of beam deflection and beam torsion are used. Several steps are needed to establish these equations.

Ski model. The ski is modeled as an elastic beam with varying width and thickness. The beam is composed of several layers consisting of different materials with varying cross sections. We assume that each material is homogeneous and isotropic. It is well known that e.g. for wood Young's modulus of elasticity E is not isotropic. However, the influence of this anisotropy is small since the materials in

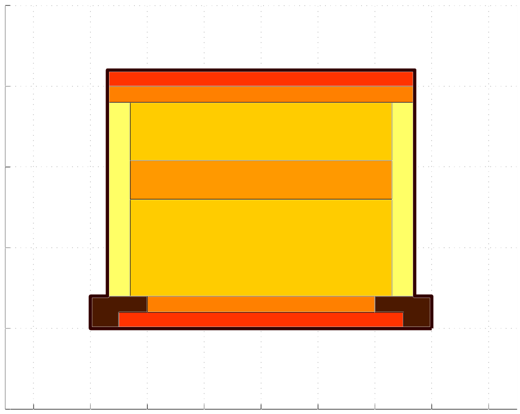

Fig. 5.5: Construction of a ski.

the top and bottom layer are considerable stiffer than the wood in the core. We use a coordinate system (Fig 5.1) with the x-axis along the ski axis, the y-axis in transversal direction and the z-axis normal to the running surface of the ski in upward direction. The ski extends from x_T at the tail to x_S at the shovel. The origin is at the mounting point of the binding, which is the midpoint between the front and the rear part of the binding. To compute the deflection $h(x)$ and the torsion $\varphi(x)$ of the beam one needs the elastic properties of the ski: the flexural stiffness EI and the torsional stiffness GJ. To obtain these quantities we have two options. We can compute both EI and GJ from the construction of the ski (Fig 5.5) when the geometric dimensions, the mass density ρ and the elastic properties, i.e. Young's modulus E and the shear modulus G of the components are known. Then, for each cross section $A(x)$ both E and G are given functions of y and z. In a first step, we calculate the neutral axis z_0 of the beam. The neutral axis is that position in the cross section of the beam where the stress field changes from tension to compression. As shown in textbooks [107, 118] the neutral axis is given as the center of the Young's moduli of elasticity

$$z_0(x) = \frac{\int_{A(x)} E(y,z) z \, dy \, dz}{\int_{A(x)} E(y,z) \, dy \, dz}, \qquad EI(x) = \int_{A(x)} E(y,z)(z - z_0(x))^2 \, dy \, dz,$$

$$GJ(x) = 2 \int_{A(x)} G(x,y) \left(y \frac{\partial \Phi}{\partial y} + (z - z_0(x)) \frac{\partial \Phi}{\partial z} \right) dy \, dz.$$

Next, the flexural stiffness EI is obtained by averaging over all materials with respect to the neutral line. For the torsional stiffness GJ one has to compute the torsion function Φ, which is a solution of the Poisson equation ($\Delta\Phi = 1$ with $\Phi|_{\partial A(x)} = 0$. Since the series expansion of the torsion function converges rapidly, we use the first terms, only [21].

Alternatively, the elastic properties of a ski can be measured [54]. The ski deflection is determined for a given load. To avoid influences due to the dead load of the ski two measurements with different loads were done and the difference of the deflections h is used for the calculations. The flexural stiffness is given by

$$EI = -\frac{M}{h''}. \tag{5.5}$$

The bending moment M can be computed from the load. In the experiment, the ski is supported at two points a and b near to tail and shovel of the ski. The load F is introduced at the position p of the mounting point of the ski. In this case the bending moment M is given by

$$M = F\frac{(b-p)(x-a)}{b-a} - F\begin{cases} 0, & a \le x \le p, \\ x-p, & p \le x \le b. \end{cases}$$

The displacement data are erroneous. Since the second derivative h'' occurs, one cannot just interpolate the data, but has to use an approximation. Because of physical reasons, h and h'' vanish at the points of support a and b. Due to the point load the third derivative h''' makes a jump at p by $F/EI(p)$ units. Therefore, h is written as $h_1 + h_2$. $h_1|_{[a,p]}$ and $h_1|_{[p,b]}$ are polynomials that match the boundary and the jump conditions. The smooth remainder h_2 is approximated by a smoothing spline with vanishing boundary conditions [24].

Snow model. The snow is supposed to be compacted, homogeneous and isotropic. A tool that penetrates into snow generates reaction forces of the snow, which are assumed to be proportional to penetration depth e. The reaction forces occur during loading only. During unloading we assume that the snow remains in its deformed state. Therefore, during loading the pressure p at a point (x, y) of the running surface of the ski is given by the constitutive equation of snow

$$p(x,y) = \begin{cases} k\ e(x,y), & \text{if } e \ge 0, \\ 0, & \text{else.} \end{cases} \tag{5.6}$$

The parameter k is determined by the hardness of snow. Reasonable values for k are between $5 \cdot 10^6$ and 10^{11} N/m^3. In our calculations we use $k = 6.25 \cdot 10^6$ N/m^3. This value corresponds to rather soft snow. When the compaction pressure exceeds a certain limiting value, yielding occurs. Yielding may start at 40-340 kPa, depending on the shear strength of snow [90]. In the case of slopes prepared for world cup races the values might even be higher.

Loading of the ski. In the equation of beam deflection and torsion Eq 5.8 one has to provide the applied load per unit length f and the applied torque per unit length m along the ski. The line load f and the line torque m are composed of three parts:

1. the loading in the boot region due to the skier $f_1(x, F_z, M_y)$ and $m_1(x, M_x)$,
2. the dead load of the ski $f_2(x, \varphi, \rho)$, and

3. the line force $f_3(x, w, d, c, h, \varphi, k)$ and line torque $m_3(x, w, d, c, h, \varphi, k)$ generated by the ground reaction force of the snow.

To compute the line loading f_1 and m_1 we assume that the skier transmits a normal force F_z, a transversal torque M_y, and an edging torque M_x in the boot-binding region. The force and the torques are introduced as piecewise linear line loading, which are nonzero in the region of the ski boot ($-0.15 \leq x \leq 0.15$) and zero elsewhere.

The dead load is the normal component of the weight of the ski. The line force is given by $f_2 = -\rho \mathrm{g} \cos\varphi$, with ρ the line density and $\mathrm{g} = 9.806$ m/s^2 the constant of gravitation. The line torque is zero by symmetry reasons.

The third part is a bit more complicated. In our model the pressure at a point (x, y) on the running surface of the ski is proportional to the elongation $e(x, y)$ of the snow. This elongation is normal to the running surface of the ski and not normal to the snow surface. We have

$$e(x, y) = -\left(h(x) + c(x) + y \tan\varphi(x)\right) \tag{5.7}$$

We denote by

$$\begin{aligned} e_1(x) &= -\min\left(h(x) + c(x) - w(x)\tan\varphi(x), 0\right), \\ e_2(x) &= -\min\left(h(x) + c(x) + w(x)\tan\varphi(x), 0\right) \end{aligned}$$

the left- and rightmost point of contact of a specific cross section with snow. Then, the contributions f_3 and m_3 to the line load can be calculated as follows

$$\begin{aligned} f_3(x) = \int k\, e(x, y)\, dy \quad &= \frac{-k}{2\tan\varphi(x)} \left(e_2^2(x) - e_1^2(x)\right), \\ m_3(x) = \int k\, y\, e(x, y)\, dy \quad &= \frac{k}{\tan^2\varphi(x)} \left(\frac{e_2^3(x) - e_1^3(x)}{3} + (h(x) + c(x))\frac{e_2^2(x) - e_1^2(x)}{2}\right). \end{aligned}$$

Boundary value problem for beam deflection and torsion. When the ski is modeled as an elastic beam, the deflection h and the torsion angle φ of the ski are given by the differential equation for the elastic beam deflection and torsion. We have free boundary conditions as in [112]

$$\begin{aligned} \frac{d^2}{dx^2}\left(EI\frac{d^2}{dx^2}h\right) &= f(x, w, d, c, h, \varphi, F_z, M_y, \rho, k), \\ \frac{d}{dx}\left(GJ\frac{d}{dx}\varphi\right) &= -m(x, w, d, c, h, \varphi, M_x, k), \\ h''(x_T) = h'''(x_T) = h''(x_S) = h'''(x_S) = 0, &\qquad \varphi'(x_T) = \varphi'(x_S) = 0. \end{aligned} \tag{5.8}$$

These equations are a system of two coupled, nonlinear ordinary differential equations with boundary values. One has to solve this boundary value problem numerically. Due to the hardness of the snow, even small changes of the penetration depth result in large changes of the load. Therefore, suitable methods have to be selected for the solution of these equations.

Numerical solution. In a first step we introduce the new variables $\psi = -h'$ (inclination), $M = EI\psi'$ (bending moment), $Q = M'$ (transversal force), and $N = GJ\varphi'$ (torsion moment). We collect these variables in the state vector $y = (h, \psi, M, Q, \varphi, N)^t$. The differential equations become a first order system $y' = F(x, y)$. The boundary value problem can be rewritten in the form

$$\frac{d}{dx}\begin{pmatrix} h \\ \psi \\ M \\ Q \\ \varphi \\ N \end{pmatrix} = \begin{pmatrix} -\psi \\ \frac{M}{EI} \\ Q \\ -f \\ \frac{N}{GJ} \\ -m \end{pmatrix}, \qquad \text{with} \qquad \begin{pmatrix} M(x_T) \\ Q(x_T) \\ N(x_T) \\ M(x_S) \\ Q(x_S) \\ N(x_S) \end{pmatrix} = 0. \tag{5.9}$$

To solve this problem we use an optimization technique. It starts by selecting an initial value for $y_0 = (h(0), \psi(0), M(0), Q(0), \varphi(0), N(0))^t$. The initial value problem $y' = F(x, y)$, y_0 given, is integrated numerically to obtain the solutions at the boundaries $x = x_T$ and $x = x_S$. With help of the integration results at the ski ends one can compute the boundary conditions $B(y_0) = (M(x_T), Q(x_T), N(x_T), M(x_S), Q(x_S), N(x_S))^t$. Note, that the boundary conditions depend on the initial values and do not satisfy that $B(y_0) = 0$. Thus, the boundary value problem is transformed to an optimization problem: Find starting values such that $B(y_0) = 0$ holds. This optimization problem is solved by a damped Newton technique [23]. The algorithm requires the sensitivity matrix, i.e. the derivative of B with respect to y_0. It is computed with variational equations [40].

Turn radius and pressure distribution. From the numerical results the penetration depth of the ski into the snow can be computed as function of x and y. The pressure distribution under the ski follows from the constitutive equation Eq 5.6. The position of the loaded ski edge can be computed as 3-D curve. This curve is projected onto the snow surface and approximated by a circle with a least squares fit. The radius of this circle is called turn radius r. The errors in the least squares fit are very small. Thus, one could apply Howe's formula Eq 5.4 in a good approximation. However, correct values for the ski length L and the penetration depth e have to be inserted. During an actual turn shearing is minimized if the ski is directed tangentially to the trajectory of the turn. In such a situation the skier has to choose a turn radius that is equal to the radius of curvature of the trajectory. This technique is called carving.

Dynamics of a carved turn. In real turns, the skier follows a certain trajectory with a given velocity. To determine the load cases for our computation we recall some results of Howe [50] and [66]. With these results one can explain two important facts:

1. For a given instantaneous turn radius the skier can perform a carved turn only if the velocity is small enough. If the velocity exceeds a certain limiting value

the skier will loose the equilibrium and fall outwards if he tries to continue the carved turn or he has to start with skidding which could be a rather difficult task.

2. The instantaneous turn radius decreases at the end of a real turn [94].

Let m be the mass, v the velocity, φ the edging angle, r the turn radius, α the inclination of the slope, and β the traverse angle between the direction of the ski and the horizontal. During carving, the normal component N of the gravitational force and the lateral force L

$$N = mg\cos\alpha, \qquad L = \frac{mv^2}{r} - mg\sin\alpha\cos\beta \tag{5.10}$$

act on the skier. The lateral force consists of two parts, the centrifugal force and the lateral component of the gravitational force. In the uphill quadrant of a turn, $\cos\beta$ is positive and both terms have a different sign. In the downhill quadrant, $\cos\beta$ is negative and both terms are added. We consider a limiting situation in which the vector sum of N and L, the resultant or total force T is directed from the center of gravity of the skier to the loaded edge of the outer ski. In equilibrium the inner lean angle χ of the skier holds the relation $\tan\chi = N/L$. In our case no angulation is introduced. The skier will loose its equilibrium if the centrifugal force gets slightly larger. For smaller values of the centrifugal force the skier can distribute the resulting force on both ski. Without angulation, the inner lean angle and the edging angle are related by $\chi = \pi/2 - \varphi$. Therefore, in the limiting situation it holds

$$\tan\varphi = \frac{L}{N}. \tag{5.11}$$

Usually, the edging angle is larger than in the above situation, since a part of the resultant force may act on the inner ski or the skier may perform an angulation. We assume that a negative angulation is not possible. Thus, the turn radius will usually be smaller than the limiting value derived below. Eliminating φ with the equation for the turn radius on hard snow Eq 5.3 and inserting N and L from Eq 5.10 yields the skiing equation (Howe [50] p. 117, with a typing error)

$$r^2(\cos^2\alpha + \sin^2\alpha\cos^2\beta) - 2r\frac{v^2}{g}\sin\alpha\cos\beta + \frac{v^4}{g^2} - R^2\cos^2\alpha = 0. \tag{5.12}$$

From the skiing equation the radius of a carved turn r in equilibrium situation can be calculated. It depends on the velocity v of the skier, on the ski radius R, on the steepness of the hill α, and on the traverse angle β. In the downhill quadrant of a carved turn, the lateral component of the gravity force has the same direction as the centrifugal force. Thus, the inner lean angle gets smaller and the edging angle gets larger. Additionally, the resultant force increases. Due to both effects the instantaneous turn radius decreases at the end of a turn.

To derive the skiing equation Eq 5.12 the turn radius on hard snow Eq 5.3 is used. Obviously, it would be better to use Eq 5.4 instead. However, the penetration depth e cannot be computed analytically. Thus, we have to apply our model. Here, the turn radius depends not only on the edging angle φ, but also on further variables, which influence the penetration depth e in Eq 5.4. We determine these parameters iteratively in such a way that they correspond to an equilibrium situation in a circular carved turn with the finally obtained turning radius. We start with a given velocity v of the skier. As starting value for the turn radius r we use the turn radius r_0 from the skiing equation Eq 5.12. With this turn radius the lateral force L in Eq 5.10 is computed. The resultant or total force T

$$T = \sqrt{N^2 + L^2} \tag{5.13}$$

is used as initial value for the normal force F_z. The edging angle φ follows from Eq 5.11. Then, starting with an edging moment $M_x \approx Tl$ and a lever arm l of 2 to 3 cm the deflection and the torsion of the ski are calculated. The torsion $\varphi(0)$ at the mounting point of the ski is compared to the edging angle φ of the ski in Eq 5.11. The edging moment is changed until $\varphi(0)$ equals φ. The new turn radius r is calculated from the deflection of the ski edge in the snow foundation. It is usually smaller than r_0. While r and r_0 are not equal, r is used as new starting value r_0. The whole procedure is repeated iteratively. With the new starting value r_0 one computes a new centrifugal force, a new lateral force, a new normal force F_z and a new edging angle φ until r equals r_0.

Ski data. In this study two carving ski, denoted by ski A and ski B, were investigated. Both ski were equipped with a binding plate and bindings. Basic data for these ski are given in Tab 5.1. The geometrical properties of the ski are plotted in Fig 5.6. Ski A is more waisted and has a wider shovel and tail. Ski A is thicker than ski B. The flexural stiffness EI was obtained from bending experiments. The results are plotted in Fig 5.7. The maximum flexural stiffness is larger for ski A (763 and 631 Nm^2) but the mean is smaller than for ski B (246 and 235 Nm^2). Ski A has softer ends than ski B.

We did not measure torsional stiffness GJ and density ρ since both quantities have little influence on the results of our computations [54]. We used $GJ = 1.2\ EI$ and calculated the line density ρ from the total mass and the geometry of the ski.

		A	B
Projected length [m]	l	1.79	1.79
Contact length [m]	L	1.60	1.60
Side cut [mm]	D	20.5	15.0
Ski radius [m]	R	15.8	20.9
Mass [kg] of one ski	m	3.8	3.7

Tab. 5.1: Properties of ski A and B.

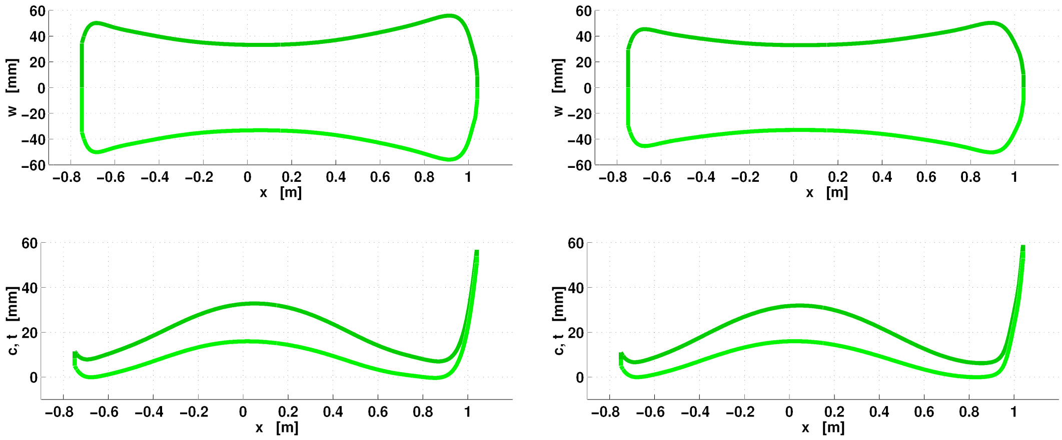

Fig. 5.6: Top and side view. Ski A (left) and B (right).

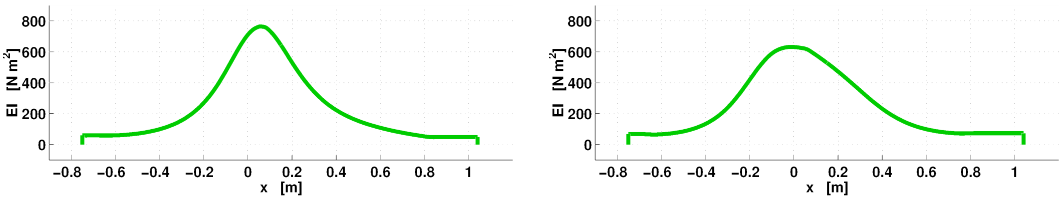

Fig. 5.7: Flexural stiffness EI. Ski A (left) and B (right).

5.3 Results

Turn radius for different load cases. For two carving ski the bedding of the ski on snow was investigated for load cases that correspond to schussing and turns at traverse angles β of 45, 90, and 135°. For demonstration we give the results for two similar velocities: 9 and 10 m/s.

Although these velocities are not high at all, the corresponding turn radii are small (Tab 5.3). The higher velocity is near to the region in which the skiing equation Eq 5.12 has no real solution since the expression under the square root becomes negative. The mass of the skier was 80 kg and the inclination of the slope 20°. The normal force is 737 N. The ski radius for ski A is $R = 15.8$ m and for ski B $R = 20.9$ m. The lateral force L, the normal force N Eq 5.10, the loading of the ski F_z, M_x with $M_y = 0$, the turn radius r and the edging angle φ for these turns are summarized in Tab 5.2. In Tab 5.3, turn radii resulting from different models are compared: the geometric models of Howe [50] for hard snow r_{hard} Eq 5.3, for soft snow r_{soft} Eq 5.4, for the skiing equation r_{seq} Eq. 5.12, and finally for our model r.

$\beta = 45°$	$\beta = 90°$	$\beta = 135°$		v [m/s]	$\beta = 45°$	$\beta = 90°$	$\beta = 135°$
332	740	1249	L [N]	9	165	477	873
808	1045	1451	$F_z = T$ [N]	9	755	878	1142
24.80	33.86	47.23	M_x [Nm]	9	20.07	26.84	35.76
12.40	8.75	6.11	r [m]	9	18.27	13.56	9.47
24.28	45.13	59.45	φ [°]	9	12.59	32.95	49.82
667	1524	2229	L [N]	10	309	779	1430
1001	1692	2348	$F_z = T$ [N]	10	799	1073	1609
32.35	54.96	75.52	M_x [Nm]	10	23.47	33.50	50.37
9.22	5.24	3.92	r [m]	10	16.01	10.26	6.44
42.58	64.16	71.68	φ [°]	10	22.78	46.58	62.73

Tab. 5.2: Turns for ski A (left) and B (right). Velocity 9 m/s (above) and 10 m/s (below).

$\beta = 45°$	$\beta = 90°$	$\beta = 135°$		v [m/s]	$\beta = 45°$	$\beta = 90°$	$\beta = 135°$
15.58	13.72	11.33	r_{seq} [m]	9	21.30	19.68	17.06
14.40	11.14	8.03	r_{hard} [m]	9	20.39	17.53	13.48
11.95	7.65	4.95	r_{soft} [m]	9	18.48	12.53	8.06
12.40	8.75	6.11	r [m]	9	18.27	13.56	9.47
14.68	12.16	9.44	r_{seq} [m]	10	20.85	18.12	15.61
11.63	6.88	4.96	r_{hard} [m]	10	19.26	14.36	9.55
8.15	4.13	2.84	r_{soft} [m]	10	15.53	8.84	5.10
9.22	5.24	3.92	r [m]	10	16.01	10.26	6.44

Tab. 5.3: Comparison of the turn radii r_{hard}, r_{soft}, r_{seq} according to Howe, and our model r. Velocity 9 m/s (above) and v = 10 m/s. Ski A (left) and B (right).

Contact area between ski and snow. Tab 5.4 gives the numerical ratios of the contact area to the total area of the running surface. The results are shown graphically in Fig 5.8. The thick line represents the surface of the ski. In schussing approximately two thirds of the ski have snow contact. The area of contact is symmetric about the longitudinal ski axis. In turns only a small fraction of ski has contact to the snow. The larger the edging angle gets the smaller and the longer the area of contact will be. Especially for large edging angles the whole edge cuts into the snow.

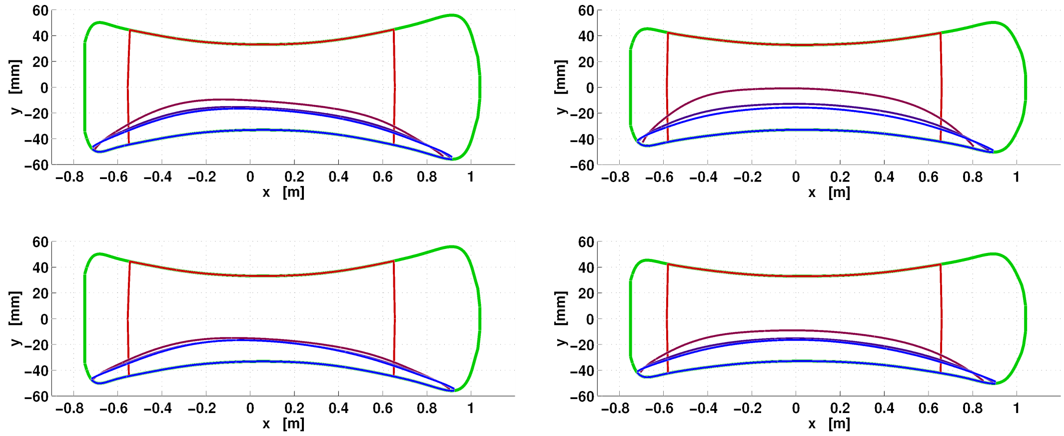

Fig. 5.8: Contact area for schussing and turns at traverse angles of 45, 90, and 135° at a velocity of 9 m/s (above) and 10 m/s (below). Ski A (left) and ski B (right).

schuss	$\beta = 45°$	$\beta = 90°$	$\beta = 135°$	v [m/s]	schuss	$\beta = 45°$	$\beta = 90°$	$\beta = 135°$
0.61	0.20	0.16	0.14	9	0.65	0.29	0.19	0.16
0.61	0.16	0.14	0.13	10	0.65	0.22	0.16	0.15

Tab. 5.4: Ratio of contact area A_c to area of running surface A. Velocity 9 m/s (above) and 10 m/s (below). Ski A (left) and B (right).

Bending of the ski. The deformation of the loaded ski edge is studied for the two skis and the load cases of Tab 5.2. In Fig 5.9, the projection of the loaded ski edge onto the snow surface is shown. In Fig 5.10 the penetration depth of the loaded ski edge is plotted. The thick parts of the lines indicate the parts of the ski edge having snow contact. In all cases the maximal penetration depth and, hence, the largest reaction pressure occurs in the middle of the ski, approximately at the heel of the boot. Apart from very small edging angles the maximum penetration over the ski width is taken at the loaded edge.

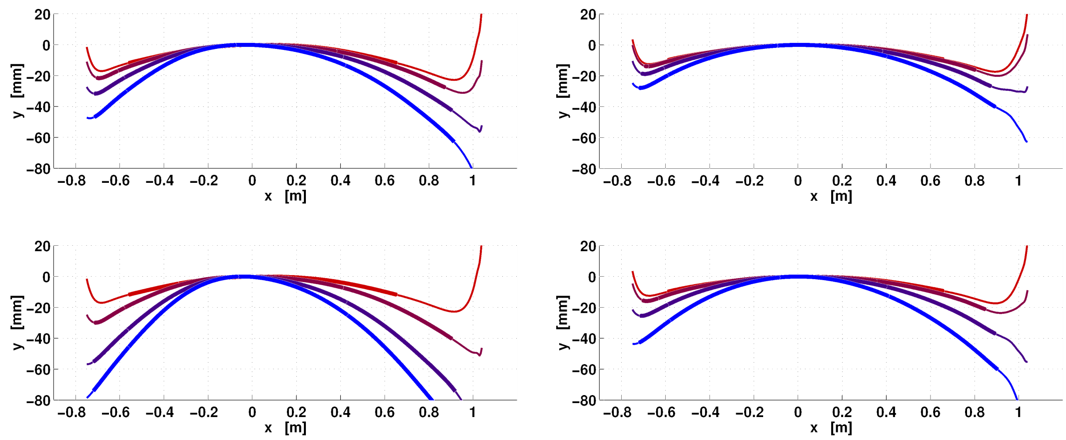

Fig. 5.9: Projection of the loaded ski edge onto the snow surface for schussing and turns at traverse angles of 45, 90, and 135°. Velocity 9 m/s (above) and 10 m/s (below). Ski A (left) and B (right).

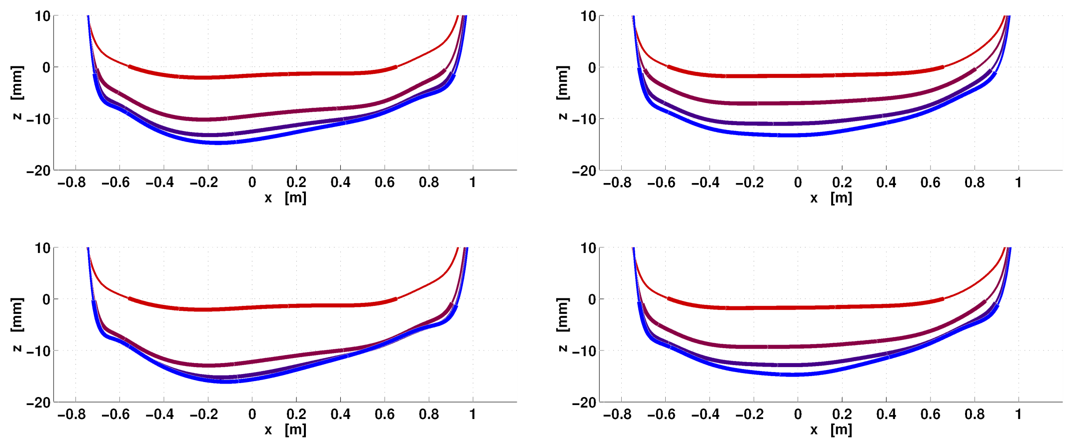

Fig. 5.10: Penetration depth of the loaded ski edge for schussing and turns at traverse angles of 45, 90, and 135° at a velocity of 9 m/s (above) and 10 m/s (below). Ski A (left) and B (right).

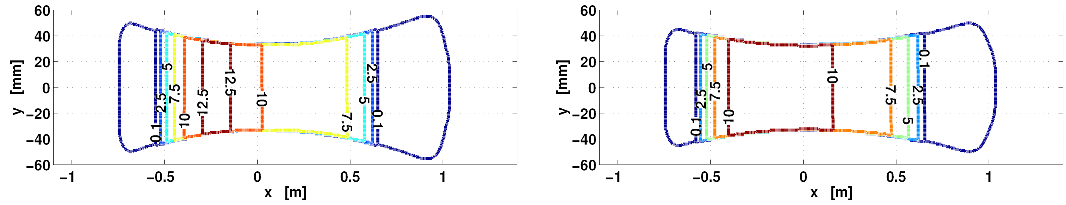

Fig. 5.11: Pressure distribution for schussing at a velocity of 9 m/s. Ski A (left) and B (right).

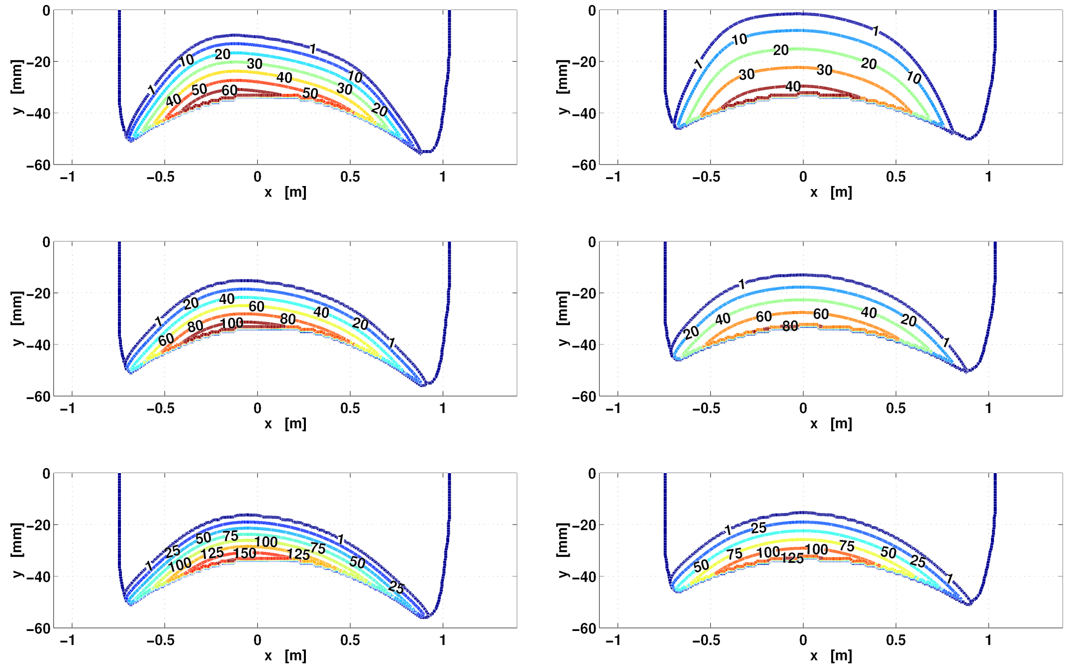

Fig. 5.12: Pressure distribution for a carved turn with a velocity of 9 m/s. Traverse angles of 45, 90, and 135°. Ski A (left) and B (right).

Pressure distribution. Finally, the pressure distribution under the ski is investigated. Fig 5.11 shows contour lines for the pressure distribution in schussing. The pressure does not depend on the actual velocity of the skier. It is largest below the boot of the skier. Similar to the behavior of the flexural stiffness EI, the maximum pressure is larger for ski A but the mean pressure is lower for ski B.

Fig 5.12 shows the pressure distribution at begin, middle, and end of a carved turn with 9 m/s. More exactly, the three positions correspond to circular turns at traverse angles of 45, 90, and 135°. Radii and load cases are given in Tab 5.2. We show just the lower half of the ski in which the snow contact occurs. Along a turn, i.e. with increasing traverse angle, the ski has to be edged more and more. As a consequence the contact area gets smaller and smaller and the pressure distribution concentrates along the edge. The maximum pressure is obtained at the boot position. In the final part of the turn the pressure reaches up to 180 kPa for 9 m/s and up to 320 kPa for

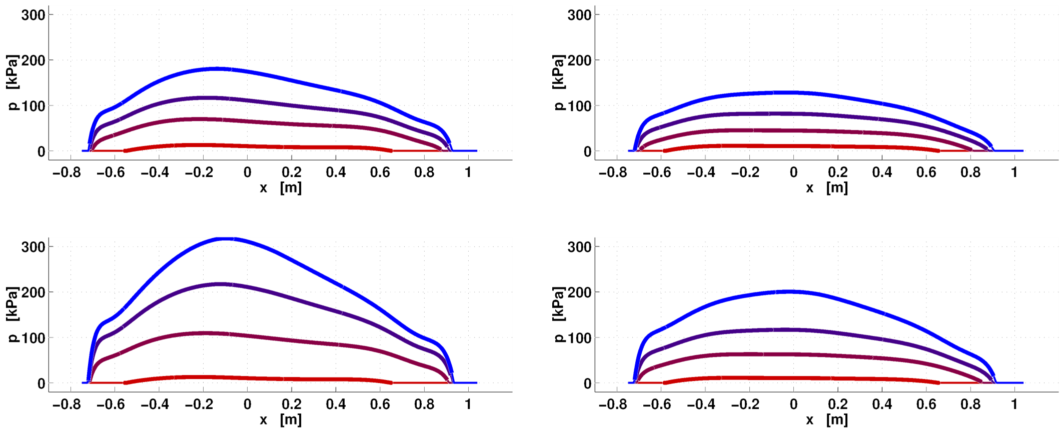

Fig. 5.13: Edge pressure for schussing and turns at traverse angles of 45, 90, and 135°. Velocity 9 m/s (above) and 10 m/s (below). Ski A (left) and B (right).

10 m/s. From shearing experiments [90] it is known, that shearing starts between 40 and 340 kPa, depending on snow hardness. Thus, in narrow turns shearing might occur. As it is difficult to represent maxima in contour plots, the pressure along the loaded ski edge is presented in Fig 5.13.

5.4 Discussion

In this theoretical study we have investigated the pressure distribution under an edged ski during carved turns. A ski-snow interaction model for purely carved turns is presented. The model allows to calculate the deflection and torsion of a loaded ski penetrating into snow and from this the ski-snow contact area and the pressure distribution under the ski. Additionally, the radius of the least square circle of the deflected edge of the ski is presented which is assumed to be the instantaneous radius of the carved turn.

The interaction depends on ski and snow properties. The ski is modeled as an elastic beam with varying bending and torsional stiffness along the ski. The bending stiffness of the two skis investigated is obtained by bending measurements. Validation experiments show that the elastic beam model is appropriate to predict the deflection of a ski in various load cases [54, 91].

The snow is assumed to be compacted. In our snow model the compaction pressure depends linearly on the penetration. Recently, snow measurements were conducted in order to determine the force-deformation relation and the yield shear pressure on ski slopes [90]. According to these measurements the snow modeled in this paper can be classified as soft snow on ski slopes.

The ski-snow interaction reveals that the contact area is surprisingly small with

63 % for schussing and around 15 % for turning. The maximum pressure under the ski reaches up to 320 kPa at the end of the studied turns. Preliminary snow measurements on ski slopes show maximum shear strengths of 40 kPa for soft snow and 340 kPa for very hard snow. Thus, in the studied soft situation the ski would not carve purely as assumed for the calculations but would shear off snow leading to skidding of the whole ski or at least parts of the ski. When skidding occurs the velocity has a radial component and the centrifugal force decreases. Both load and edging angle become smaller and hence the turn radius larger. By these effects the pressure under the ski is reduced. Under this aspect the values given for radius and pressure at the end of turns have to be interpreted with caution. For future work we plan a dynamic investigation of a skier including the modeling of the shearing action of the ski and to validate the model by measurements.

Regarding the calculated turn radii our study shows remarkable results. The turn radius becomes considerably smaller during a turn. In the investigated situations the turn radius in the first part of the turn (45° traverse angle) is twice as large as in the last part of the turn (135° traverse angle). This is due to the increasing lateral force during a turn. It requires an increase of the inward lean of the skier. Consequently, the edging angle of the ski is increased causing a reduction of the turn radius. By positive angulation it is possible to edge more and to reduce the turn radius even more. However, an increase of the turn radius is hardly possible since negative angulation of the skier is very limited. The lateral force is mainly influenced by the speed of the skier. Consequently, the turn radius of a purely carved turn is strongly determined by the speed of the skier. If the speed reaches a certain limiting value a purely carved turn is no longer possible because the edging angle would approach 90°.

The validation of the developed model is difficult since one has to measure the pressure distribution at the running surface of a ski. Attempts were started to implement pressure sensors in the running base of a ski. If this succeeds one could obtain pressure values at certain points of the running surface in real skiing situations. By measuring the path of a ski in a certain snow and comparing the obtained pressure with the yield shear pressure of that snow we know that skidding is an integral part of a carved turn. Thus, skidding has to be implemented in a realistic ski-snow interaction model.

Thanks

This work was supported in part by the Austrian Ski Federation and the ski binding company Tyrolia.

6 Selection of Abstracts

6.1 W. Nachbauer, P. Kaps, and M. Mössner, Determination of Kinetic Friction in Downhill Skiing, 8th Meeting of the European Society of Biomechanics, 1992

Reference: W. Nachbauer[1], P. Kaps[2], and M. Mössner[3], *Determination of Kinetic Friction in Downhill Skiing*, Book of Abstracts, 8th Meeting of the European Society of Biomechanics (ESB) (Rome, IT), 1992, p. 333.

Introduction

A thin melt water film caused by frictional heating is thought to be the reason for the low friction between skis and snow. The coefficient of kinetic friction of skis on snow appears to be influenced by several factors e.g. speed, contact area, snow type (temperature, liquid-water, hardness, texture), and ski properties (stiffness, thermal conductivity, base material, base roughness). In laboratory investigations, the coefficient of friction meters consisting of rotational devices with built-in force transducers (e.g. Kuroiwa [62]). In skiing investigations measurements were done in straight running using the towing method (e.g. Habel [39]) or the run-out method (e.g. Leino and Spring [63]). The purpose of this study was to present a method to determine the coefficient of kinetic friction in straight running on a slope with varying inclination and in traversing on an inclined plane.

Data Collection

The straight running experiments were conducted on a 342 m long run with altitudinal difference of 73 m. Nine photocells were installed about 25 cm above the snow surface and distributed along the run. Geodetic measurements of track and photocells were made using a theodolite. Time data of a skier gliding straight down the fall line in a tucked position was collected from all photocells. Several runs were recorded.

In the traverse, the path of the downhill ski boot was determined by film analysis. The length of the run was about 25 m, located on an 18° inclined plane. The traversing angle was about 40° to the horizontal. The sides of the traverse were marked by ropes equipped with black painted tennis balls that defined a 1 m reference marker system. The skier was filmed with a 16 mm high-speed camera located laterally to the plane of motion of the skier. The camera operator followed

[1]Dept. of Sport Science, Univ. Innsbruck, AT. email: Werner.Nachbauer@uibk.ac.at
[2]Inst. for Basic Sciences in Engineering, Univ. Innsbruck, AT
[3]Dept. of Sport Science, Univ. Innsbruck, AT

the skier with the camera. The width of the film field ranged from 4 to 6 m. The film speed was set 100 Hz. Ball-shaped markers were placed on the toe part of the binding. The skier had to traverse in a straight line in an upright position. Side slipping had not occur. Barometric pressure and air temperature were measured in order to calculate the air density. The mass of the skier including equipment was taken as well.

Data Analysis

In straight running, one run was selected for analysis. The time history of the coordinates of the shell of the ski boot was established by the releasing times and the position of the photocells. In traversing, three runs of one skier were analyzed. In each film frame, the binding marker of the lower ski as well as 4 reference markers were digitized. The time history of the coordinates of the toe part of the binding was calculated from digitized data. The skier was modeled as a particle that moves on the surface of the slope given by $z = h(x, y)$. The track of the skier was given by its projection on the x-y-plane: $y = kx + d$. Following forces were assumed to act on the particle: the weight F_w, the aerodynamic drag F_d, and the snow friction F_f, both in the tangent direction opposite the velocity. Due to its minor influence, the lift component of the air resistance was neglected. Hence, the equation of motion was given by

$$ma = F_w + F_d + F_f + F_r, \tag{6.1}$$

where m denotes the mass of the skier with the equipment, a the acceleration, and F_r the reaction forces. The equation of motion combined with the geometric constraints defining the track of the skier represents an index 3 differential-algebraic equation. The numerical solution was obtained by the code MEXX21 of Lubich [68]. Note, that the reaction forces F_r must not be provided by the user , but are computed automatically by the program. The snow friction force was assumed to be proportional to the reaction force normal to the slope $F_f = \mu F_n$. The drag force was set according to $F_d = \frac{1}{2}\rho C_d A v^2$. The coefficient of kinetic friction μ and the drag area $C_d A$ were kept constant. These parameters were calculated by minimizing the sum of squared errors between computed and measured times.

Results

For straight running the computed coefficient of friction was 0.00085, which is in the same range as obtained by the towing and run-out method. The drag area was 0.22 m^2. This is in agreement with unpublished wind tunnel experiments on the Austrian Ski Federation, where the drag area of male world class racers was between 0.13 and 0.19 m^2.

In Tab 6.1, the traversing results for different velocities are summarized. The computed coefficients of friction were between 0.06 and 0.15. The increase of μ with increasing velocity may not be interpreted as a velocity effect, as the snow conditions varied considerably throughout the measurements due to increasing sun radiation. For the drag area the value 0 was obtained. The confidence interval was infinitely large.

μ	$\Delta\mu$	v_i [m/s]	v_f [m/s]
0.064	0.060–0.067	0.6	10.6
0.128	0.108–0.150	11.0	13.4
0.153	0.136–0.171	14.7	16.6

Tab. 6.1: Coefficients of kinetic friction μ, 10 % confidence intervals $\Delta\mu$, and initial v_i and final velocities v_f of the traversing measurements.

Conclusions

The results of the study indicate that the applied method is adequate for the determination of the coefficient of kinetic friction in skiing. For traversing, however, we did not succeed in calculating the drag area. We believe that the accuracy of the measurements has to be improved and/or the model has to be refined by considering the drag area function for gliding velocity. Furthermore, the proposed method allows to calculate reaction forces which becomes important when the skier is modeled as a multibody system.

Acknowledgment

This study was supported in part by a grant of the Austrian Research Foundation and the Austrian Ski Federation.

6.2 M. Mössner, P. Kaps, and W. Nachbauer, Smoothing the DLT-Parameters for Moved Cameras, XVth Congress of the International Society of Biomechanics, 1995

Reference: M. Mössner[4], P. Kaps[5], and W. Nachbauer[6], *Smoothing the DLT-Parameters for Moved Cameras*, Book of Abstracts: XVth Congress of the International Society of Biomechanics (ISB) (Jyväskylä, FI) (K. Häkkinen, K.L. Keskinen, P.V. Komi, and A. Mero, eds.), University of Jyväskylä, 1995.

Introduction

For many sport-biomechanical analyses, e.g. in Alpine ski racing, the athletes have to be filmed over a large object space. To digitize body landmarks a sufficiently large image of the athlete is necessary. Thus, one has to follow the athlete with the cameras and to zoom the lenses. Our group collected data of the jumping movement during the downhill events of the 1994 Winter Olympic Games in Lillehammer. For 3-D reconstruction the DLT-parameters were calculated for every frame of each camera separately [85]. The data reconstructed by this method were suitable for computing resultant knee joint forces and moments by inverse dynamics [101]. Since the control points were surveyed geodetically, errors in the reconstruction are mainly caused by digitization. In [101] the errors in calibration were averaged by using 10 control points. If only 6 control points are available the reconstruction error might be enlarged by more than an order of magnitude. For frames with less than 5 control points the DLT-parameters can not be determined. In the present paper the DLT-parameters are smoothed to overcome these difficulties.

Method

Direct Linear Transformation. Between a space point with object coordinates $(X, Y, Z)^t$ and its image coordinates $(x, y)^t$ it holds the relation:

$$x = \frac{b_1 X + b_2 Y + b_3 Z + b_4}{b_9 X + b_{10} Y + b_{11} Z + 1}, \qquad y = \frac{b_5 X + b_6 Y + b_7 Z + b_8}{b_9 X + b_{10} Y + b_{11} Z + 1}\,. \tag{6.2}$$

The coefficients $b_1, \ldots, b_{11}$ are called DLT-parameters. From the basic photogrammetric relations Hatze [43] obtained a condition for the DLT-parameters which can be written as follows [85]:

$$(b_9^2 + b_{10}^2 + b_{11}^2)(b_1 b_5 + b_2 b_6 + b_3 b_7) = (b_1 b_9 + b_2 b_{10} + b_3 b_{11})(b_5 b_9 + b_6 b_{10} + b_7 b_{11})\,. \tag{6.3}$$

Calibration. The DLT-parameters are computed for every frame of each camera. The image and the object coordinates of at least 6 control points are inserted into

[4]Dept. of Sport Science, Univ. Innsbruck, AT. email: Martin.Moessner@uibk.ac.at
[5]Inst. for Basic Sciences in Engineering, Univ. Innsbruck, AT
[6]Dept. of Sport Science, Univ. Innsbruck, AT

Eq 6.2. By multiplying Eq 6.2 with the denominators one obtains an overdetermined linear system for the DLT-parameters. The results can be used as initial guess for solving the nonlinear system Eqs 6.2,6.3 by standard Newton techniques. For smooth camera movements the DLT-parameters are smooth functions of time which are approximated by smoothing splines.

Reconstruction. The 3-D object coordinates of an unknown space point are computed from its coordinates in synchronized images of two cameras. Inserting the DLT-parameters and the image coordinates into Eq 6.2 yields four linear equations in the unknown object coordinates.

Data Collection. The investigation is based on a data set which shows the flight and the landing phase of a ski racer [101]. The 3-D reconstruction of 23 landmarks was done for 180 frames taken at a rate of 180 fps. In 95 % of the frames 10 control points were used for calibration. The smoothing spline approximations to the reconstructed 3-D coordinates of the landmarks are the best solutions available and therefore taken as „true“ solutions for error estimations. The error of a certain reconstruction is defined by the absolute values of the differences to the „true“ solutions averaged over the 23 landmarks, the 180 time steps, and the 3 coordinates. The error of the above data is 3.8 cm.

Results

For illustration we give a plot of the DLT-parameters b_5 and b_6 together with the corresponding smoothing splines:

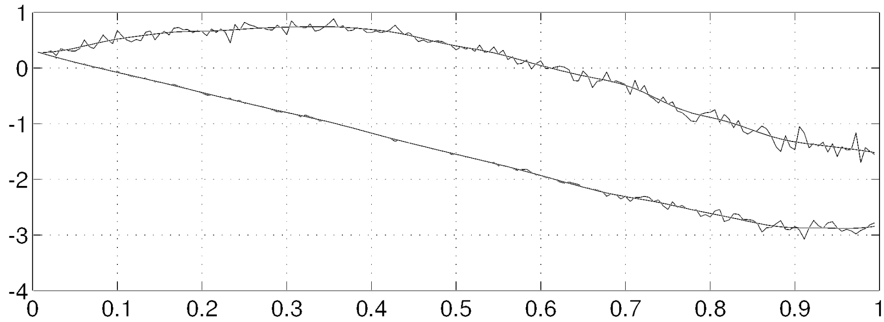

Smoothing the DLT-parameters reduced the error to 3.3 cm. The effect of smoothing the image coordinates was investigated, too. It reduced the error to 2.9 cm. Smoothing both DLT-parameters and image coordinates halved the error to 2.0 cm. The smoothing parameter had to be chosen carefully, since oversmoothing resulted in drifting away from the true solution.
To estimate the effect of hidden control points frames 50 to 70 as well as frames 110 to 130 were not calibrated. As DLT-parameters we used the interpolation values of the smoothing spline. This resulted in an error of 2.3 cm.
A reconstruction based on a calibration using only six control points gave an error of 70 cm. By omitting time steps with obviously wrong DLT-parameters and successive smoothing the error could be reduced to 6.7 cm.

Discussion

The results show that smoothing of DLT-parameters can successfully be applied to reduce the influence of digitization errors on the calibration and to interpolate the DLT-parameters in cases where the calibration is impossible over same frames. However, the smoothing parameter can not yet be determined automatically.

6.3 P. Kaps, M. Mössner, W. Nachbauer, and R. Stenberg, Pressure Distribution under an Edged Ski, 2nd International Congress on Skiing and Science, 2000

Reference: P. Kaps[7], M. Mössner[8], W. Nachbauer[9], and R. Stenberg[10], *Pressure Distribution under an Edged Ski*, Abstract Book, 2nd International Congress on Skiing and Science (ICSS) (St. Christoph am Arlberg, AT) (E. Müller, R. Roithner, W. Niessen, C. Raschner, and H. Schwameder, eds.), 2000, pp. 48–49.

Introduction

The pressure distribution on the running surface of a ski is an important factor in ski design. However, it is a difficult task to measure the pressure distribution or to determine it computationally. There are several factors with significant influence. Among these we mention the contact area between ski and snow, the penetration depth into the snow surface as well as stiffness properties of the ski and the hardness of the snow.

Due to the side cut of the ski, the edged ski touches a rigid and plane surface on two points near its tip and its tail. After loading the ski is bent until the whole edge has contact with the surface. The line of contact is a circle with radius

$$R_s = r_s \cos(\theta),$$

where θ denotes the edging angle of the ski and r_s is the ski radius.

On a non-rigid surface the ski compacts the snow and the edge penetrates into the snow. In the area of contact the snow reaction forces act on the ski. We assume that these forces are proportional to the penetration depth and act normal to the running surface. Thus, the pressure distribution under the ski can be computed, if the penetration of the ski into the snow and its deformation is known.

Obviously, the pressure distribution depends on several parameters: 1) On the hardness of the snow which is described by the constitutive equation. 2) On the loading of the ski which is characterized by the normal force F_z and the torques M_x and M_y with respect to the longitudinal and transversal axis. 3) On geometric properties of the ski like length, width, camber height, side cut and thickness as well as on mechanical properties like flexural and bending stiffness. These factors can be used by the ski design to build an optimal ski.

[7]Inst. for Basic Sciences in Engineering, Univ. Innsbruck, AT. email: Peter.Kaps@uibk.ac.at
[8]Dept. of Sport Science, Univ. Innsbruck, AT
[9]Dept. of Sport Science, Univ. Innsbruck, AT
[10]Dept. of Mathematics, Univ. Tampere, FI

Ski model

A modern ski is built up in a complicated way. We model the ski as an elastic beam consisting of several layers of different materials. For the physical dimensions we use data of real skis. Additionally, one needs the mass density ρ, the Young module E and the Poisson number ν for each material. First, the total mass, the center of gravity, and the inertia tensor are computed. Then, the position of the neutral line is calculated. Finally, the flexural stiffness EI is obtained by averaging over all materials. For the torsional stiffness GJ one has to compute the torsion function, which is a solution of the Poisson equation. Since the series expansion converges rapidly, we use the first terms, only.

Snow model

In our model we assume compacted, homogeneous snow. The pressure p on a small flat plate penetrating a distance d into the snow is given by

$$p = kd.$$

The constant k is a measure for the hardness of the snow.

Pressure distribution under the ski

The pressure distribution follows from the deflection h and torsion φ of the ski. To obtain these quantities, one has to solve the differential equations for the elastic beam deflection and for the torsion angle. The line load f and the torque m are computed from the loading of the ski and the pressure distribution under the ski belonging to a certain deflection and torsion. In formulas, one has to integrate the following nonlinear boundary value problem numerically:

$$\frac{d^2}{dx^2}\left(EI\frac{d^2h}{dx^2}\right) = f(x, h, \varphi, F_z, M_y), \qquad h''(x_t) = h'''(x_t) = h''(x_s) = h'''(x_s) = 0,$$

$$\frac{d}{dx}\left(GJ\frac{d\varphi}{dx}\right) = -m(x, h, \varphi, M_x), \qquad \varphi'(x_t) = \varphi'(x_s) = 0,$$

Results

In the figure above the pressure distribution on the running surface of an edged ski is shown. The situation refers to hard snow conditions. The loading $F_z = 2$ kN, $M_y = 20$ Nm, and $M_x = 55$ Nm leads to an edging angle of 58°.

The x-y plane describes the running surface of the ski. The x- and y-coordinate give the position on the curved longitudinal and transversal ski axis, respectively. Note, that the two axes are scaled differently. The edges of the ski are denoted by the two thick lines in the top and bottom of the figure. The thin lines give levels of constant pressure. In the region without snow contact there is no pressure. In the investigated case, only a small portion of the ski has contact with the snow. The pressure is largest along the inner edge and reaches a peak value of 250 kPa.

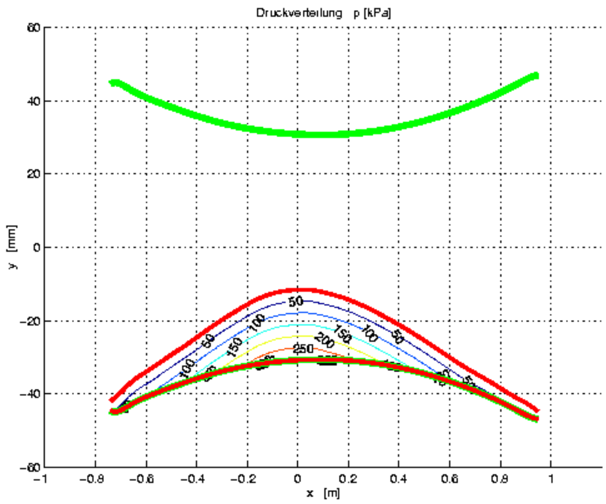

If the curve that represents the edge of the ski is projected orthogonally to the snow surface, one obtains a curve which is nearly part of a circle. The radius of this circle represents the radius of a purely carved turn. This radius might be considerably smaller than the radius predicted by the formula in the introduction.

6.4 B. Knünz, W. Nachbauer, M. Mössner, K. Schindelwig, and F. Brunner, Track Analysis of Giant Slalom Turns of World Cup Racers, 5th Annual Congress of the European College of Sport Science, 2000

Reference: B. Knünz[11], W. Nachbauer[12], M. Mössner[13], K. Schindelwig[14], and F. Brunner[15], *Track Analysis of Giant Slalom Turns of World Cup Racers*, Proceedings of the 5th Annual Congress of the European College of Sport Science (ECSS) (Jyväskylä, FI) (J. Avela, P.V. Komi, and J. Komulainen, eds.), University of Jyväskylä, FI, 2000, p. 399.

Introduction

The track of a perfect giant slalom turn is meant to show no skidding. There are only a view publications dealing with trajectories in different disciplines of Alpine ski racing e.g. Förg-Rob and Nachbauer [32]. However, there are no studies giving information on the amount of skidding during a turn. The purpose of the study was to evaluate the carving and skidding behavior during giant slalom turns of elite skiers.

Method

Three Alpine world cup racers (R1, R2, R3) performed giant slalom turns on a course with 8 open gates on an approximately plain slope of 16° inclination. The snow conditions were hard packed. Control points were distributed along the path of the skier and geodetically surveyed (Nachbauer et al., [101]). The subjects were recorded by a video camera at 50 frames/s. In the laboratory 4 points of each ski and at least 8 control points were digitized per frame. The position of the ski points on the slope were computed using the 2d DLT-method. 3d coordinates of the ski points were obtained from the 3d model of the slope. The data were smoothed using smoothing splines (Woltring [125]). For this study five runs were processed. Analyzed parameters are shear off area per cm track length (A) and the angle of the ski relative to the moving direction (α). These parameters were calculated for the inner and outer ski for two turns of each run (T1, T2). The beginning and the end of the turns were determined by the edge change.

Results

Fig 6.1 shows the track of racer R1. The markers on the track indicate the edge changes. Turn duration for T1 was 1,48 s and for T2 1,40 s. For T1 A was 20 cm^2 for the inner ski and 9 cm^2 for the outer ski. For T2 A was 9 cm^2 for the inner ski

[11] Dept. of Sport Science, Univ. Innsbruck, AT
[12] Dept. of Sport Science, Univ. Innsbruck, AT
[13] Dept. of Sport Science, Univ. Innsbruck, AT
[14] Dept. of Sport Science, Univ. Innsbruck, AT
[15] Dept. of Sport Science, Univ. Innsbruck, AT

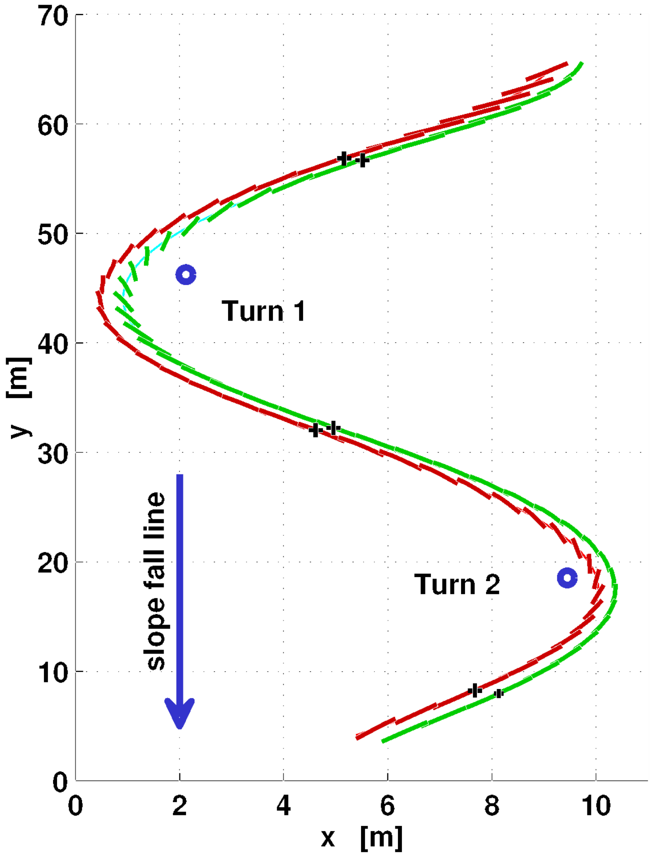

Fig. 6.1: Track of racer R1.

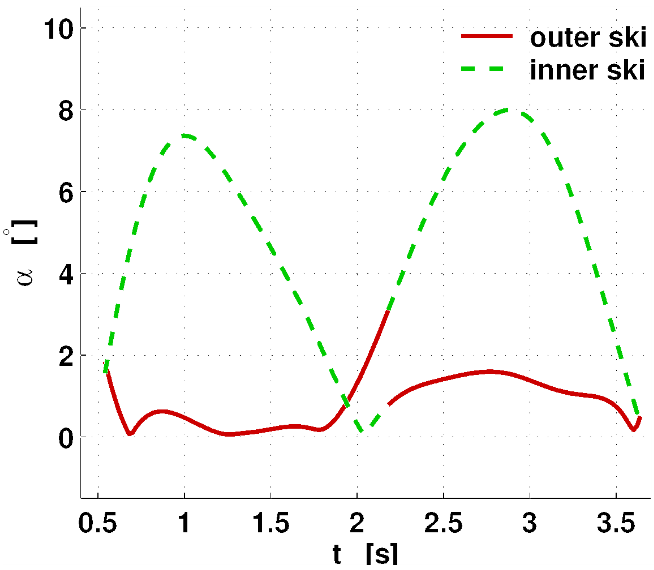

Fig. 6.2: Angle of the ski relative to the traveling direction (α) of racer R3.

and 5 cm^2 for the outer ski.

Fig 6.2 shows the angle (α) of the ski relative to the traveling direction of skier R3. The vertical line indicates the edge change. For T1 peak values of equal 7° for the inner ski and about 1° for the outer ski were observed. For T2 values up to 8° for the inner and 2° for the outer ski were calculated.

The mean value for the turn duration was 1.47 s, the track length was 28.5 m, and the velocity was 19.4 m/s. The turn radius was approximately 20 m. The range of the analyzed parameters in the 5 runs were as following: For T1 A varied between 10-19 cm^2 for the inner ski and 2-10 cm^2 for the outer ski. For T2 A showed a variation of 4-20 cm^2 for the inner ski and 4-5 cm^2 for the outer ski. For T1 and T2 peak values for α were between $2 - 12°$ for the inner ski and $1 - 8°$ for the outer ski.

Discussion

Even highly skilled world cup racers do not purely carve giant slalom turns. There was considerably more skidding for the inner ski than for the outer ski. The amount of skidding differs between the subjects and within their runs. Skidding occurs both in the initiation and the steering phase of the turn. During the unloaded part of the initiation phase this might be a technique used by skilled racers. In the steering phase it results in increased friction and, hence, in a velocity reduction. In order to verify these statements more runs have to be analyzed.

6.5 M. Mössner, W. Nachbauer, G. Innerhofer, and H. Schretter, Mechanical Properties of Snow on Ski Slopes, 15th International Congress on Skiing Trauma and Skiing Safety. 2003

Reference: M. Mössner[16], W. Nachbauer[17], K. Schindelwig[18], G. Innerhofer[19], and H. Schretter[20], *Mechanical Properties of Snow on Ski Slopes*, Poster presented at the 15th International Congress on Skiing Trauma and Skiing Safety (ICSTSS), St. Moritz / Pontresina, CH, April 27th - May 2nd 2003.

Purpose

The aim of this study was to obtain the force-penetration relationship and the ultimate shear pressure of snow on ski slopes.

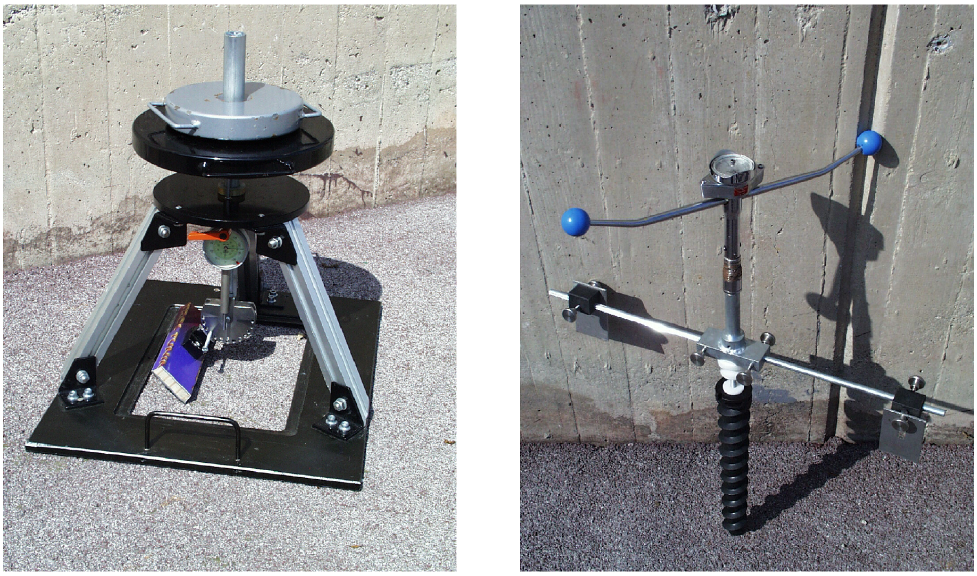

Fig. 6.3: Snow penetration tool (left) and snow shear tool (right).

Force Penetration Relationship

Data Collection.

For determining the force-penetration relationship, the device in Fig 6.3 left was used. Weights were loaded onto the top of the device. The resultant load was applied

[16]Dept. of Sport Science, Univ. Innsbruck, AT. email: Martin.Moessner@uibk.ac.at
[17]Dept. of Sport Science, Univ. Innsbruck, AT
[18]Dept. of Sport Science, Univ. Innsbruck, AT
[19]Dept. of Sport Science, Univ. Innsbruck, AT
[20]HTM Tyrolia, Schwechat, AT

through the vertical pole to the edged ski with the length L. Penetration depth e and edging angle β were recorded with respect to the load F supplied. Snow hardness H varied from 0.1 N/mm^3 for groomed new snow to 70 N/mm^3 for glacier ice. Edging angles were prescribed with 15, 30, 45, and 60°. 224 series of measurements with loads ranging from 12 to 408 N were taken.

Model.

The contact pressure p at the base of the tool is modeled as a polynomial in e, β, and H. Integration over the contact area gives the reaction force $F = \int_A p\,dxdy$. The recorded amount of data leads to a large set of least squares equations for the coefficients of the contact pressure p, respectively, the reaction force F. Additionally pressure and reaction force have to be positive and must increase with increasing penetration depth. The regression equations and the constraints lead to a linearly constrained linear least squares problem, which is solved by NAG library functions. Techniques of mathematical statistics are supplied to select the terms needed in the representation of p and to calculate confidence intervals.

Results.

The force-penetration relationship shows that the reaction force is proportional to the volume of the displaced snow: $p = cHe$ and $F = cHV$ with $V = Le^2/2tan\beta$. The constant of proportionality c is 1.21±0.06.

Higher order correction terms depending on the edging angle and the snow hardness could be obtained

$$\begin{aligned} p &= a + be \\ F &= \frac{L}{\tan\beta}\left(ae + b\frac{e^2}{2}\right) \end{aligned} \qquad \begin{aligned} a &= c_1\beta + c_2H + c_3\beta^2H, \\ b &= c_4H \end{aligned}$$

Coefficients and 10 % confidence intervals are $c_1 = 0.45 \pm 0.14$, $c_2 = 0.06 \pm 0.02$, $c_3 = 0.20 \pm 0.07$, and $c_4 = 0.45 \pm 0.18$.

Ultimate Shear Pressure of Snow

Data Collection.

The tool showed in Fig 6.3 right was fixed with a slalom pole anchorage into the snow. Plates with the width B were positioned with prescribed penetration depth e and edging angle β in the snow and a moment M about the vertical axis was supplied by hand until shearing started. Through the lever arm r the moment was assigned as shearing Force F to the snow. 79 experiments were conducted for various types of snow and different edging angles β.

Model.

From the data the ultimate shear pressure p is calculated by

$$p = \frac{M}{rBe}.$$

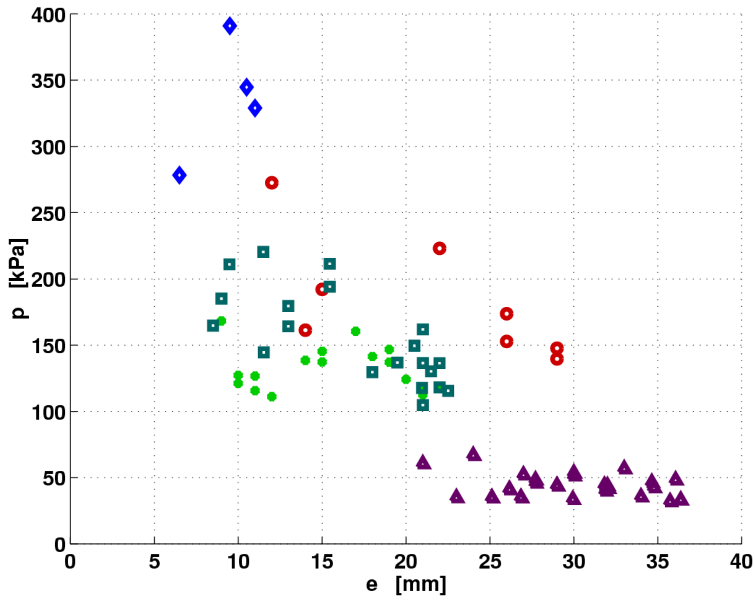

Fig. 6.4: Ultimate shear pressure of snow

Results.

The entity of our measurements is given in Fig 6.4. Different colors refer to different snow conditions. The ultimate shear pressure ranged from 50 to 400 kPa. No significant dependency of the ultimate shear pressure on penetration depth or edging angle could be verified.

Summary

Devices for the determination of mechanical properties of snow were developed. Considerably different snow conditions were investigated. From the data, models for the force-penetration relationship and the ultimate shear pressure were obtained. These models proved to be suitable for the simulation of the ski-snow interaction.

6.6 P. Kaps, W. Nachbauer, and M. Mössner, Snow Friction and Drag in Alpine Downhill Racing, 4th World Congress of Biomechanics. 2002

Reference: P. Kaps[21], W. Nachbauer[22], and M. Mössner[23], *Snow Friction and Drag in Alpine Downhill Racing*, Abstract Book, 4th World Congress of Biomechanics (Calgary, CA), Aug 2002.

Introduction

For training purposes we want to visualize an Alpine downhill slope from the view of an elite skier. As slope we have chosen the Streif, a famous and difficult Alpine downhill run in Kitzbühel, AT. The surface of the slope between the starting area and the end of the Steilhang was geodetically surveyed. The length is approximately 700 m, the difference in height 300 m. The first 30 runners of the FIS World Cup downhill event 2002 were recorded by video cameras. With direct linear transformation we obtained the trajectory of the fastest skier as a function of the time. We call the trajectory with the time history a path. It depends not only on the trajectory but also on the velocity of the skier. It is well known that the speed depends on the drag and the snow friction. These parameters depend strongly on the situation and the skill of the skier. Minimal values occur during straight running when the skier takes an egg position. The snow friction is considerably increased during turns when the skier edges, especially, if the turn is not optimally carved. The drag is increased during difficult parts of the track when the skier takes an upright position. Additionally, the optimal path depends on the strength of the skier. The skier has to exert forces onto the snow to keep his trajectory. These forces are limited due to the constitution of the skier and the consistency of snow.

Methods

For the fastest skier, a video analysis was performed. A typical frame is given in Fig 6.5. Here, the trajectory is represented, additionally. In each frame, the positions of the toe pieces of the bindings as well as the visible control points were manually digitized. With help of the direct linear transformation the position of the skier was obtained in real 3D object coordinates. Finally, the path was obtained by smoothing. For dynamic analyses, the skier is modeled as a mass point. The equation of motion is established in descriptor form Eq 6.4. The constraint g is given by the trajectory of the skier.

[21]Inst. for Basic Sciences in Engineering, Univ. Innsbruck, AT. email: Peter.Kaps@uibk.ac.at
[22]Dept. of Sport Science, Univ. Innsbruck, AT
[23]Dept. of Sport Science, Univ. Innsbruck, AT

$$
\begin{pmatrix} I & 0 & 0 & 0 \\ 0 & I & 0 & 0 \\ 0 & 0 & 0 & 0 \\ 0 & 0 & 0 & 0 \end{pmatrix} \begin{pmatrix} x \\ v \\ a \\ \lambda \end{pmatrix}' = \begin{pmatrix} v \\ a \\ Ma - f - r \\ Gv - g' \end{pmatrix} \tag{6.4}
$$

$$
g(x,t) = 0, \quad G = \frac{\partial g}{\partial x}, \quad g' = \begin{pmatrix} 0 \\ 0 \end{pmatrix}
$$

The applied forces f are assumed in the form

$$
f = \begin{pmatrix} 0 \\ 0 \\ -mg \end{pmatrix} - \mu N t - \frac{1}{2} c_d A \rho v^2 t, \qquad \text{with} \qquad \mathrm{t} = \frac{\mathrm{v}}{\|\mathrm{v}\|}. \tag{6.5}
$$

For the reaction forces r and the normal force N it holds

$$
r = -G^T \lambda, \qquad N = \|r\|. \tag{6.6}
$$

We assume that the drag $c_d A$ and the snow friction μ are piecewise constant. The values are determined by a least squares argument: the error between measured and computed positions is minimal.

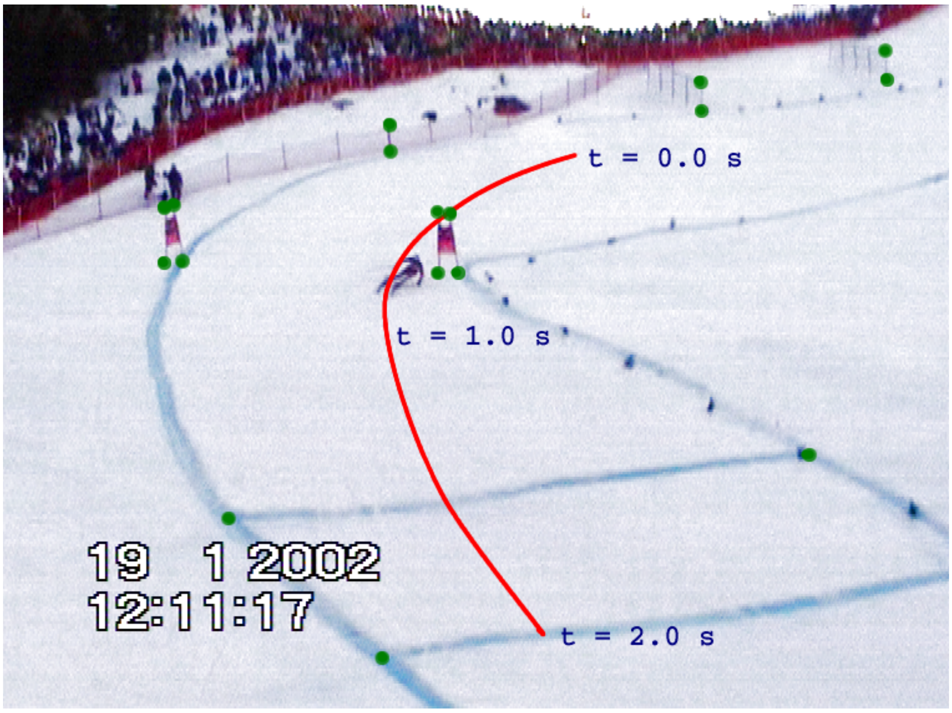

Fig. 6.5: Video frame with trajectory of the ski racer.

Results

We have computed snow friction and drag for the turn in Fig 6.5. The turn starts at t = 0 s end ends at t = 1.92 s. The results are given in Tab 6.2. The root mean square error is less than 2 cm.

	$t < 0.2$	$0.2 < t < 0.75$	$t > 0.75$
μ	0.2	0.45	0.05
$c_d A$	0.7	0.95	0.3

Tab. 6.2: Snow friction and drag for the turn in Fig 6.5.

Discussion

Despite of the short time passed since data collection we can present some preliminary results on a small portion of the investigated slope. We plan to visualize the downhill race from the view of a skier. We hope that the results can be used by the Austrian ski team for training purposes.

Acknowledgment

The research was supported by a Top Sport Austria project of the Austrian Ski Federation.

6.7 M. Mössner, D. Heinrich, P. Kaps, K. Schindelwig, P. Lugner, H.B. Schmiedmayer, H. Schretter, and W. Nachbauer, Modeling of the Ski-Snow Contact for a Carved Turn, International Congress on Mountain and Sport, 2005

Reference: M. Mössner[24], D. Heinrich[25], K. Schindelwig[26], P. Lugner[27], H.B. Schmiedmayer[28], H. Schretter[29], and W. Nachbauer[30], *Modeling of the Ski-Snow Contact for a Carved Turn*, Programme and Book of Abstracts, International Congress on Mountain and Sport (Rovereto, IT) (F. Schena, G. Ferretti, P. Tosi, C. Capelli, and G. Fumagalli, eds.), Nov 2005, p. 64.

Introduction

We investigate carved turns with Alpine skis. During the movement of a ski, snow is loaded and unloaded. Compacted snow is not elastic, i.e. deformations remain. Such effects are modeled by a hypoplastic constitutive equation. During a turn the shovel digs into the snow and the rear part of the ski keeps nearly the same penetration depth as the part with maximum load. This results in a higher resistance against shearing for the afterbody of the ski. In the present work we investigate the benefits of the hypoplastic against the elastic force law. Simulation results for a sledge on two skis will be compared to experimental track data.

Method

The sledge and the skis were modeled as a system of rigid bodies. Bending and torsional stiffness were translated to rotational springs with given spring and damping coefficients. The values for the constants were taken from experiments on real skis [13, 14]. For the calculation of the contact forces we attached a smooth surface at the bottom of the rigid segments of each ski. This surface coincides with the midpoints and tangential directions of the bases of the ski segments. We call this surface the running surface of the ski. All force calculations were calculated with respect to the running surface. For penetration the contact forces were modeled using a hypoplastic constitutive equation [29]. Because of this, reaction forces are different during loading and unloading of the ski. Shearing forces were limited by supplying an ultimate pressure that snow can withstand.

Three experiments were designed in order to determine the properties of snow: 1) the elastic force-penetration relationship for static loading was obtained, 2) the ultimate shear pressure of snow was determined, and 3) the dynamic behavior of snow, such as loading/unloading and cutting, was investigated.

[24]Dept. of Sport Science, Univ. Innsbruck, AT. email: Martin.Moessner@uibk.ac.at
[25]Dept. of Sport Science, Univ. Innsbruck, AT
[26]Dept. of Sport Science, Univ. Innsbruck, AT
[27]Dept. of Mechanics and Mechatronics, Vienna Univ. of Technology, AT
[28]Dept. of Mechanics and Mechatronics, Vienna Univ. of Technology, AT
[29]HTM Tyrolia, Schwechat, AT
[30]Dept. of Sport Science, Univ. Innsbruck, AT

In order to assess the validity of the improved snow contact model the movement of the sledge was recorded on a slope. Simulation results for the hypoplastic and the elastic constitutive equation were compared to the measured track data.

Results/Discussion

The implementation proofed to be suitable to simulate the movement of a self-running sledge on skis. The penetration depth is more realistic for the hypoplastic than for the elastic constitutive equation. For the hypoplastic force law the rear part of the ski penetrates deeper into the snow than for the elastic force law. The sledge on skis gets a better side guidance. Hence faster turn velocities are possible.

The model can be used to study the influence of construction properties of the skis (bending/torsional stiffness, shape, ...) as well as of the snow conditions. Results to such investigations will be published elsewhere.

Acknowledgment

The investigation was supported by HTM Tyrolia.

References

[1] Y.I. Abdel-Aziz and H.M. Karara, *Direct Linear Transformation from Comparator Coordinates into Object Space Coordinates in Close-Range Photogrammetry*, ASP Symposium on Close Range Photogrammetry (Falls Church, US-VA), American Society of Photogrammetry (ASP), 1971, pp. 1–18.

[2] N. Aichner, *Bodendruckverteilung und Formänderungswiderstand beim gleitenden Schi*, Ph.D. Thesis, Graz University of Technology, AT, 1978.

[3] M. Akkok and C.M. Ettles and, *Parameters Affecting the Kinetic Friction of Snow*, Journal of Tribology **109** (1987), 552–561.

[4] W. Ambach and, *Ski Gliding and Water Film*, Cold Regions Science and Technology **5** (1981), 59–65.

[5] E. Anderson, Z. Bai, C.H. Bischof, J.W. Demmel, J.J. Dongarra, J. du Croz, A. Greenbaum, S. Hammarling, A. McKenney, S. Ostrouchov, and D. Sorensen, *LAPACK Users' Guide*, Society for Industrial and Applied Mathematics (SIAM), Philadelphia, US-PA, 1992.
`http://netlib.org/lapack/index.html`

[6] R.M. Angulo and J. Dapena, *Comparison of Film and Video Techniques for Estimating Three-Dimensional Coordinates within a Large Field*, International Journal of Sport Biomechanics **8** (1992), 145–151.

[7] K.A. Ball and M.R. Pierrynowski, *A Modified Direct Linear Transformation (DLT) Calibration Procedure to Improve the Accuracy of 3D Reconstruction for Large Vols*, Biomechanics XI-B (Amsterdam, NL) (G. de Groot, A.P. Hollander, P.A. Huijing, and G.J. van Ingen Schenau, eds.), Free University Press, 1988, pp. 1045–1050.

[8] H. Bopp and H. Krauss, *A Simple and Rapidly Converging Orientation and Calibration Method for non Topographic Applications*, Proceedings of the ASP (Falls Church, US-VA), American Society of Photogrammetry (ASP), 1977, pp. 425–432.

[9] F.P. Bowden, *Friction on Snow and Ice*, Proceedings of the Royal Society of London **A217** (1953), 462–478.

[10] F.P. Bowden and T.P. Hughes, *The Mechanism of Sliding on Ice and Snow*, Proceedings of the Royal Society of London **A172** (1939), 280–298.

[11] V. Brasey, *HEM5 User's Guide*, Report, Section de Mathématiques, Université de Genéve, CH, 1995.
`http://www.unige.ch/ hairer/software.html`

[12] C.A. Brown and J.O. Outwater, *On the Skiability of Snow*, Skiing Trauma and Safety, 7th vol., ASTM STP 1022 (Philadelphia, US-PA) (R.J. Johnson, C.D. Mote, and M.H. Binet, eds.), American Society for Testing and Materials (ASTM), 1989, pp. 329–336.

[13] F. Bruck, *Das dynamische Verhalten von Schi und Schnee im alpinen Schilauf. Modellbildung, Simulation, Validierung*, Ph.D. Thesis, Department of Mechanics and Mechatronics, Vienna University of Technology, AT, 2003.

[14] F. Bruck, P. Lugner, and H. Schretter, *A Dynamic Model for the Performance of Carving Skis*, Skiing Trauma and Safety, 14th vol., ASTM STP 1440 (West Conshohocken, US-PA) (R.J. Johnson, M.K. Lamont, and J.E. Shealy, eds.), American Society for Testing and Materials (ASTM), 2003, pp. 10–23.

[15] F. Casolo, V. Lorenzi, M. Giorla, and R. Messironi, *Relevance of Ski Mechanical and Geometrical Properties in Carving Technique: A Dynamic Simulation*, 2nd International Congress on Skiing and Science (ICSS) (St. Christoph am Arlberg, AT) (E. Müller, R. Roithner, W. Niessen, C. Raschner, and H. Schwameder, eds.), International Congress on Skiing and Science (ICSS), 1999, pp. 46–47.

[16] J.H. Challis and D.G. Kerwin, *Accuracy Assessment and Control Point Configuration when Using the DLT for Photogrammetry*, Journal of Biomechanics **25** (1992), 1053–1058.

[17] S.C. Colbeck, *A Review of the Processes that Control Snow Friction*, Technical Report 92-2, Cold Regions Research and Engineering Laboratory (CRREL), Hanover, US-NH, 1992.

[18] S.C. Colbeck, *The Kinetic Friction of Snow*, Journal of Glaciology **34** (1988), 78–86.

[19] S.C. Colbeck and G.C. Warren, *The Thermal Response of Downhill Skis*, Journal of Glaciology **37** (1991), 228–235.

[20] J. Dapena, *Three-Dimensional Cinematography with Horizontal Panning Cameras*, Sciences et Motricité **1** (1978), 3–15.

[21] A. Deak, J. Jorgensen, and J. Vagners, *The Engineering Characteries of Snow Skis. Part 1: Static Bending and Torsional Characteristics*, Transactions of the American Society of Mechanical Engineers (ASME) Journal of Engineering for Industry **97** (1975), 131–137.

[22] C. de Boor, *A Practical Guide to Splines*, Springer, New York, US-NY, 1978.

[23] P. Deuflhard, *A Modified Newton Method for the Solution of Ill-Conditioned Systems of Nonlinear Equations with Applications to Multiple Shooting*, Numerische Mathematik **22** (1974), 289–315.

[24] P. Dierckx, *Curve and Surface Fitting with Splines*, Oxford University Press, Oxford, GB, 1993.

[25] M.P. do Carmo, *Differentialgeometrie von Kurven und Flächen*, Vieweg, Wiesbaden, DE, 1983.

[26] V. Drenk, *Erarbeitung von photogrammetrischen Auswerteverfahren für den Einsatz schwenkbarer Kameras in der Leistungssportforschung (Photogrammetric Analysis Methods for Pan and Tilt Cameras in Sports Research)*, Ph.D. Thesis, Forschungsinstitut für Körperkultur und Sport, Leipzig, DE, 1988.

[27] J. Erkkilä, T. Hämäläinen, P. Pihkala, S. Savolainen, and E. Spring, *A Cinematographic Method for Determination of the Kinetic Friction of Skis on Snow*, Report Series in Geophysics, vol. 21, University of Helsinki, FI, 1985.

[28] C.D.B. Evans, J.F. Nye, and K.J. Cheeseman, *The Kinetic Friction of Ice*, Proceedings of the Royal Society of London **A347** (1976), 493–512.

[29] W. Fellin, *Hypoplastizität für Einsteiger (Hypoelasticity for beginners)*, Bautechnik **77** (2000), 10–14.
`http://geotechnik.uibk.ac.at/res/hypopl.html`

[30] F. Fetz, *Biomechanische Analyse alpiner Zieleinfahrtechniken (Biomechanical analysis of finishing techniques in alpine ski racing)*, Zur Biomechanik des Schilaufs (F. Fetz, ed.), Inn-Verlag, Innsbruck, AT, 1977, 68–79.

[31] J.M. Figueras, F. Escalas, A. Vidal, R. Morgenstern, J.M. Buló, J.A. Merino, and J.M. Espada-Gamisans, *The Anterior Cruciate Ligament Injury in Skiers*, Skiing Trauma and Safety 6th vol., ASTM STP 938 (Philadelphia, US-PA) (C.D. Mote and R.J. Johnson, eds.), American Society for Testing and Materials (ASTM), 1987, pp. 55–60.

[32] W. Förg-Rob and W. Nachbauer, *Use of Spline-Functions in the Smoothing of Film Data for Slalom Ski Racers*, International Journal of Sport Biomechanics **4** (1988), 166–177.

[33] K.G.M. Gerritsen, W. Nachbauer, and A.J. van den Bogert, *Simulation of Landing Movement in Downhill Skiing: Validation Using Experimental Data*, Proceedings of the Eighth Biennial Conference (Calgary, CA), Canadian Society for Biomechanics, 1994, pp. 192–163.

[34] P.E. Gill, W. Murray, and M.H. Wright, *Practical Optimization*, Academic Press, Inc., London, GB, 1995.

[35] B. Glenne, *Sliding Friction and Boundary Lubrication of Snow*, Journal of Tribology **109** (1987), 614–617.

[36] G.H. Golub and C.F. van Loan, *Matrix Computations*, 2nd ed., The Johns Hopkins University Press, Baltimore, US-MD, 1991.

[37] G.H. Golub and C.F. van Loan, *An Analysis of the Total Least Squares Problem*, SIAM Journal on Numerical Analysis **17** (1980), 883–893.

[38] S.M. Gorlin, M.M. Maseev, W.A. Zyrjanow, and L.L. Remizov, *Sliding Friction and Boundary Lubrication of Snow*, Teorija i praktika fizicheskoj kultury **2** (1972), 65–66.

[39] B. Habel, *Über die Bestimmung von Luftwiderstand und Gleitreibung beim Skilauf*, Europa-Sport **20** (1968), 950–955.

[40] E. Hairer, S.P. Nørsett, and G. Wanner, *Solving Ordinary Differential Equations I. Nonstiff Problems*, 2nd ed., Springer Series in Computational Mathematics, vol. 8, Springer, Berlin, DE, 1993.

[41] E. Hairer and G. Wanner, *Solving Ordinary Differential Equations II. Stiff and Differential-Algebraic Problems*, Springer Series in Computational Mathematics, vol. 14, Springer, Berlin, DE, 1991.

[42] E.P. Hanavan, *A Mathematical Model of the Human Body*, AMRL-TR-64-102, Wright-Patterson Air Force Base, US-OH, 1964.

[43] H. Hatze, *High-Precision Three-Dimensional Photogrammetric Calibration and Object Space Reconstruction Using a Modified DLT-Approach*, Journal of Biomechanics **21** (1988), 533–538.

[44] E.J. Haug, *Computer Aided Kinematics and Dynamics of Mechanical Systems. Vol. I: Basic Methods*, Allyn and Bacon, Boston, US-MA, 1989.

[45] D. Heinrich, M. Mössner, P. Kaps, H. Schretter, and W. Nachbauer, *Influence of Ski Bending Stiffness on the Turning Radius of Alpine Skis at Different Edging Angles and Velocities*, 6th Engineering of Sport Conference (Munich, DE), 2006.

[46] D. Heinrich, M. Mössner, P. Kaps, H. Schretter, and W. Nachbauer, *Influence of Ski Bending Stiffness on the Turning Radius of Alpine Skis at Different Edging Angles and Velocities - A Computer Simulation*, Programme and Book of Abstracts, International Congress on Mountain and Sport (Rovereto, IT) (F. Schena, G. Ferretti, P. Tosi, C. Capelli, and G. Fumagalli, eds.), Nov 2005, p. 44.

[47] W. Herzog and L. Read, *Anterior Cruciate Ligament Forces in Alpine Skiing*, Journal of Applied Biomechanics **9** (1993), 260–278.

[48] Y. Hirano and N. Tada, *Mechanics of the turning snow ski*, International Journal on Mechanical Sciences **36** (1994), 421–429.

[49] S.F. Hoerner, *Fluid-Dynamic Drag, Practical Information on Aerodynamic Drag and Hydrodynamic Resistance*, published by the author, New York, US-NY, 1965.

[50] J. Howe, *Skiing Mechanics*, Poudre Press, Laporte, US-CO, 1983.

[51] E. Jenner, *Ausgewählte Einflussgrößen auf den Kurvenradius von Alpinschiern unter spezieller Berücksichtigung spezieller Fußstellungen*, Diploma Thesis, Department of Sport Science, University of Innsbruck, AT, 1997.

[52] P. Kaps, *Pressure Distribution under an Edged Ski*, Public Lecture held at the 2nd International Congress on Skiing and Science (ICSS), St. Christoph am Arlberg, AT, 9-15 Jan 2000.

[53] P. Kaps, *Determination of Kinetic Friction and Drag Area in Alpine Skiing*, Public Lecture held at the 10th International Congress on Skiing Trauma and Skiing Safety (ICSTSS), International Society for Skiing Safety (ISSS), Kaprun/Zell am See, AT, 17-21 May 1993.

[54] P. Kaps, M. Mössner, and W. Nachbauer, *Kurvenradius bei geschnittenen Schwüngen*, Report 3-2000, Institute for Basic Sciences in Engineering, University of Innsbruck, AT, Feb 2000.

[55] P. Kaps, M. Mössner, and W. Nachbauer, *Messung von Gleitreibung und Luftwiderstand bei Hangschrägfahrt*, Report, Institute for Basic Sciences in Engineering, University of Innsbruck, AT, May 1992.

[56] P. Kaps, M. Mössner, W. Nachbauer, and R. Stenberg, *Pressure Distribution Under a Ski During Carved Turns*, Science and Skiing (Hamburg, DE) (E. Müller, H. Schwameder, C. Raschner, S. Lindiger, and E. Kornexl, eds.), Verlag Dr. Kovac, 2001, pp. 180–202.

[57] P. Kaps, M. Mössner, W. Nachbauer, and R. Stenberg, *Pressure Distribution under an Edged Ski*, Abstract Book, 2nd International Congress on Skiing and Science (ICSS) (St. Christoph am Arlberg, AT) (E. Müller, R. Roithner, W. Niessen, C. Raschner, and H. Schwameder, eds.), 2000, pp. 48–49.

[58] P. Kaps, W. Nachbauer, and M. Mössner, *Snow Friction and Drag in Alpine Downhill Racing*, Abstract Book, 4th World Congress of Biomechanics (Calgary, CA), Aug 2002.

[59] P. Kaps, W. Nachbauer, and M. Mössner, *Determination of Kinetic Friction and Drag Area in Alpine Skiing*, Ski Trauma and Skiing Safety: 10th Volume, ASTM STP 1266 (Philadelphia, US-PA) (C.D. Mote, R.J. Johnson, W. Hauser, and P.S. Schaff, eds.), American Society for Testing and Materials (ASTM), 1996, pp. 165–177.

[60] P.W. Kennedy, D.L. Wright, and G.A. Smith, *Comparison of Film and Video Techniques for Three-Dimensional DLT Repredictions*, International Journal of Sport Biomechanics **5** (1989), 457–460.

[61] B. Knünz, W. Nachbauer, M. Mössner, K. Schindelwig, and F. Brunner, *Track Analysis of Giant Slalom Turns of World Cup Racers*, Proceedings of the 5th Annual Congress of the European College of Sport Science (ECSS) (Jyväskylä, FI) (J. Avela, P.V. Komi, and J. Komulainen, eds.), University of Jyväskylä, FI, 2000, p. 399.

[62] D. Kuroiwa, *The Kinetic Friction on Snow and Ice*, Journal of Glaciology **19** (1977), 141–152.

[63] M.A.H. Leino and E. Spring, *Determination of the Coefficient of Kinetic Friction between Ski and Snow from Gliding Velocity of a Skier*, Report Series in Geophysics, vol. 19, University of Helsinki, FI, 1984.

[64] M.A.H. Leino, E. Spring, and H. Suominen, *Methods for the Simultaneous Determination of Air Resistance to a Skier and the Coefficient of Friction of his Skis on the Snow*, Wear **86** (1983), 101–104.

[65] D.K. Lieu and C.D. Mote, *Experiments in the Machining of Ice at Negative Rake Angles*, Journal of Glaciology **30** (1984), 77–81.

[66] D. Lind and S.P. Sanders, *The Physics of Skiing*, Springer, New York, US-NY, 1996.

[67] LMS International, Leuven, BE.
email: `info@lms.be`. URL: `http://www.lmsintl.com/`.

[68] C. Lubich, *Extrapolation Integrators for Constrained Multibody Systems*, Impact of Computing in Science and Engineering **3** (1991), 213–234.

[69] C. Lubich, U. Nowak, U. Pöhle, and C. Engstler, *MEXX – Numerical Software for the Integration of Constrained Mechanical Multibody Systems*, Preprint SC 92-12, Konrad-Zuse-Zentrum für Informationstechnik (ZIB), Berlin, DE, 1992.
`http://www.zib.de/Numerik/numsoft/CodeLib/index.en.html`

[70] L. Magerl, *Untersuchungen zur Dynamik von Alpinschiern mit einem Mehrkörperdynmaik-Simulations-Programm*, Diploma Thesis, Department of Mechanics and Mechatronics, Vienna University of Technology, AT, 2003.

[71] C.T. Marzan and H.M. Karara, *A Computer Program for Direct Linear Transformation Solution of the Collinearity Condition, and some Applications of it*, ASP Symposium on Close Range Photogrammetry (Falls Church, US-VA), American Society of Photogrammetry (ASP), 1975, pp. 420–449.

[72] S.M. Maxwell and M.L. Hull, *Measurement of Strength and Loading Variables on the Knee During Alpine Skiing*, Skiing Trauma and Safety, 7th vol., ASTM STP 1022 (Philadelphia, US-PA) (R.J. Johnson and C.D. Mote, eds.), American Society for Testing and Materials (ASTM), 1989, pp. 231–251.

[73] M. Mössner, *Reaktionskraft und Abscherfestigkeit von Pistenschnee*, Oral Presentation at the Department of Mechanics and Mechatronics, Vienna University of Technology, AT, 23 Mai 2000.

[74] M. Mössner, *Reaktionskraft und Abscherfestigkeit von Pistenschnee*, Oral Presentation at HTM Tyrolia, Schwechat, AT, 10 Dez 1999.

[75] M. Mössner, *Datenerfassung und Auswertung von Riesentorlauf- und Carving-Schwüngen*, Oral Presentation at HTM Tyrolia, Schwechat, AT, 10 Dez 1999.

[76] M. Mössner, *Digitize, Version 3.0, Deutsche Version*, Instruction Manual, Department of Sport Science, University of Innsbruck, AT, May 1999.

[77] M. Mössner, *Instruction Manual for F3D, ver. 3.02*, Instruction Manual, Department of Sport Science, University of Innsbruck, AT, Jan 1996.

[78] M. Mössner, *3-D Reconstruction of 2-D Video Data. The F3D Software Package*, Poster presented at the 15th Congress of the International Society of Biomechanics (ISB), Jyväskylä, FI, 2-6 Jul 1995.

[79] M. Mössner, *A Method for Obtaining 3-D Data in Alpine Skiing Using Pan and Tilt Cameras with Zoom Lenses*, Public Lecture held at the 10th International Congress on Skiing Trauma and Skiing Safety (ICSTSS), International Society for Skiing Safety (ISSS), Kaprun/Zell am See, AT, 17-21 May 1993.

[80] M. Mössner, *3D-Filmauswertung bei mitgeschwenkter und gezoomter Kamera*, Internal Report, Institute for Basic Sciences in Engineering, University of Innsbruck, AT, Aug 1992.

[81] M. Mössner, *3D-Filmanalyse von Skischwüngen bei mitgeschwenkter Kamera*, Public Lecture held at the Department of Sport Science, University of Innsbruck, AT (Lectures for guest professor B.M. Nigg, Human Performance Laboratorium (HPL), Calgary, CA), 22-27 Mar 1992.

[82] M. Mössner, D. Heinrich, K. Schindelwig, P. Kaps, P. Lugner, H.B. Schmiedmayer, H. Schretter, and W. Nachbauer, *Modelling of the Ski-Snow*

Contact for a Carved Turn, 6th Engineering of Sport Conference (Munich, DE), 2006.

[83] M. Mössner, D. Heinrich, P. Kaps, K. Schindelwig, P. Lugner, H.B. Schmiedmayer, H. Schretter, and W. Nachbauer, *Modeling of the Ski-Snow Contact for a Carved Turn*, Programme and Book of Abstracts, International Congress on Mountain and Sport (Rovereto, IT) (F. Schena, G. Ferretti, P. Tosi, C. Capelli, and G. Fumagalli, eds.), Nov 2005, p. 64.

[84] M. Mössner, G. Innerhofer, and W. Nachbauer, *Reaktionskräfte und Abscherfestigkeit von Pistenschnee*, Report, Department of Sport Science, University of Innsbruck, AT, Dez 1999.

[85] M. Mössner, P. Kaps, and W. Nachbauer, *A Method for Obtaining 3-D Data in Alpine Skiing Using Pan and Tilt Cameras with Zoom Lenses*, Skiing Trauma and Safety, 10th vol., ASTM STP 1266 (Philadelphia, US-PA) (C.D. Mote, R.J. Johnson, W. Hauser, and P.S. Schaff, eds.), American Society for Testing and Materials (ASTM), 1996, pp. 155–164.

[86] M. Mössner, P. Kaps, and W. Nachbauer, *Smoothing the DLT-Parameters for Moved Cameras*, Book of Abstracts: 15th Congress of the International Society of Biomechanics (ISB) (Jyväskylä, FI) (K. Häkkinen, K.L. Keskinen, P.V. Komi, and A. Mero, eds.), University of Jyväskylä, FI, 1995.

[87] M. Mössner, P. Kaps, and W. Nachbauer, *Smoothing the DLT-Parameters for Moved Cameras*, Poster presented at the 15th Congress of the International Society of Biomechanics (ISB), Jyväskylä, FI, 2-6 Jul 1995.

[88] M. Mössner and W. Nachbauer *Reaktionskraft und Abscherfestigkeit von Pistenschnee II*, Report, Department of Sport Science, University of Innsbruck, AT, Nov 2001.

[89] M. Mössner and W. Nachbauer, *Druckverteilung des Atomic Beta Ride und des Head Cyber Cross bei geschnittenen Schwüngen*, Report, Department of Sport Science, University of Innsbruck, AT, Aug 2000.

[90] M. Mössner, W. Nachbauer, *Reaktionskraft und Abscherfestigkeit von Pistenschnee*, Report, Department of Sport Science, University of Innsbruck, AT, Jun 2000.

[91] M. Mössner, W. Nachbauer, *Einfluss der Einstellung der Tyrolia Power Select Bindung auf den Schwungradius*, Report, Department of Sport Science, University of Innsbruck, AT, Dez 1999.

[92] M. Mössner, W. Nachbauer, G. Innerhofer, and H. Schretter, *Mechanical Properties of Snow on Ski Slopes*, Abstract Book, 15th International Congress on Skiing Trauma and Skiing Safety (ICSTSS) (St. Moritz / Pontresina, CH)

(G. Ahlbäumer, M.H. Binet, J. Haury, B.H. Hörterer, V. Senner, A.U. Urfer, and W. Vogt, eds.), 2003, pp. P–1.

[93] M. Mössner, W. Nachbauer, G. Innerhofer, and H. Schretter, *Mechanical Properties of Snow on Ski Slopes*, Poster presented at the 15th International Congress on Skiing Trauma and Skiing Safety (ICSTSS), St. Moritz / Pontresina, CH, 27 Apr - 2 May 2003.

[94] M. Mössner, W. Nachbauer, and K. Schindelwig, *Einfluss der Skitaillierung auf Schwungradius und Belastung*, Sportverletzung Sportschaden **11** (1997), 140–145.

[95] M. Mössner, W. Nachbauer, K. Schindelwig, G. Innerhofer, and H. Schretter, *Mechanical Properties of Snow on Ski Slopes*, Abstract Book, 5th International Congress on Snow Engineering (ICSE) (Davos, CH) (E. Adams, W. Ammann, E. Hjorth-Hansen, H. Norem, M.J. O'Rourke, A. Sato, and J. Johnson, eds.), 2004.

[96] E. Müller, F. Brunner, E. Kornexl, and C. Raschner, *Biomechanische Analyse von Starttechniken im alpinen Skirennlauf (Biomechanical Analysis of Starting Techniques in Alpine Ski Racing)*, Biomechanik der Sportarten. Band 2: Biomechanik des alpinen Skilaufs (F. Fetz and E. Müller, eds.), Ferdinand Enke Verlag, Stuttgart, DE, 1991, pp. 112–123.

[97] A. Murua, *PHEM56 user's guide*, Report, Konputazio Zientzia eta A. A., Informatika Fakultatea, EHU/UPV Donostia/San Sebastian, SP, 1995. `http://www.unige.ch/ hairer/software.html`

[98] W. Nachbauer, *Fahrlinie in Torlauf und Riesentorlauf (Line in Slalom and Giant Slalom)*, Leistungssport **17** (1987), 17–21.

[99] W. Nachbauer and P. Kaps, *Fahrzeitbestimmende Faktoren beim Schussfahren*, Biomechanik der Sportarten. Band 2: Biomechanik des alpinen Skilaufs (F. Fetz and E. Müller, eds.), Ferdinand Enke Verlag, Stuttgart, DE, 1991, pp. 101–111.

[100] W. Nachbauer, P. Kaps, and M. Mössner, *Determination of Kinetic Friction in Downhill Skiing*, Book of Abstracts, 8th Meeting of the European Society of Biomechanics (ESB) (Rome, IT), 1992, p. 333.

[101] W. Nachbauer, P. Kaps, B.M. Nigg, F. Brunner, A. Lutz, G. Obkircher, and M. Mössner, *A Video Technique for Obtaining 3-D Coordinates in Alpine Skiing*, Journal of Applied Biomechanics **12** (1996), 104–115.

[102] W. Nachbauer, P. Schröcksnadl, and B. Lackinger, *Effects of Snow and Air Conditions on Ski Friction*, Skiing Trauma and Safety, 10th vol., ASTM STP 1266 (Philadelphia, US-PA) (C.D. Mote, R.J. Johnson, W. Hauser, and

P.S. Schaff, eds.), American Society for Testing and Materials (ASTM), 1996, pp. 178–185.

[103] A.A. Nordt, *Design of Alpine Skis*, Ph.D. Thesis, Department of Aeronautics and Astronautics, Stanford University, US-CA, 1999.

[104] A.A. Nordt, G.S. Springer, and L.P. Kollr, *Computing the Mechanical Properties of Alpine Skis*, Sports Engineering **2** (1999), 65–84.

[105] Numerical Algorithms Group, NAG Ltd., Oxford, GB.
email: `sales@nag.co.uk www`. URL: `http://www.nag.co.uk/`.

[106] R.I. Perla and B. Glenne, *Skiing*, Handbook of snow (D.M. Grey and D.H. Male, eds.), Pergamon Press, Toronto, CA, 1981, pp. 709–740.

[107] E. Pestel and J. Wittenburg, *Technische Mechanik. Band 2: Festigkeitslehre*, BI Wissenschaftsverlag, Mannheim, DE, 1992.

[108] R. Preiss, *PHANA, Fortran Program to Compute the Inertia Parameter according to Hanavan*, Tech. Report, Department of Sport Science, University of Frankfurt, DE, 1983.

[109] W.H. Press, S.A. Teukolsky, W.T. Vetterling, and B.P. Flannery, *Numerical Recipes in Fortran. The Art of Scientific Computing*, Cambridge University Press, Cambridge, GB, 1992.

[110] T.P. Quinn and C.D. Mote, *Prediction of the Loading Along the Leg During Snow Skiing*, Skiing Trauma and Safety, 9th vol., ASTM STP 1182 (Philadelphia, US-PA) (R.J. Johnson, C.D. Mote, and J. Zelcer, eds.), American Society for Testing and Materials (ASTM), 1993, pp. 128–149.

[111] L. Read and W. Herzog, *External Loading at the Knee Joint for Landing Movements in Alpine Skiing*, International Journal of Sport Biomechanics **8** (1992), 63–80.

[112] A.A. Renshaw and C.D. Mote, *A Model for the Turning Snow Ski*, Skiing Trauma and Safety, 8th vol., ASTM STP 1104 (Philadelphia, US-PA) (C.D. Mote and R.J. Johnson, eds.), American Society for Testing and Materials (ASTM), 1991, pp. 217–238.

[113] C.C. Roberts, *Numerical Modeling of the Transient Dynamics of a Skier while Gliding*, Biomechanics in Sport – A (E.D. Rekow et al., ed.), The American Society of Mechanical Engineers, New York, US-NY, 1987, pp. 77–82.

[114] P.S. Schaff and W. Hauser, *3-D Video Motion Analysis on the Slope - A Practical Way to Analyze Motion Patterns in Alpine Skiing*, Skiing Trauma and Safety, 9th vol., ASTM STP 1182 (Philadelphia, US-PA) (R.J. Johnson, C.D. Mote, and J. Zelcer, eds.), American Society for Testing and Materials (ASTM), 1993, pp. 165–177.

[115] M. Schiestl, P. Kaps, M. Mössner, and W. Nachbauer, *Calculation of Friction and Reaction Forces During an Alpine World Cup Downhill Race*, 6th Engineering of Sport Conference (Munich, DE), 2006.

[116] M. Schiestl, P. Kaps, M. Mössner, and W. Nachbauer, *Snow Friction and Drag During the Downhill Race in Kitzbühel*, Programme and Book of Abstracts, International Congress on Mountain and Sport (Rovereto, IT) (F. Schena, G. Ferretti, P. Tosi, C. Capelli, and G. Fumagalli, eds.), Nov 2005, p. 54.

[117] H. Schlichting, *Grenzschichttheorie*, Verlag G. Braun, Karlsruhe, DE, 1958.

[118] W. Schnell, D. Gross, and W. Hauger, *Technische Mechanik. Band 2: Elastostatik*, Springer Lehrbuch, vol. 2, Springer, Berlin, DE, 1995.

[119] E. Spring, S. Savolainen, J. Erkkilä, T. Hämäläinen, and P. Pihkala, *Drag Area of a Cross-Country Skier*, International Journal of Sport Biomechanics **4** (1988), 103–113.

[120] B. van Gheluwe, *Computerized Three-Dimensional Cinematography for any Arbitrary Camera Setup*, Biomechanics VI-A (E. Asmussen and K. Jorgensen, eds.), University Park Press, Baltimore, US-MD, 1978, pp. 343–348.

[121] S. van Huffel and J. Vandewalle, *The Total Least Squares Problem. Computational Aspects and Analysis*, Society for Industrial and Applied Mathematics (SIAM), Philadelphia, US-PA, 1991.

[122] G.J. van Ingen Schenau, *The Influence of Air Friction in Speed Skating*, Journal of Biomechanics **15** (1982), 449–458.

[123] J.S. Walton, *Close-Range Cine-Photogrammetry: A Generalized Technique for Quantifying Gross Human Motion*, Ph.D. Thesis, The Pennsylvania State University, US-PA, 1981.

[124] G.C. Warren, S.C. Colbeck, and F.E. Kennedy, *Thermal Response of Downhill Skis*, Technical Report 89-23, Cold Regions Research and Engineering Laboratory (CRREL), Hanover, US-NH, 1989.

[125] H.J. Woltring, *A Fortran Package for Generalized Cross Validatory Spline Smoothing and Differentiation*, Adv. Eng. Software **8** (1986), 104–107.

[126] G.A. Wood and R.N. Marshall, *The Accuracy of DLT Extrapolation in Three-Dimensional Film Analysis*, Journal of Biomechanics **19** (1986), 781–785.

[127] C. Wurm, *Untersuchungen und Parameterstudien zur dynmaischen Simulation von Carvingschwüngen im alpinen Schilauf mit einem MKS-Modell*, Diploma Thesis, Department of Mechanics and Mechatronics, Vienna University of Technology, AT, 2002.

[128] M.R. Yeadon, *A Method for Obtaining Three-Dimensional Data on Ski Jumping Using Pan and Tilt Cameras*, International Journal of Sport Biomechanics **5** (1989), 238–247.

The Author's Publication List

Several of the publications given below can be obtained as pdf-document form the author's home page:

`http://sport1.uibk.ac.at/mm/publ/`

Papers

[10] M. Mössner, D. Heinrich, K. Schindelwig, P. Kaps, P. Lugner, H.B. Schmiedmayer, H. Schretter, and W. Nachbauer, *Modelling of the Ski-Snow Contact for a Carved Turn*, 6th Engineering of Sport Conference (Munich, DE), 2006.

[9] D. Heinrich, M. Mössner, P. Kaps, H. Schretter, and W. Nachbauer, *Influence of Ski Bending Stiffness on the Turning Radius of Alpine Skis at Different Edging Angles and Velocities*, 6th Engineering of Sport Conference (Munich, DE), 2006.

[8] M. Schiestl, P. Kaps, M. Mössner, and W. Nachbauer, *Calculation of Friction and Reaction Forces During an Alpine World Cup Downhill Race*, 6th Engineering of Sport Conference (Munich, DE), 2006.

[7] P. Kaps, M. Mössner, W. Nachbauer, and R. Stenberg, *Pressure Distribution Under a Ski During Carved Turns*, Science and Skiing (Hamburg, DE) (E. Müller, H. Schwameder, C. Raschner, S. Lindiger, and E. Kornexl, eds.), Verlag Dr. Kovac, 2001, pp. 180–202.

[6] M. Mössner, W. Nachbauer, and K. Schindelwig, *Einfluss der Skitaillierung auf Schwungradius und Belastung*, Sportverletzung Sportschaden **11** (1997), 140–145.

[5] W. Nachbauer, K. Schindelwig, and M. Mössner, *Standhöhe und Kniebelastung im alpinen Skilauf*, SKI. Mitteilungen des Österreichischen Arbeitskreises Skilauf an Schulen & Hochschulen **20** (Mar 1997), 18–19.

[4] W. Nachbauer, P. Kaps, B.M. Nigg, F. Brunner, A. Lutz, G. Obkircher, and M. Mössner, *A Video Technique for Obtaining 3-D Coordinates in Alpine Skiing*, Journal of Applied Biomechanics **12** (1996), 104–115.

[3] P. Kaps, M. Mössner, and W. Nachbauer, *Determination of Kinetic Friction and Drag Area in Alpine Skiing*, Skiing Trauma and Safety, 10th vol., ASTM STP 1266 (Philadelphia, US-PA) (C.D. Mote, R.J. Johnson, W. Hauser, and P.S. Schaff, eds.), American Society for Testing and Materials (ASTM), 1996, pp. 165–177.

[2] M. Mössner, P. Kaps, and W. Nachbauer, *A Method for Obtaining 3-D Data in Alpine Skiing Using Pan and Tilt Cameras with Zoom Lenses*, Skiing Trauma and Safety, 10th vol., ASTM STP 1266 (Philadelphia, US-PA) (C.D. Mote, R.J. Johnson, W. Hauser, and P.S. Schaff, eds.), American Society for Testing and Materials (ASTM), 1996, pp. 155–164.

[1] M. Mössner and J. Pfleiderer, *Automatic Analysis for Time-Series with Large Gaps*, Proceedings of the 5th ESO/ST-ECF Data Analysis Workshop (Munich/Garching, DE) (P.J. Grosbøl and R.C.E. de Ruijsscher, eds.), European Southern Observatory (ESO), Sep 1993, pp. 197–202.

Reports

[20] W. Nachbauer, E. Kornexl, G. Daringer, M. Mössner, and A. Niederkofler, *Einrichtung eines Messplatzes zur Technikanalyse von Skispringern an der Skisprungschnaze Bergisel*, Report, Department of Sport Science, Österreichischer Skiverband (ÖSV), University of Innsbruck, AT, 2004.

[19] M. Mössner and W. Nachbauer, *Dehnungseigenschaften von Bändern*, Report, Department of Sport Science, University of Innsbruck, AT, Aug 2003.

[18] P. Kaps, W. Nachbauer, and M. Mössner, *Simulation in Alpine Skiing*, Report, Institute for Basic Sciences in Engineering, University of Innsbruck, AT, Mar 2003.

[17] M. Mössner, W. Nachbauer, K. Schindelwig, F. Brunner, F. Rainer, and C. Wurm, *Versuche mit dem Skischlitten am Kaunertaler Gletscher*, Report, Department of Sport Science, University of Innsbruck, AT, Nov 2002.

[16] M. Mössner and W. Nachbauer *Reaktionskraft und Abscherfestigkeit von Pistenschnee II*, Report, Department of Sport Science, University of Innsbruck, AT, Nov 2001.

[15] M. Mössner, W. Nachbauer, K. Schindelwig, F. Brunner, G. Innerhofer, and F. Bruck, *Versuche mit dem Skischlitten in Stuben*, Report, Department of Sport Science, University of Innsbruck, AT, May 2001.

[14] M. Mössner, *Berechnung der Biegesteifigkeit von Skiern*, Internal Report, Department of Sport Science, University of Innsbruck, AT, Jan 2001.

[13] M. Mössner and W. Nachbauer, *Versuche mit dem Skischlitten: Materialdaten*, Report, Department of Sport Science, University of Innsbruck, AT, Sep 2000.

[12] M. Mössner and W. Nachbauer, *Druckverteilung des Atomic Beta Ride und des Head Cyber Cross bei geschnittenen Schwüngen*, Report, Department of Sport Science, University of Innsbruck, AT, Aug 2000.

[11] M. Mössner and W. Nachbauer, *Reaktionskraft und Abscherfestigkeit von Pistenschnee*, Report, Department of Sport Science, University of Innsbruck, AT, Jun 2000.

[10] P. Kaps, M. Mössner, and W. Nachbauer, *Kurvenradius bei geschnittenen Schwüngen*, Report 3-2000, Institute for Basic Sciences in Engineering, University of Innsbruck, AT, Feb 2000.

[9] M. Mössner, G. Innerhofer, and W. Nachbauer, *Reaktionskräfte und Abscherfestigkeit von Pistenschnee*, Report, Department of Sport Science, University of Innsbruck, AT, Dez 1999.

[8] M. Mössner and W. Nachbauer, *Einfluss der Einstellung der Tyrolia Power Select Bindung auf den Schwungradius*, Report, Department of Sport Science, University of Innsbruck, AT, Dez 1999.

[7] M. Mössner, *Ski-Modellierung*, Internal Report, Department of Sport Science, University of Innsbruck, AT, Mar 1998.

[6] M. Mössner, *Fast Nonuniform Random Number Generation*, Report, Department of Sport Science, University of Innsbruck, AT, Jun 1997.

[5] W. Nachbauer, K. Schindelwig, and M. Mössner, *Zur Auswirkung der Standhöhe auf Verletzungen im alpinen Skirennsport*, Report, Department of Sport Science, University of Innsbruck, AT, Apr 1997.

[4] W. Nachbauer, *Verstellbare Bindungsplatte*, Report, Department of Sport Science, Österreichischer Skiverband (ÖSV), University of Innsbruck, AT, Jan 1997.

[3] M. Mössner, N. Netzer, and J. Pfleiderer, *Efficient Computing of the Anderson-Darling Test Statistic*, Internal Report, Institut of Astronomy, University of Innsbruck, AT, 1994.

[2] M. Mössner, *3D-Filmauswertung bei mitgeschwenkter und gezoomter Kamera*, Report, Institute for Basic Sciences in Engineering, University of Innsbruck, AT, Aug 1992.

[1] P. Kaps, M. Mössner, and W. Nachbauer, *Messung von Gleitreibung und Luftwiderstand bei Hangschrägfahrt*, Report, Institute for Basic Sciences in Engineering, University of Innsbruck, AT, May 1992.

Abstracts

[16] M. Mössner, D. Heinrich, P. Kaps, K. Schindelwig, P. Lugner, H.B. Schmiedmayer, H. Schretter, and W. Nachbauer, *Modeling of the Ski-Snow Contact for a Carved Turn*, Programme and Book of Abstracts, International Congress on Mountain and Sport (Rovereto, IT) (F. Schena, G. Ferretti, P. Tosi, C. Capelli, and G. Fumagalli, eds.), Nov 2005, p. 64.

[15] D. Heinrich, M. Mössner, P. Kaps, H. Schretter, and W. Nachbauer, *Influence of Ski Bending Stiffness on the Turning Radius of Alpine Skis at Different Edging Angles and Velocities - A Computer Simulation*, Programme and Book of Abstracts, International Congress on Mountain and Sport (Rovereto, IT) (F. Schena, G. Ferretti, P. Tosi, C. Capelli, and G. Fumagalli, eds.), Nov 2005, p. 44.

[14] M. Schiestl, P. Kaps, M. Mössner, and W. Nachbauer, *Snow Friction and Drag During the Downhill Race in Kitzbühel*, Programme and Book of Abstracts, International Congress on Mountain and Sport (Rovereto, IT) (F. Schena, G. Ferretti, P. Tosi, C. Capelli, and G. Fumagalli, eds.), Nov 2005, p. 54.

[13] D. Heinrich, M. Mössner, W. Nachbauer, and H. Schretter, *Zum Einfluss der Biegesteifigkeit auf dne Schwungradius von Alpinski*, Kurzfassungen der Beiträge der 10-ten Tagung der Österreichischen Sportwissenschaftlichen Gesellschaft (ÖSG) (Schladming/Pichl, AT) (M. Sust and S. Titze, eds.), 17-19 Nov 2004.

[12] M. Mössner, W. Nachbauer, K. Schindelwig, G. Innerhofer, and H. Schretter, *Mechanical Properties of Snow on Ski Slopes*, Abstract Book, 5th International Congress on Snow Engineering (ICSE) (Davos, CH) (E. Adams, W. Ammann, E. Hjorth-Hansen, H. Norem, M.J. O'Rourke, A. Sato, and J. Johnson, eds.), 2004.

[11] M. Mössner, W. Nachbauer, G. Innerhofer, and H. Schretter, *Mechanical Properties of Snow on Ski Slopes*, Abstract Book, 15th International Congress on Skiing Trauma and Skiing Safety (ICSTSS) (St. Moritz / Pontresina, CH) (G. Ahlbäumer, M.H. Binet, J. Haury, B.H. Hörterer, V. Senner, A.U. Urfer, and W. Vogt, eds.), 2003, pp. P–1.

[10] P. Kaps, W. Nachbauer, and M. Mössner, *Snow Friction and Drag in Alpine Downhill Racing*, Abstract Book, 4th World Congress of Biomechanics (Calgary, CA), Aug 2002.

[9] B. Knünz, W. Nachbauer, M. Mössner, K. Schindelwig, and F. Brunner, *Track Analysis of Giant Slalom Turns of World Cup Racers*, Proceedings of the 5th Annual Congress of the European College of Sport Science (ECSS) (Jyväskylä, FI) (J. Avela, P.V. Komi, and J. Komulainen, eds.), University of Jyväskylä, FI, 2000, p. 399.

[8] P. Kaps, M. Mössner, W. Nachbauer, and R. Stenberg, *Pressure Distribution under an Edged Ski*, Abstract Book, 2nd International Congress on Skiing and Science (ICSS) (St. Christoph am Arlberg, AT) (E. Müller, R. Roithner, W. Niessen, C. Raschner, and H. Schwameder, eds.), 2000, pp. 48–49.

[7] W. Nachbauer, K. Schindelwig, M. Mössner, and P. Kaps, *Forces and Moments at the Boot Sole During Carving*, Book of Abstracts, 17th Congress of the International Society of Biomechanics (ISB) (Calgary, CA) (W. Herzog and A. Jinha, eds.), University of Calgary, CA, 1999, p. 54.

[6] K. Schindelwig, W. Nachbauer, T. Schliernzauer, and M. Mössner, *Prediction of the Moments at the Knee Joint for Carving and Parallel Turns Technique*, Book of Abstracts, 17th Congress of the International Society of Biomechanics (ISB) (Calgary, CA) (W. Herzog and A. Jinha, eds.), University of Calgary, CA, 1999, p. 667.

[5] W. Nachbauer, M. Mössner, M. Burtscher, and K. Schindelwig, *Estimation of the Load on the Skier During Carving*, Book of Abstracts, 13th International Congress on Skiing Trauma and Skiing Safety (ICSTSS) (Breuil Cervinia, Aosta Valley, IT) (A. Ekeland, R.J. Johnson, and P. Zucco, eds.), International Society for Skiing Safety (ISSS), 1999, p. 100.

[4] P. Kaps, M. Mössner, and W. Nachbauer, *Effect of Ski and Snow Properties on the Turning Radius*, Book of Abstracts, 13th International Congress on Skiing Trauma and Skiing Safety (ICSTSS) (Breuil Cervinia, Aosta Valley, IT) (A. Ekeland, R.J. Johnson, and P. Zucco, eds.), International Society for Skiing Safety (ISSS), 1999, p. 101.

[3] J. Pfleiderer and M. Mössner, *Detection of Weak Periodic Signals from Irregularly Spaced Observations*, Astronomical Society of the Pacific Conference Series **83** (1995), 283–284.

[2] M. Mössner, P. Kaps, and W. Nachbauer, *Smoothing the DLT-Parameters for Moved Cameras*, Book of Abstracts: 15th Congress of the International Society of Biomechanics (ISB) (Jyväskylä, FI) (K. Häkkinen, K.L. Keskinen, P.V. Komi, and A. Mero, eds.), University of Jyväskylä, FI, 1995.

[1] W. Nachbauer, P. Kaps, and M. Mössner, *Determination of Kinetic Friction*

in Downhill Skiing, Book of Abstracts, 8th Meeting of the European Society of Biomechanics (ESB) (Rome, IT), 1992, p. 333.

Public Lectures

[10] M. Mössner and D. Heinrich, *Projekt: Fahrwerk. Jahresbericht 2005*, Oral Presentation at HTM Head, Kennelbach, AT, 27 Jan 2006,

[9] M. Mössner and D. Heinrich, *Projekt: Fahrwerk. Jahresbericht 2005*, Oral Presentation at HTM Tyrolia, Schwechat, AT, 16 Dez 2005,

[8] M. Mössner, *Improvement of the Model of the Ski-Snow Contact for a Carved Turn*, Oral Presentation at the International Congress on Mountain and Sport, Rovereto, IT, 12 Nov 2005.

[7] M. Mössner, *Reaktionskraft und Abscherfestigkeit von Pistenschnee*, Oral Presentation at the Department of Mechanics and Mechatronics, Vienna University of Technology, AT, 23 Mai 2000.

[6] M. Mössner, *Datenerfassung und Auswertung von Riesentorlauf- und Carving-Schwüngen*, Oral Presentation at HTM Tyrolia, Schwechat, AT, 10 Dez 1999.

[5] M. Mössner, *Reaktionskraft und Abscherfestigkeit von Pistenschnee*, Oral Presentation at HTM Tyrolia, Schwechat, AT, 10 Dez 1999.

[4] M. Mössner, *Einfluss der Einstellung der Tyrolia Power Select Bindung auf das Schwungverhalten*, Oral Presentation at HTM Tyrolia, Schwechat, AT, 10 Dez 1999.

[3] M. Mössner, *Modellierung mittels DAE's*, Oral Presentation Department of Sport Science, University of Innsbruck, AT (Biomechanische Modellierung im alpinen Skilauf, B.M. Nigg, Human Performance Laboratorium (HPL), Calgary, CA and W. Nachbauer, Department of Sport Science, AT), 14-18 Jun 1993.

[2] M. Mössner, *A Method for Obtaining 3-D Data in Alpine Skiing Using Pan and Tilt Cameras with Zoom Lenses*, Public Lecture held at the 10th International Congress on Skiing Trauma and Skiing Safety (ICSTSS), International Society for Skiing Safety (ISSS), Kaprun/Zell am See, AT, 17-21 May 1993.

[1] M. Mössner, *3D-Filmanalyse von Skischwüngen bei mitgeschwenkter Kamera*, Public Lecture held at the Department of Sport Science, University of

Innsbruck, AT (Lectures for guest professor B.M. Nigg, Human Performance Laboratorium (HPL), Calgary, CA), 22-27 Mar 1992.

Posters

[9] D. Heinrich, M. Mössner, P. Kaps, H. Schretter, and W. Nachbauer, *Influence of Ski Bending Stiffness on the Turning Radius of Alpine Skis at Different Edging Angles and Velocities - A Computer Simulation*, Poster presented at the International Congress on Mountain and Sport, Rovereto, IT, 11-12 Nov 2005.

[8] M. Schiestl, P. Kaps, M. Mössner, and W. Nachbauer, *Friction During Alpine Ski Racing*, Poster presented at the International Congress on Mountain and Sport, Rovereto, IT, 11-12 Nov 2005.

[7] M. Mössner, W. Nachbauer, G. Innerhofer, and H. Schretter, *Mechanical Properties of Snow on Ski Slopes*, Poster presented at the 15th International Congress on Skiing Trauma and Skiing Safety (ICSTSS), St. Moritz / Pontresina, CH, 27 Apr - 2 May 2003.

[6] B. Knünz, W. Nachbauer, M. Mössner, K. Schindelwig, and F. Brunner, *Track Analysis of Giant Slalom Turns of World Cup Racers*, Poster presented at the 5th Annual Congress of the European Colledge of Sport Science (ECSS), Jyväskylä, FI, 19-23 Jul 2000.

[5] K. Schindelwig, W. Nachbauer, T. Schliernzauer, and M. Mössner, *Forces and Moments at the Knee Joint for Carving and Parallel Turning*, Poster presented at the 2nd International Congress on Skiing and Science (ICSS) St. Christoph am Arlberg, AT, 9-15 Jan 2000.

[4] K. Schindelwig, W. Nachbauer, T. Schliernzauer, and M. Mössner, *Force and Moment at the Knee Joint for Carving and Parallel Turning*, Poster presented at the 17th Congress of the International Society of Biomechanics (ISB), Calgary, CA, 8-13 Aug 1999.

[3] M. Mössner, *3-D Reconstruction of 2-D Video Data. The F3D Software Package*, Poster presented at the 15th Congress of the International Society of Biomechanics (ISB), Jyväskylä, FI, 2-6 Jul 1995.

[2] M. Mössner, P. Kaps, and W. Nachbauer, *Smoothing the DLT-Parameters for Moved Cameras*, Poster presented at the 15th Congress of the International Society of Biomechanics (ISB), Jyväskylä, FI, 2-6 Jul 1995.

[1] M. Mössner and J. Pfleiderer, *Automatic Analysis for Time-Series with Large Gaps*, Poster presented at the 5th ESO/ST-ECF Data Analysis Workshop,

European Southern Observatory (ESO), Munich/Garching, DE, 26-27 Apr 1993.

Undisclosed Collaboration

[1] *Gutachten zum tödlichen Skirennunfall von Ulrike Maier am 29. 1. 1994 in Garmisch-Partenkirchen*, Department of Sport Science, AT, Aug 1994.

Instruction Manuals

[4] M. Mössner, *Digitize, Version 3.0, Deutsche Version*, Instruction Manual, Department of Sport Science, University of Innsbruck, AT, May 1999.

[3] M. Mössner, *Druckverteilung bei aufgekanteten Ski*, Instruction Manual, Department of Sport Science, University of Innsbruck, AT, Nov 1998.

[2] M. Mössner, *MM Toolbox, ver. 2.11*, Instruction Manual, Department of Sport Science, University of Innsbruck, AT, Jan 1998.

[1] M. Mössner, *Instruction Manual for F3D, ver. 3.02*, Instruction Manual, Department of Sport Science, University of Innsbruck, AT, Jan 1996.

Diploma Thesis

[1] M. Mössner, *Fourierreihen nach Eigenfunktionen regulärer Sturm-Liouvillescher-Randwertprobleme und deren Anwendung zur Berechnung von Fehlerabschätzungen für Separationslösungen partieller Differentialgleichungen*, Diploma Thesis, Institute for Basic Sciences in Engineering, University of Innsbruck, AT, Okt 1988.

Curriculum Vitae

Martin Mössner
Galgenbühelweg 5, A–6020 Innsbruck, Austria
E-Mail: `martin.moessner@uibk.ac.at`
URL: `http://sport1.uibk.ac.at/mm/`

I was born on March 20th 1964 in Innsbruck, Austria as the son of the housewife Barbara Mössner, nèe Klammer, and the henceforth deceased plumber Heribert Mössner. I grew up in my parent's house. After attending elementary and secondary school, I finished my education with the German Matura, which qualifies for university entrance. In 1990 my daughter Elisabeth-Agnes was born.

During 1982 and 1989 I studied mathematics and physics at the Leopold Franzens University of Innsbruck. I finished my studies with a diploma thesis in mathematics on Fourier series expansions on the solutions of certain partial differential equations. Right before university entrance I began to study scientific matters at my own. For works on calculating astronomical ephemerides, for a construction plan of a sun-dial, and for calculating e and π I got two times the Austrian youth-prizes. In 1984 I got a grant for gifted students of the Faculty of Natural Sciences.

In 1986 I began to work on the Institute for Basic Sciences in Engineering, of the University of Innsbruck. There I become acquainted with Prof. Kaps, biomechanics of skiing, and the Department of Sport Science. After a while, I switched to the biomechanics group of Prof. Nachbauer at the Department of Sport Science. For the outcomes of my ongoing cooperation with Prof. Kaps and Prof. Nachbauer I refer to my publication list. Over the years I gathered, besides my scientific knowledge on biomechanics, physics, and mathematics, a lot of skills in informatics and computing. Among these are knowledge on the usage of numerous software tools, the programming in several programming and scripting languages, as well as the handling of Windows computers and UNIX servers. Beside my scientific work I gave several years exercise courses for the students of civil engineering as well as informatics.

Innsbruck, July 2006